SPACE- AND TIME-DEPENDENT ANALYSIS OF SUBCRITICAL TRANSIENTS IN A HEAVY WATER REACTOR

A DISSERTATION

Presented to

The Faculty of the Division of Graduate

Studies and Research

by

Anthony Joseph Foltman, II

In Partial Fulfillment

of the Requirements for the Degree

Doctor of Philosophy

in the School of Nuclear Engineering

Georgia Institute of Technology

May, 1972

SPACE- AND TIME-DEPENDENT ANALYSIS

OF SUBCRITICAL TRANSIENTS IN A HEAVY WATER REACTOR

Approved:

W. Waverly Graham, III, Chairman

J. D. Clement

L. J. Gallaher

R. J. Johnson

Date approved by Chairman: May 12, 1972

In presenting the dissertation as a partial fulfillment of the requirements for an advanced degree from the Georgia Institute of Technology, I agree that the Library of the Institute shall make it available for inspection and circulation in accordance with its regulations governing materials of this type. I agree that permission to copy from, or to publish from, this dissertation may be granted by the professor under whose direction it was written, or, in his absence, by the Dean of the Graduate Division when such copying or publication is solely for scholarly purposes and does not involve potential financial gain. It is understood that any copying from, or publication of, this dissertation which involves potential financial gain will not be allowed without written permission.

7/25/68

ACKNOWLEDGMENTS

A great many individuals have significantly contributed to all phases of this thesis. I therefore wish to take this opportunity to express my sincere thanks and appreciation to all concerned for the helpfulness they exhibited.

My advisor, Dr. W. Waverly Graham, III, admirably fulfilled his role with many suggestions and much guidance over the past three years. I especially appreciate the support he gave me in my numerous moments of doubt and confusion. The members of my reading committee, Dr. J. D. Clement, Dr. L. J. Gallaher, and Dr. R. J. Johnson, provided many timely and thoughtful suggestions throughout the research and during the writing of the dissertation.

I wish to thank Dr. C. J. Roberts and the National Science Foundation for the financial support which they provided. Dr. G. G. Eichholz was also helpful in obtaining financial aid for me during the final phases of this work.

My occasional employer, Dr. Stephen Spooner, was quite helpful over the past years by furnishing both advice and encouragement, not to mention gainful employment. His confidence in my abilities was always well appreciated.

The efforts of my good friend, Dr. Gabe Weaver, in providing assistance were exceptional. He never failed to take the time necessary to offer all the help possible, and he readily involved himself in many

long hours of discussions and labors. In addition, the high quality of his own research provided firm foundation for the continuation of my work.

I wish to thank my friend, Dr. Dave Ebert, for taking the time to discuss many aspects of my research. His continued encouragements were quite favorably received.

The experiments reported in this dissertation would never have been performed without the excellent equipment and services provided by four individuals. Mr. Stanley Beavers of Mobesco, Inc. was very helpful in the design and construction of the hydraulic system, while Mr. J. C. Gundlach of Reactor Controls, Inc. supplied an excellent neutron detection system which operated flawlessly. Mr. Billy D. Statham also proved very helpful in coaxing two occasionally balky computers into cooperating. Finally, Mr. Mike Burke repeatedly demonstrated his first-rate abilities as a machinist, and the many enjoyable and animated discussions we had were a relaxing respite from my frequently tiring labors.

The staff of the Georgia Tech Research Reactor furnished a great deal of assistance. Mr. Fred Apple and Mr. Robert Kirkland were very understanding in providing procedural advice and in scheduling the experiments. The reactor operators, Messrs. Lamar Bennett, Sam Kirbo, Dean McDowell, John Moon, and Sonny Pruett, could not have been more helpful, patient, and understanding. Their continual eagerness to cooperate and to offer assistance was greatly appreciated during the experimental phase of this research. I am obliged to Messrs. Bob Boyd, Martin Mitchell, Jerry Taylor, and John Wright of Health Physics for their alert efforts which facilitated the smooth and safe operation of the experiments.

I wish to thank Mrs. Lydia Geeslin for her accurate typing of this dissertation. Mrs. Martha Shoemaker was also very helpful in offering advice and suggestions on the preparation of the figures.

My mother- and father-in-law, Mr. and Mrs. R. J. Kovac, have often expressed interest in my work. I want to thank them for their many heartening and reassuring comments.

I am very appreciative of the generous assistance and unwavering support that my parents have given during my many years at Georgia Tech. Their confidence in me was always very encouraging and satisfying.

Finally, my appreciation of the countless contributions of my darling wife, Karen, is too great to possibly express. Suffice it to say that without her love, devotion, understanding, and just plain, hard work, none of this would have been meaningful, or even possible.

TABLE OF CONTENTS

TABLE OF CONTENTS (Concluded)

LIST OF TABLES

LIST OF TABLES (Concluded)

LIST OF ILLUSTRATIONS

LIST OF ILLUSTRATIONS (Concluded)

SUMMARY

Consideration of the time dependence of neutrons in multiplying media, that is, reactor kinetics, has interested engineers and physicists since the nuclear industry began. Calculations for the early, small reactors proved that the point kinetics formulation, even with its lack of spatial detail, was sufficient. However, the design and construction of larger power reactors provided impetus for the examination of spatial effects. Kinetics programs employing finite-differenced, multigroup diffusion theory (such as WIGLE) served as standards for accurately calculating space-dependence. However, these standards proved to be economically impractical for industrial design purposes. This led to the development of several calculational methods involving even more approximations, but permitting greater economy. The accuracy of these approximate methods was estimated by comparisons to the standards, but it is now desirable to verify both the standards and the approximate methods by comparison with experiments.

Therefore, the purpose of this research was to provide data in order to make model comparisons for essentially two-dimensional, fast subcritical transients similar in nature to the operational transients experienced in power reactors. The experimental program employed the highly enriched, heavy water moderated Georgia Tech Research Reactor (GTRR). The results were compared with two-dimensional, two-group calculations from both finite-differenced diffusion theory and the adiabatic

approximation model.

The adiabatic model utilizes the assumption that spatial changes in the flux at any time during a transient may be approximated by the calculated statics flux shapes associated with the physical reactor configuration at that time. The neglect of delayed neutrons is a potential source of serious error in the method.

The GTRR shim-safety blades could not be used to generate the desired subcritical transients since their complex movements were three-dimensional. The generation of meaningful kinetics data for comparisons with the two-dimensional models thus required the construction of a hydraulically operated control rod which was inserted along the GTRR core axis. In this configuration there was no angular dependence on position, resulting in a two-dimensional experiment.

The control rod was worth about 5.6 percent $\Delta k/k$ and could be inserted into the core in 0.5 second or longer. In order not to complicate the comparisons, feedback effects were not considered. Thus, the transients were initiated from a power level of 50 kilowatts. During an experiment, miniature boron ionization chambers were used to obtain data at several positions throughout the core. These detectors were also used to obtain axial flux shapes versus various control rod positions at different radial core locations. The rapid transients required the use of a computerized data acquisition system which monitored eight channels of data 200 times per second, and stored the information on magnetic tape for later analysis.

The comparisons of statics calculations with the experimental

results illustrated good agreement for general spatial features. For positions within the core, the greatest difference noted was about 25 percent. The reflector regions exhibited differences greater than 50 percent for certain control rod positions. This deviation was concluded to be due to the inadequacy of diffusion theory in regions with large flux gradients.

As with the statics results, the kinetics simulations using the standard model illustrated good agreement for spatially-dependent effects. For the insertions longer than one second, the differences noted could be directly attributed to the differences observed in the statics results. Significantly larger differences between the standard model's calculations and experimental data resulted for the faster insertions. It was therefore concluded that insertions slower than one second do not require stringent statics modeling if the adequacy of the statics model is known. For fast insertions, typical of operational transients in a power reactor, however, the model must calculate the actual flux shape and eigenvalue within a few percent for the standard methods to be accurate. This is especially true if the rapidly changing portion of the transient is under consideration.

The results of the adiabatic model calculations exhibited the expected delayed neutron holdback, but also a 50 percent savings in computation time. For insertions as fast as one second, the method lagged the standard model calculations by about 40 percent during the prompt drop. If the asymptotic portion of a fast transient is of primary importance, the adiabatic method is as accurate as the standard methods.

Simulations of insertions faster than one second exhibited large error, and consequently the need for accurate representations of delayed neutrons.

CHAPTER I

INTRODUCTION

The study of the time dependence of the neutron population in multiplying media, that is, reactor kinetics, has been a subject of much interest. It has its origins even before it was decided to build the first nuclear reactor during the Manhattan Project in the early 1940's. In a paper reviewing reactor kinetics, Henry[1] discusses the nature of these origins in such areas as Brownian motion and stellar radiation. The study of such phenomena led to a formulation of the time dependence of small numbers of particles of a statistical nature. Henry states that this type of statistical formulation was first examined with respect to the neutrons during the early atomic bomb work.

The essence of the statistical approach is a consideration of all possible states of neutrons and the probabilities of their changing to another state. The mainstay of the technique is a balance equation of the nature of the presently used Boltzmann transport equation on which kinetics theory is founded.

Point Kinetics

The next stage in the development of reactor kinetics leads to the study of very large populations of neutrons. Deterministic, rather than statistical, equations are now necessary, and the results were the point reactor kinetics equations. The essential assumption of the point kinetics

approach is that the reactor can be represented as a point, thereby giving consideration only to the magnitude, or amplitude, of the neutron population. Mathematically, this is equivalent to stating the neutron population, or flux, as a function of time and position, is separable into distinct functions of time and position along with the position, or shape, function being constant.

The point kinetics equations can be derived in several different ways utilizing many degrees of complexity. These range from a simple balance equation for neutrons involving physical considerations,[2] to a derivation by Henry[3] based on the full Boltzmann transport equation. Recently, Becker[4] has even generalized and extended the method of Henry by assuming time-dependent weighting. The relationship of the point kinetics equations to the techniques employed in the present research is outlined in Chapter IV which deals with those techniques.

Intuitively, applying point kinetics to the huge, 3,000 megawatt reactors now being ordered would appear to be unreasonable and unsafe, which it has proven to be. Nevertheless, point kinetics still has important utility in nuclear engineering. Typical uses include: the calculation of total energy release in prompt critical excursions[5] along with other safety calculations such as determining reactor performance limits; preliminary feasibility studies and design calculations; and control and stability predictions.[6] In addition to these uses, point kinetics is the basis for an entire family of spatially-dependent kinetics approximations[7] which will be discussed later in this chapter, and will be examined in detail in Chapter IV. Since the solution of point kinetics for such

practical problems as those listed requires the use of digital computers, the easily obtained, exact exponential solution must be approximated using standard numerical techniques[8] which then results in the introduction of error. Much effort, therefore, has been, and is still being, devoted to providing more efficient and accurate techniques of approximating the point kinetics solutions.[8-14]

Spatially-Dependent Kinetics

With the advent of large power reactors, with their inherent spatial characteristics, it became clear that some spatial information had to be included in the kinetics solutions.[15,16] Besides building larger reactors, space-time analysis is required to build these reactors economically by predicting the limits of reactor response, instead of the procedure of merely overdesigning to accommodate any conceivable situation. Kaplan[15] also states the need to apply space-time analysis when attempting to obtain basic reactor parameters in order to refine the precision of the parameters, or else to be assured error is not introduced due to spatial effects. Kasten[17] concurs in this and adds that experimental data have frequently been forced to fit point kinetics solutions without any justification. He also says that there are questions in applying point kinetics to the areas of safety and stability. Besides the above reasons, space-time analysis will be necessary to design the fast breeder reactors of the future. Many of the techniques proposed for spatial analysis are also readily applied to the fast reactor problem of predicting the energy-time response accurately. Butler and Meneley[18] and Stacey[19] have recently

written excellent review articles on application of these techniques to fast reactor spectral analysis.

With the need for space and time analysis established, the method of solving for the spatial response becomes of some concern. Solving the transport equation will provide the necessary answers, but obviously this is a totally unreasonable approach for practical problems. The approximation of transport theory, that is, multigroup, multi-dimensional diffusion theory, provides part of the answer. Numerical techniques,[23] such as the finite-difference method, applied to diffusion theory will result in a set of equations which can be solved on a computer. This has been done for one dimension to yield well-known programs like WIGLE.[20] Two dimensions and thermal-hydraulic feedback equations further complicate the problem, but are still manageable resulting in such programs as TWIGL[21] and WIGL2.[22] The essentials in the development of these types of solutions, using finite-difference techniques, will be presented in Chapter IV. Such solutions are occasionally called "exact" methods, but will be called standard or space-time solutions in this dissertation.

The difficulty in using these programs for detailed reactor design work is the use of inordinate amounts of computer time. Therefore, a great deal of effort has been expended in the development of various approximate solutions which will require significantly less time to produce with only a minimal loss of accuracy. However, the finite-difference solutions of diffusion theory are still regularly used as standards to which the various approximate methods can be compared.

There are several fine papers reviewing the approximate methods

commonly used, including those by Henry,[1] Kaplan,[15] Kerlin,[16] Butler,[18] and Stacey.[19] The common methods, in addition to the standard methods, include: nodal analysis; modal analysis or synthesis; and the adiabatic approximation, a method considered in this research. There are also other less common methods such as Alternating Direction Implicit (ADI)[24] and harmonic analysis techniques[25] which have proven to be less useful. The major methods listed above will be described in the following sections.

Nodal Analysis

This method assumes the reactor consists of a small number of nodes or channels.[26] The average flux for each of these nodes, obtained by integrating the diffusion equations over each node, provides the temporal information, while calculations of leakage into and out of each node provides the spatial information. Finite-difference solutions of diffusion theory may be thought of as an extreme case of nodal analysis in which the nodes are very small and closely spaced.[15,19]

Because of the coarse nature of the nodes, the method has been frequently considered for separated but coupled cores, although it can be used for single, contiguous cores. Its advantages include the use of the simple standard point kinetics formulation, while feedback is readily incorporated using the standard engineering equations.[16]

In past years, this method enjoyed greater popularity than it does now. The minimal spatial information obtainable from large nodes was probably acceptable when early space-time calculations were being carried out, but now much finer spatial detail is required, and the method has been replaced by more sophisticated techniques. In addition to the lack

of spatial detail, the programs using the technique have generally been limited to one-dimension and one energy group because of the long and expensive computer time necessary to calculate the coupling parameters. Since the calculation of coupling also requires the use of the static flux and the static adjoint, the method has been questioned for transients in which the spatial shape may undergo extensive changes.[19,27]

Modal Analysis

This method is currently being given a great deal of consideration as a technique for spatial analysis, and also for the similar energy-time analysis necessary for designing fast reactors.[19] Its accuracy and the detail which it can provide can be quite good. Kaplan[15] and Yasinsky[27] have even suggested the technique may eventually prove to be practical for realistic, three-dimensional reactor calculations.

The essence of the procedure is to approximate the unknown space- and time-dependent flux with a linear combination of carefully chosen, known spatial "trial functions" or "modes" weighted by unknown, time-dependent "mixing coefficients."[15] The actual scheme consists of substituting the combination of trial functions into the diffusion equations, and then weighting the result with the time-dependent mixing coefficients. This equation is then integrated over the reactor volume to yield a set of differential equations which can be solved for the mixing coefficients. Practically, the solution requires a digital computer and the use of finite-difference techniques.

The exact choice of the trial functions requires some insight and experiment and improper choices can obviously lead to bad kinetics results.

Likewise, judicious selection of the trial functions can simplify the work necessary to obtain the time dependence. The degree of improvisation allowed to the analyst is, therefore, substantial, and some experience is necessary to use the techniques. As a result of this freedom, many different types of trial functions have been investigated and reported. Some of the simpler, and less exotic choices, include Helmholtz modes, omega modes, lambda modes, and Green's function modes.[17]

Helmholtz modes consist of the solutions to the Helmholtz wave equation. This type of trial function has the desirable attribute of being orthogonal, which proves to be very useful in simplifying aspects of modal analysis. Complicated geometries or transients with severe spatial changes lead to an excessive number of these trial functions with ensuing large computation costs. The omega modes are derived by assuming exponential solutions to the diffusion equation; the type of omega mode is dependent on whether the delayed neutrons are included. These are considered the "natural modes" of a problem. As with Helmholtz modes, a great number are necessary to describe real assemblies, and they are frequently difficult to calculate. Lambda modes, also called reactivity modes, are essentially the solutions of the statics equations of the assembly during the transient. They suffer from the same drawbacks as the omega modes. Finally, Green's function modes are obtained by dividing the reactor into nodes, setting all fission cross sections to zero, and then calculating the static and adjoint fluxes when the appropriate portion of the unperturbed fission distribution for a given mode is introduced into each of the nodes successively. The desirability of this

scheme is that realistic geometries can be considered with reasonable amounts of computer time.

The most accurate results are obtained from this method when "synthesis" modes are used. In this situation, the method is sometimes referred to as flux or time-synthesis.[19] Synthesis modes are flux shapes, such as the static and asymptotic shape and possibly others, which are predicted to bracket the shapes expected during the transient. If such shapes can be obtained readily, the results can be quite accurate with only a few modes and reasonable computer time.

The major hindrance in the use of modal analysis is the lack of usable error criteria. A common method of evaluating the error is to recalculate the result using additional modes and compare to the previous solution. However, this method has been known to give worse results.[28] Henry[29] has recently stated that methods of applying bounds to the error are now available.

Adiabatic Approximation

This method, along with a standard method, are the ones of concern in this dissertation. A more detailed look at the method will be provided in Chapter IV.

After Henry[3] had presented his work on the point kinetics formulation, discussed earlier, he and Curlee[30] extended the approach and proposed the adiabatic approximation. While the method of recalculating the spatial shape from time to time during solution of the point kinetics equation had been intuitively considered for some time,[19] this was the first practical approach. The adiabatic method as proposed by Henry and

Curlee makes the assumption that the reactor spatial shape instantly adjusts to the state of the reactor variables at any time during the transient. Point kinetics is then used for the time dependence. This is equivalent to saying that the lambda mode, or static flux shape, of the reactor for a given state is used to provide the input to the point kinetics equations. Kerlin[16] notes that even for infinitesimally small time steps the result is not exact, but still gives substantial improvement over point kinetics.

One cause for inexactness is the lack of consideration for the effects of delayed neutrons. The most common form of the adiabatic method assumes the shape of the delayed neutron distribution to be the same as that of the prompt neutrons.[18] This is easily seen to be a serious source of error since during transients the prompt fission distribution may be greatly different from the delayed neutron distribution, which essentially has the shape of the prompt neutrons at some earlier time. Stacey[19] refers to this effect as delayed neutron holdback. A more detailed consideration of the effect is discussed in Chapter IV.

Because of the delayed neutron holdback, the adiabatic method is most accurate in situations where delayed neutrons are less important, such as large cores undergoing prompt critical transients.[31] In order to apply this type of analysis to other situations Ott and Maddell[32] and Stacey and Adams[33] agree that only the delayed neutron shape need be accurately represented to achieve good results. Ott and Meneley[34] have formulated the equations necessary to achieve more accurate results and a discussion of their development is given in Chapter IV.

If the delayed neutron shape is properly handled, the approach is generally referred to as the quasistatic method. Such methods can be as accurate as necessary, and for decreasing time steps will approach standard method results. A computer program,[34] QX1, has utilized this method and found to yield excellent agreement with WIGLE. It is the only code capable of dealing with as many as 30 energy groups with any desired accuracy.

Review of Numerical Studies

The first step in assessing the validity of such methods of approximation as those discussed above is to make comparisons of results of test cases with those of accepted standard methods such as WIGLE. Several such comparison studies have been published on the methods discussed above.[35, 36,37] A particularly thorough study of the approximations for large and small reactor models and two types of positive transients was carried out by Yasinsky and Henry.[38] The study included WIGLE as the standard along with the adiabatic, synthesis, nodal, and point kinetics approximations.

The results of the Yasinsky and Henry comparisons are typical of the expected responses, and of other such studies. The transients were designed to exhibit significant spatial effects, and the point kinetics results, as expected, were in considerable error. However, the magnitude of the error was greater than expected, especially on the large reactor model. This further confirmed the conclusion that point kinetics should never be used for large reactors or transients with severe spatial changes, and also established the need for more accurate space-time calculational procedures. Of the spatially dependent approximate methods, nodal analy-

sis yielded the worst prediction of the spatial changes, as would be expected from its coarse nature. The adiabatic approximation provided significant improvement over point kinetics, but overpredicted the magnitude due to the effect of the delayed neutron holdback. Synthesis appeared to be the most accurate and yielded excellent results for all test cases.

Review of Space-Time Experiments

The need to account for spatial dependence in the course of undertaking kinetics calculations has been well established as outlined earlier. As a result, much theoretical work has been done in developing a great many space-time approximations to multigroup diffusion theory. Some of the more important methods, along with their relative merits and disadvantages, have been presented in this chapter. Deciding which one is "best" in some sense is a difficult task, but numerical studies, such as those reported in the preceding section, provide partial answers. However, Hassan and Miley[39] and Rydin[40] point out that the many assumptions and approximations necessary to develop the standard methods leaves even them open to question as to their accuracy with respect to experiments. Their use as standards of comparison is, therefore, in need of verification. In addition, many other authors[1,16,18,41] have stressed the need for experiments with which to compare the various other approximate methods. The requirement for spatially dependent experimental data to compare to model predictions is consequently well established. Unfortunately, little work has been carried out in this area.

Of the many experiments performed, a large number have been on

non-multiplying media and are beyond the scope of this paper. Such experiments are generally involved in pulsing the media to obtain isolated reactor parameters, and as previously stated, space-time effects must be considered even in this type of experiment to account for possible interference.

Experiments in multiplying media also involve measuring reactor parameters, calculating accident consequences, and verifying space-time models such as those discussed. However, only the latter types will be reviewed in this section.

Of the experiments performed for model verification purposes, most are of the type Kaplan[15] refers to as linear; that is, feedback from the neutron behavior to the nuclear properties has not been considered. Non-linear experiments, those with feedback, have been much more limited.

The most notable of the non-linear experiments have been the Special Power Excursion Reactor Test or SPERT experiments[42] which provided data on very fast, positive transients. Much of the data is not specifically concerned with space-time effects, but rather with the interrelation of the neutronics with the thermal-hydraulic aspects of the reactor. The complete analysis of these data, especially with respect to spatial effects, has not been completed.

The TREAT experiments,[43] on the Transient Reactor Test Facility, were performed on an air-cooled graphite reactor using fast transients. Robinson[44] attempted to apply the results to an approximate solution of the multigroup diffusion equation, but reported spatial effects were not observed.

Included in linear experiments are transfer function experiments which perturb an assembly, generally in a sinusoidal fashion, and measure the amplitude and phase shift of the response with respect to the input. Such experiments are useful in studying reactor behavior, and have been used to study space-time effects. Early work on the NORA reactor,[45] using noise techniques to develop the zero power reactor transfer function, was later extended by Johnson[46] using the NORA data, and data obtained from the Georgia Tech Research Reactor with a pile oscillator. The results exhibited significant spatial changes and were reasonably predicted using numerical methods. The use of EXTERMINATOR to analyze the two-dimensional behavior was also successful, but computation costs were large. Johnson illustrated significant spatial effects could be instituted in the Georgia Tech Research Reactor with only moderate rates of reactivity insertion. Bridges[47] recently extended Johnson's work using non-linear experiments which included temperature feedback effects, and found standard numerical techniques yielded good predictions of spatial effects.

Experiments at the University of Florida have attempted to provide verification of WIGLE by pulsing an essentially one-dimensional, light water assembly.[48] WIGLE was found to yield inconsistent results, probably due to the lack of accurate statics modeling.

Hassan and Miley[39] reported similar work designed to verify WIGLE using pulses propagating through a heavy water TRIGA assembly. They had particularly good statics modeling and the WIGLE predictions were quite accurate.

A series of experiments has been recently reported for the Solid

Homogeneous Assembly (SHA) at the Knolls Atomic Power Laboratory, which were specifically designed to test calculational models.[40] A novel scheme allowed essentially step-insertions of negative reactivity to be made near the end of the assembly. The purpose of the step-insertion was to preclude complications arising from ambiguities in the rate of reactivity insertion. The model was to be one-dimensional, and emphasis was placed on the modal synthesis model. The static modeling of the assembly was quite good, and the authors found few-group diffusion theory to be adequate. The synthesis predictions of the dynamic behavior were also reasonable, but the method did show evidence of a delayed neutron holdback and overpredicted the observed flux tilt. The results of the SHA work indicated that a statics model which predicts the initial flux shapes well, along with the perturbation worth, should yield adequate kinetics results.

Since the total worth of the reactivity in the SHA experiments was small, the ensuing transients were not very severe. No comparisons were made to the prompt drop and subsequent rapid decay portion of the transient.

A series of linear experiments has been performed on the Georgia Tech Research Reactor by Weaver,[49] with the goal of providing data for fast negative transients for comparisons of diffusion theory and the adiabatic approximation, using two energy groups and two dimensions. The statics modeling proved to be difficult, and resultant kinetics calculations were not in exact agreement with experiment. The results did give some evidence of important trends related to the rate of reactivity insertion which experimental refinements could bring out to a greater

degree. This work has provided the basis for the research reported in this dissertation, which has extended the experiment to include faster reactivity insertions.

Objectives of the Present Research

Stacey[19] has suggested the need for further experiments to confirm the limited results so far obtained on comparisons of calculational models and experiment. He has also stated the need for assessments of the practical importance of accounting for spatial effects, and the relative adequacy of the available approximate calculation schemes, especially in realistic reactor experiments. Rydin[40] has specifically affirmed the need to verify these recent results on essentially two-dimensional reactors.

The objectives of this research are, therefore, to provide additional documented data on an essentially two-dimensional, heavy water reactor to which calculational model predictions can be compared. The models of concern here will be finite-differenced, multigroup diffusion theory, and the adiabatic approximation as applied to a realistic reactor model. Feedback effects will not be included, and special emphasis will be placed on refining previous results, including importance of statics modeling, accuracy of standard methods, relative accuracy of the adiabatic approximation, and the significance of the rate of reactivity insertion. Finally, extensions of results obtained by Weaver[49] on his "mixed-method" calculational model will be undertaken.

CHAPTER II

EQUIPMENT AND INSTRUMENTATION

The experimental equipment and instrumentation consisted of four major systems. They were:

1. the Georgia Tech Research Reactor,
2. the Negative Transient Generator,
3. the Nuclear Instrumentation System, and
4. the Data Acquisition System.

These systems will be discussed in this chapter.

Georgia Tech Research Reactor

The reactor used in the experiments was the one megawatt, heavy water moderated Georgia Tech Research Reactor[50] (hereafter referred to as the GTRR). The GTRR consists of an aluminum reactor vessel, six feet in diameter, supported in a two foot thick graphite reflector. The reactor vessel contains 5.2 tons of heavy water in which the fuel assemblies and control elements are suspended. A fully loaded core of 19 fuel assemblies, arranged in a six inch triangular pitch array, approximates a right cylinder 23.5 inches in height and approximately two feet in diameter. The core utilized in the present experiments had a loading of either 17 or 18 assemblies. The heavy water provides moderation within the core and also a two foot thick reflector on all sides of the core. Above the water is a helium blanket designed to prevent contamination of the D_2O. A vertical

section of the reactor and concrete biological shield is shown in Figure 1. A horizontal section is shown in Figure 2.

The fuel is highly enriched (greater than 93 percent U-235), MTR type assemblies. Each assembly is constructed of ten curved fuel plates of aluminum clad, aluminum-uranium alloy with each plate being 0.060 inch thick, 2.796 inches wide, and 25 inches long. Each assembly has a fuel loading of 142 grams of U-235. Between the plates are coolant passages 0.183 inch wide. The complete assembly consisting of locating end fitting and lower top shield plug is shown in perspective in Figure 3.

The reactor is controlled by four, aluminum-clad, cadmium shim-safety blades, ranging in worth from 9.7 percent $\Delta k/k$ to 15.2 percent $\Delta k/k$, which are arranged in semaphore fashion at the top of the reactor. They move 55° through the core and have a full out position 6° below horizontal. The complex three-dimensional behavior of the shim-safety blades was not amenable to producing two-dimensional, experimental data. As mentioned previously, the kinetics analyses involved two-dimensional models. The generation of meaningful experimental data for comparison purposes therefore necessitated the design and construction of the Negative Transient Generator. This device, an axial control rod for kinetics experiments, is described in the next section. In addition to the shim-safety blades, a low worth regulating rod is located in the D_2O reflector for fine adjustments of power. The location of the control elements is shown in Figure 1.

Access to the core is by vertical experimental ports and fuel ports from the top of the reactor.

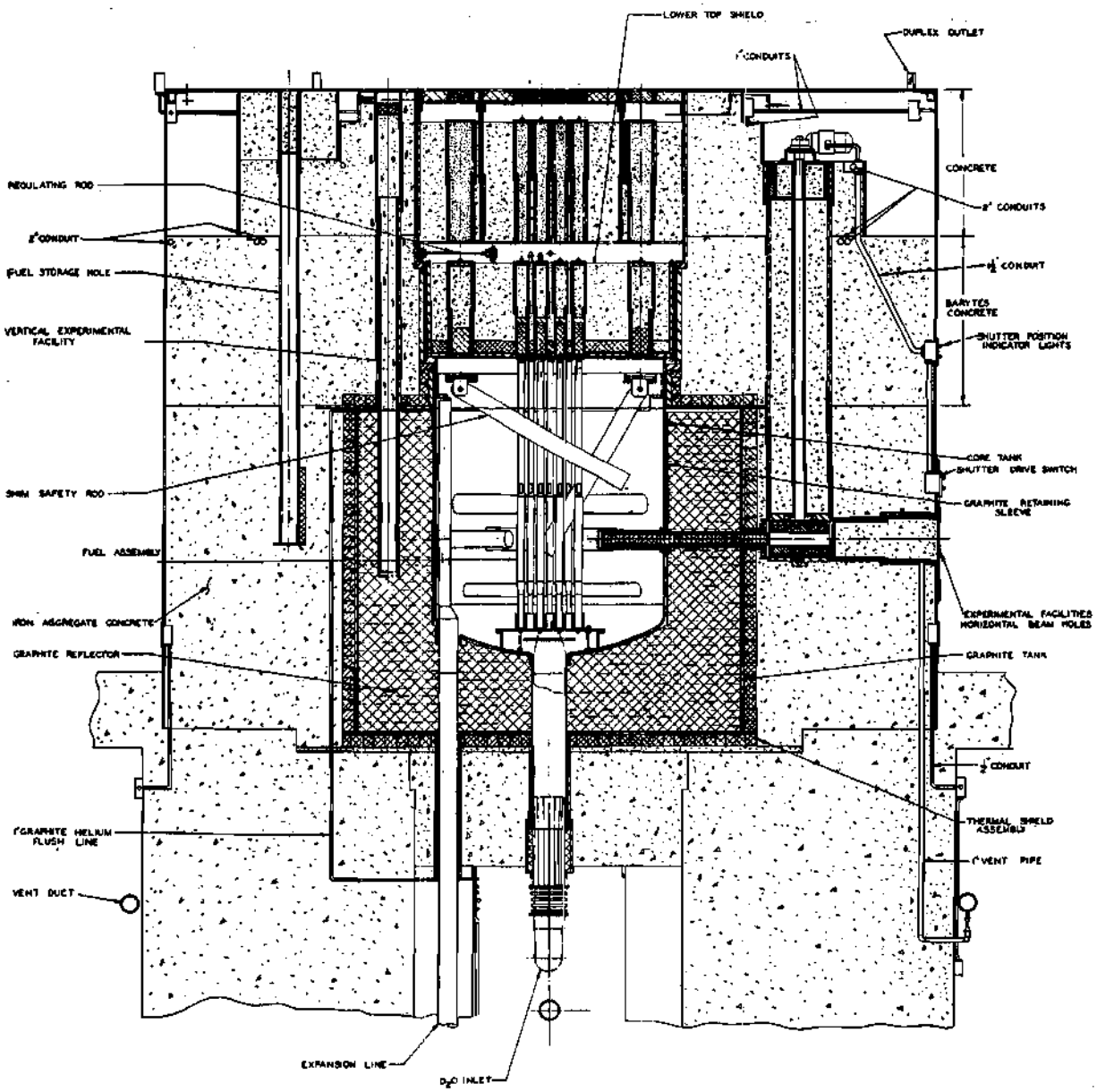

Figure 1. Vertical Section Through the GTRR

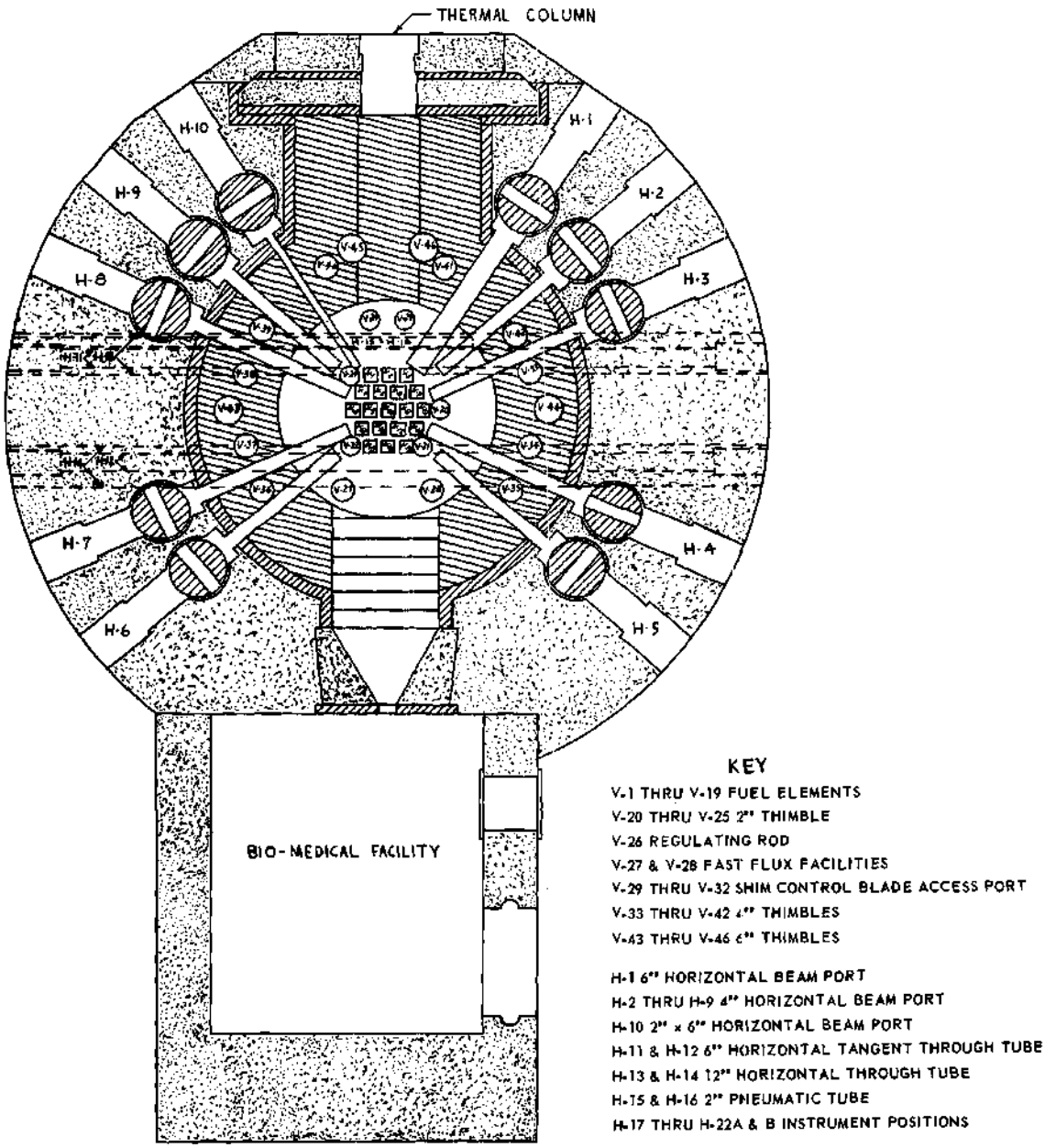

Figure 2. Horizontal Section of the GTRR at the Core Mid-Plane.

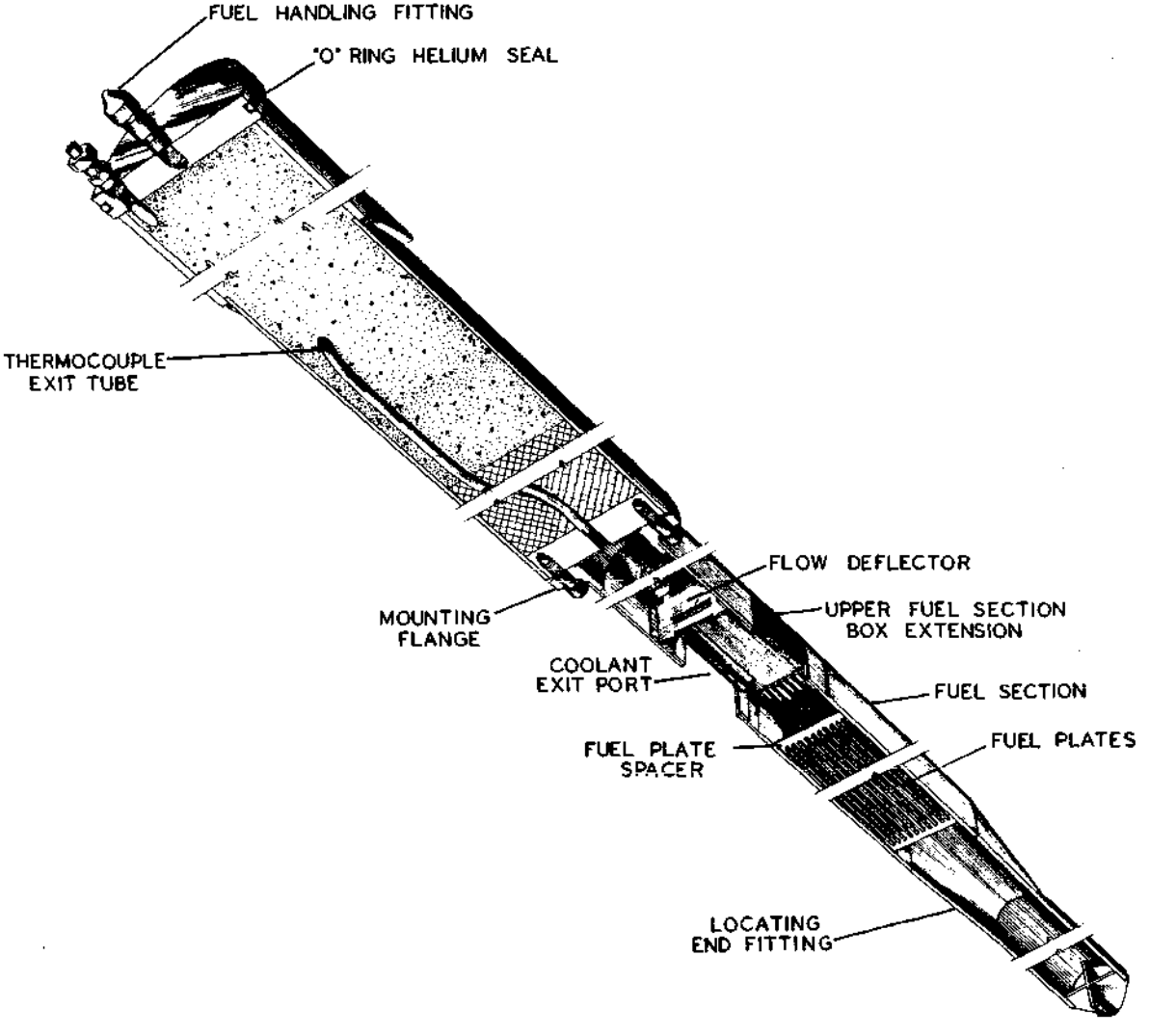

Figure 3. Perspective of a Fuel Assembly

Negative Transient Generator

The Negative Transient Generator (hereafter referred to as the NTG) was composed of four major components. They were:

1. the Control Rod Assembly,
2. the Link and Instrumentation Unit,
3. the Hydraulic Drive, and
4. the Control and Monitoring System.

Control Rod Assembly

The Control Rod Assembly was loaded into vertical fuel position V-10, and provided linear withdrawal and insertion of an absorber along the reactor core axis. Thus, two-dimensional geometry (no angular dependence about the axis) was approximated. A cutaway diagram of the assembly is shown in Figure 4, and a photograph of the detail of the lower half of the assembly is shown in Figure 5. There were provisions for changing the neutron absorbing control rod, but a type 304 stainless steel element, 30 inches long and two inches in diameter, was used exclusively in the present experiments.

The assembly was suspended in the core by the modified lower top shield plug. Bolted to the bottom of the shield plug was a three inch diameter, 0.035 inch-thick wall aluminum shroud; at the end of the shroud was a plenum plug which sealed off the channel from coolant flow. Extending through the shield plug was a one inch diameter stainless steel drive rod which was threaded to accept the neutron absorbing assembly, and was within the aluminum shroud. The top of the drive rod had connected to it a cup-like portion of the remote solenoid gripper used to couple to the Link and Instrumentation Unit. The drive rod ran on linear recirculating

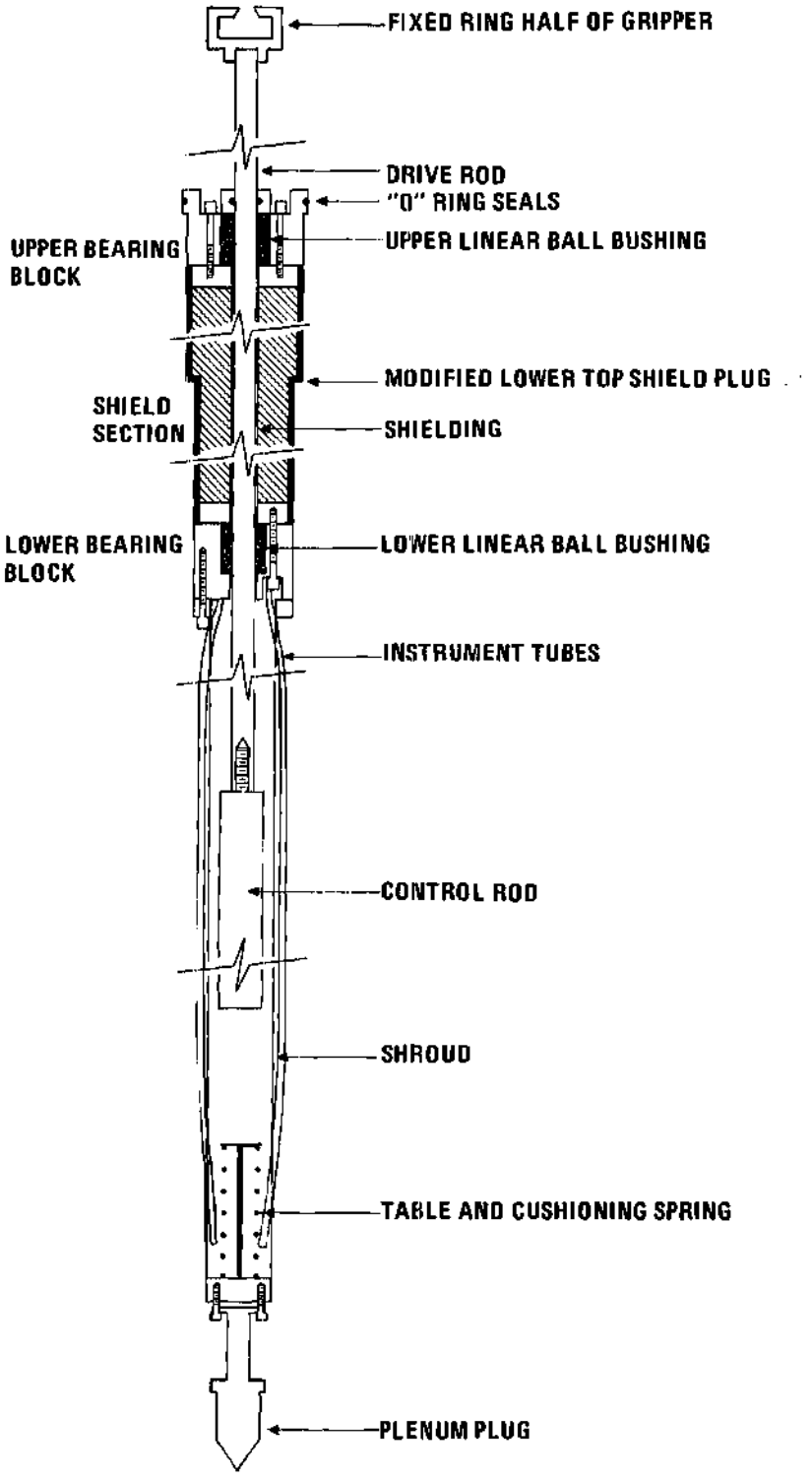

Figure 4. Cut-Away View of the Control Rod Assembly

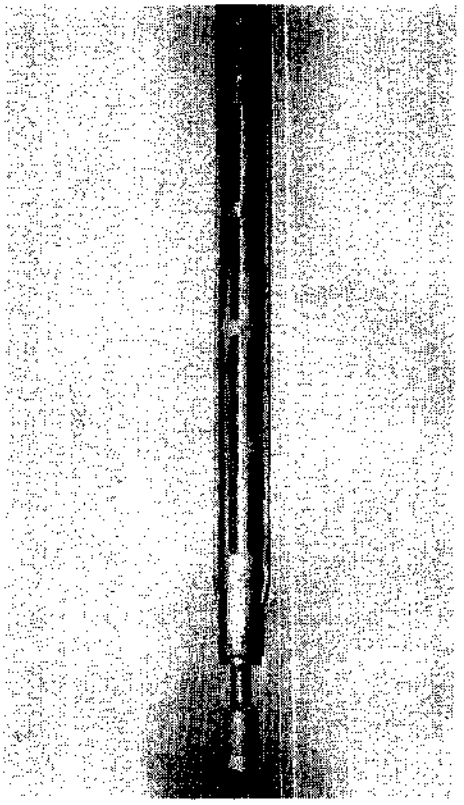

Figure 5. Detail of Control Rod Assembly

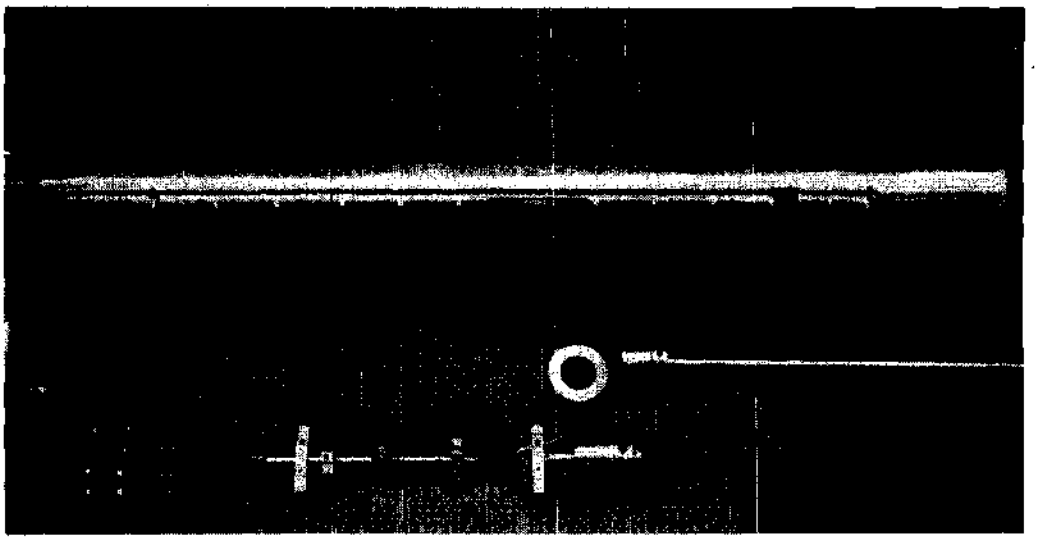

Figure 6. Disassembled Link and Instrumentation Unit

ball bearings. All possible paths of helium leakage through the assembly were sealed by "O" rings or gaskets.

When fully inserted, the control rod rested on a spring loaded cushioning table located in the bottom of the shroud, and extended three inches above and below the core boundaries.

Extending through the shield plug and along the outside of the shroud were two dry aluminum tubes into which detectors were loaded.

Finally, atop the shield plug was a standard remote gripper mast, which could be moved aside to enable coupling to the Link and Instrumentation Unit. This mast facilitated movement of the assembly with standard GTRR procedures. The Control Rod Assembly could be loaded into any available fuel lattice site.

Link and Instrumentation Unit

This unit rested in the upper top shield over the Control Rod Assembly and provided coupling to the hydraulic drive cylinder, which was on top of the reactor and bolted to the Link and Instrumentation Unit. The non-nuclear instrumentation, that is, the instrumentation which monitors the status of the equipment during the experiment, is provided by this unit. A photograph of the disassembled unit is shown in Figure 6.

The unit consisted of a six inch diameter aluminum tube with a large flange on one end; the tube extended into the upper top shield plug with the flange supporting the weight on the reactor top. The flange was held to the reactor cover plate with large bolts which fit into adjacent fuel positions when their cover plate plugs were removed. Inside the tube were two stainless steel tracks on which the instrumented extension rod ran, while two aluminum guides on the extension rod engaged these tracks

and prevented angular movement about the axis and also maintained alignments.

The extension rod connected the control rod to the hydraulic cylinder. The extension rod itself was connected to the cylinder piston rod by a chain coupling, which allowed for some small axial misalignment. The other end of the extension rod had attached to it, in a brass housing, a double-cam, rotary action, solenoid-operated gripper. The gripper had a conical shape in order to locate the cup-like portion of the coupling on the drive rod in the Control Rod Assembly. Once located, power was applied to the solenoid, which then overcame a spring, and rotated the cam to force three ball bearings under the lip of the cup-like ring of the drive rod. As long as power was applied to the solenoid the bearings remained extended, and a coupling of the extension rod to the control rod was effected. The control rod could then be withdrawn and inserted by the hydraulic unit.

Clamped to the extension rod are two spring loaded trips which triggered microswitches, located on the aluminum tube, when the control rod was either fully extended or fully withdrawn. A microswitch located on the solenoid gripper was tripped when engaged to the drive rod, and gave an indication when the extension rod was coupled to the drive rod. In addition, a multiturn potentiometer with a pulley was clamped to the extension rod. A thin, stainless steel cable was looped once around the pulley and connected at each end to the aluminum tube. Thus, as the extension rod moved through the tube, a potentiometer reading resulted, which indicated the position of the extension rod with respect to the tube and therefore the position of the NTG control rod with respect to the reactor.

Since the extension rod moved over a distance of 30 inches, it was necessary to design an electrical conductor to connect to the instrumentation located on the extension rod which could withstand such movement. This was accomplished by using plastic ties to attach ribbon conductor to surgical tubing, which resulted in a series of "S" loops when the tubing was unstretched. Therefore, with one end of the surgical tubing attached to the flange and the other attached near the bottom of the extension rod, a 3:1 extension of conductors was accomplished without entanglements or breakages over many cycles. Figure 6 also shows the extension rod and associated instrumentation.

All instrumentation wires were brought out in a channel machined into the flange, and ended in two multipin connectors to facilitate disassembly of the experimental equipment.

Finally, the aluminum tube has machined into it various slots and openings for adjustments of instrumentation in an assembled state.

Hydraulic Drive

The Hydraulic Drive provided the force necessary to withdraw and insert the control rod. A schematic diagram of the Hydraulic Drive, utilizing standard hydraulic symbols,[51] is shown in Figure 7. Appendix A describes each of the components of the diagram. Photographs of the three Hydraulic Drive components (the hydraulic cylinder, valve platform, and pump unit) are shown in Figures 8 through 10.

The Hydraulic Drive was designed to supply oil to drive the control rod over a stroke of 30 inches into the reactor core as fast as was safely possible. The fastest rate obtainable was about 1.5 seconds with 0.4 seconds required to traverse the core. While most experiments were done at

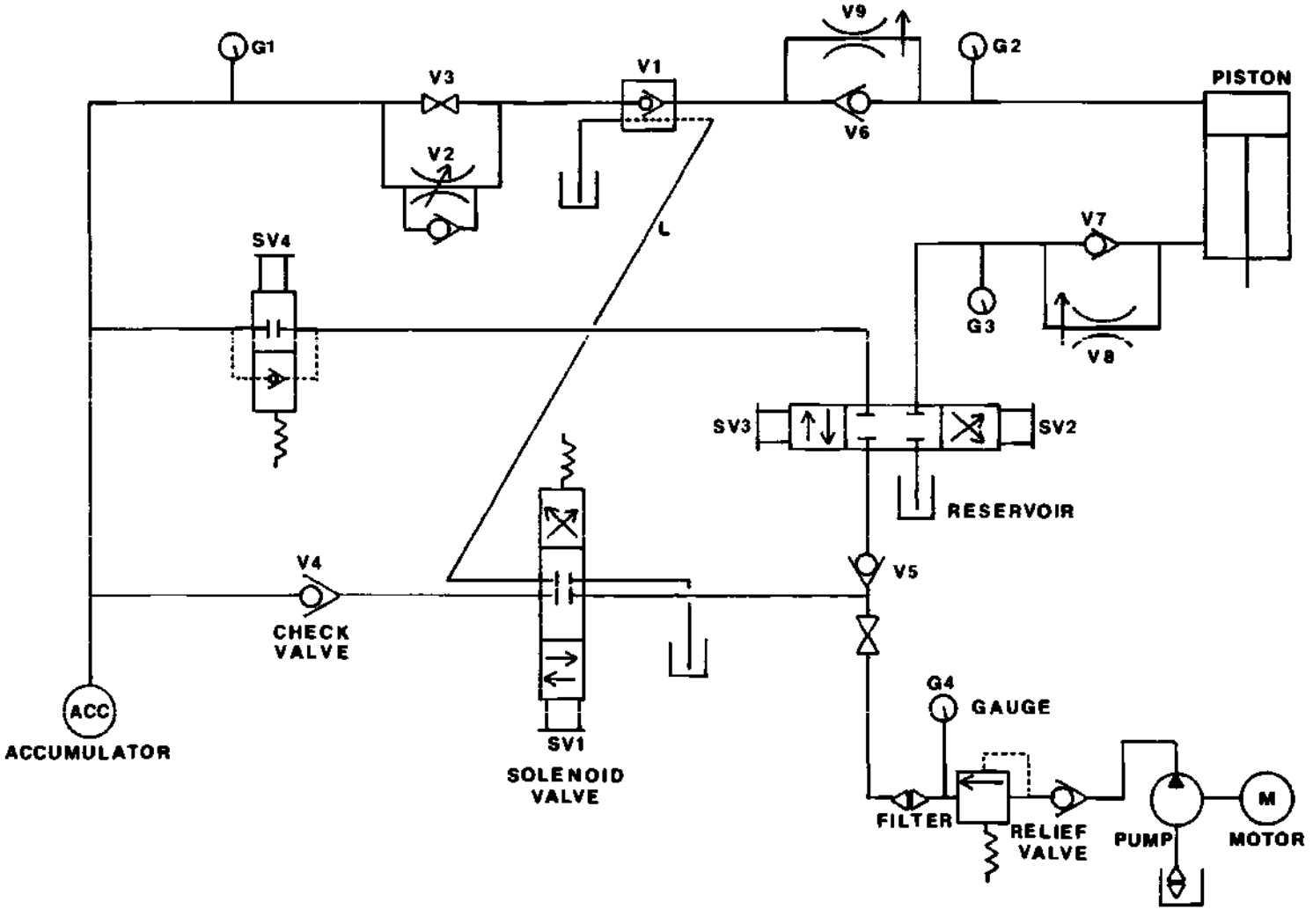

Figure 7. Schematic Diagram of the NTG Hydraulic Drive

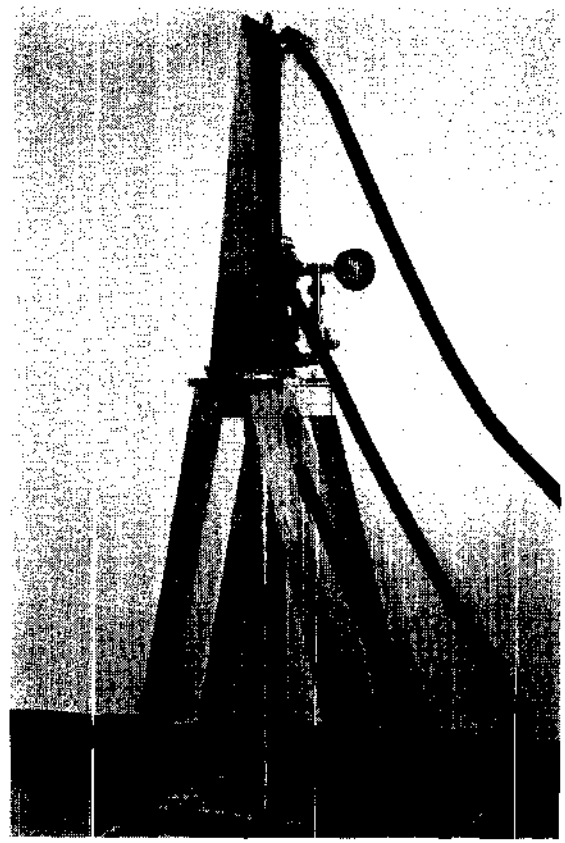

Figure 8. NTG Hydraulic Cylinder Unit

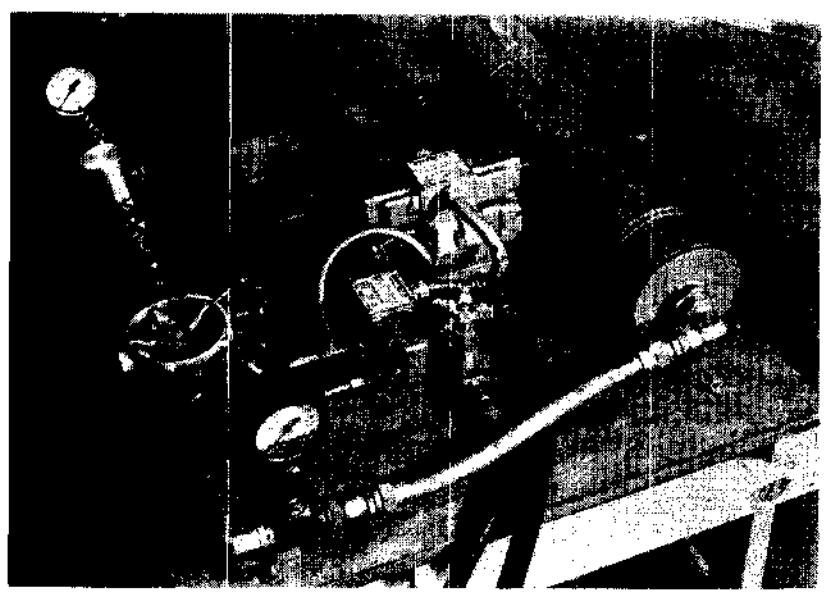

Figure 9. NTG Valve Platform

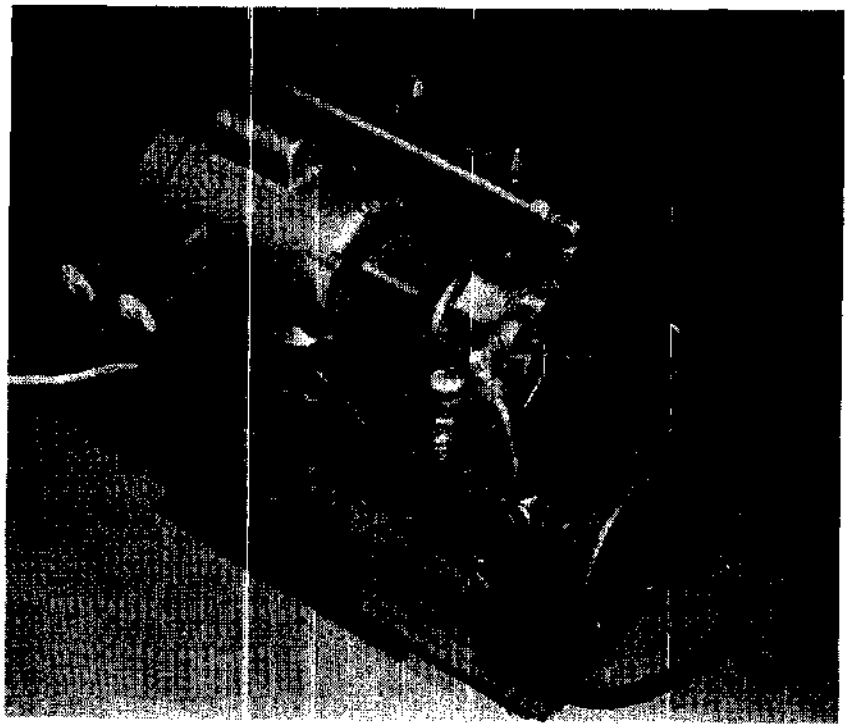

Figure 10. NTG Pump Unit

Figure 11. NTG Control and Monitoring Unit

this rate, the drive was capable of insertions of up to about 500 seconds for full travel. Withdrawal rate was preset at greater than 1,200 seconds.

The Hydraulic Drive was built to meet certain safety specifications set forth by the Atomic Energy Commission. These included redundancy of valves used to maintain the withdrawal rate and the withdrawal rate itself. Further discussion of the Hydraulic Drive operation and its specifications will be found in Appendix A.

The hydraulic cylinder piston rod was attached by way of the chain coupling to the extension rod of the Link and Instrumentation Unit discussed previously. The cylinder then bolted to the flange of the Link and Instrumentation Unit which was then securely clamped to the lead cover plate of the reactor top.

Control and Monitoring System

The four functions of the Control and Monitoring System were:

1. interlock the GTRR shim-safety blades with the experiment,
2. control the hydraulic system,
3. provide analog output to the data acquisition system on the status of the NTG, and
4. provide visual output to the operator and experimenter on the status of the NTG.

A photograph of the control and monitoring unit is shown in Figure 11. This unit was used to control the operation of the NTG experiment by the reactor operators.

The purpose of interlocking the GTRR shim-safety blades with the experiment was to preclude the possibility of starting up the reactor with

the NTG control rod. A three-position switch on the control unit was used to stop, withdraw, or insert the NTG control rod. The power to the shim blade magnetic clutches was turned off if the control unit was in a withdraw position, thus dropping the shim-safety blades into the core. In addition, the reactor can only be started up if the control rod was fully out, as indicated by a neon light on the control unit. The interlock was disabled when a key switch on the control unit was turned off, but this procedure also disabled the NTG. The GTRR shim-safety blades were always capable of being inserted.

The control unit was also used to control the hydraulic system by way of three solenoid valves on the valve platform. The three-position switch mentioned above was used to change the state of the solenoid valves and therefore the control rod. In addition, there was a switch to turn on the pump, and a switch to provide 12 vDC to power the solenoid gripper. However, 12 vDC would not cause the solenoid gripper to rotate, but would hold it without overheating once it had rotated. Thus, a momentary push-button switch was needed to supply 30 vDC to the solenoid for a short period of time to rotate the cam. A constant 30 vDC would have caused the solenoid to overheat and fail. Turning the solenoid switch off interrupted power to the solenoid and allowed uncoupling of the control rod.

Analog output to the computer data acquisition system by way of a remote monitoring unit at the computer was also provided by the control unit. A photograph of the remote monitoring unit is shown in Figure 12. The status of the experiment as determined by the microswitches of the Link and Instrumentation Unit, and also the various switches on the

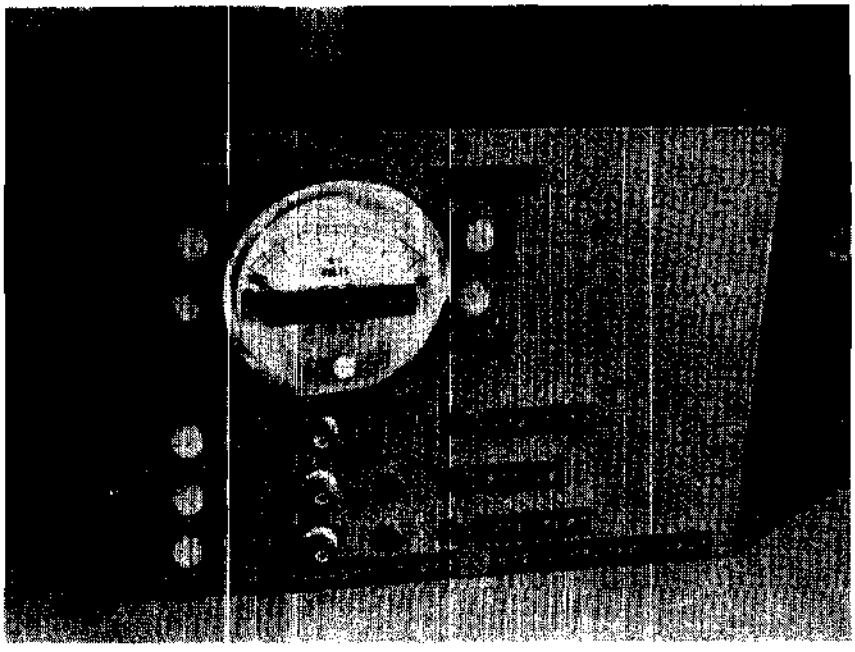

Figure 12. Remote NTG Monitoring Unit

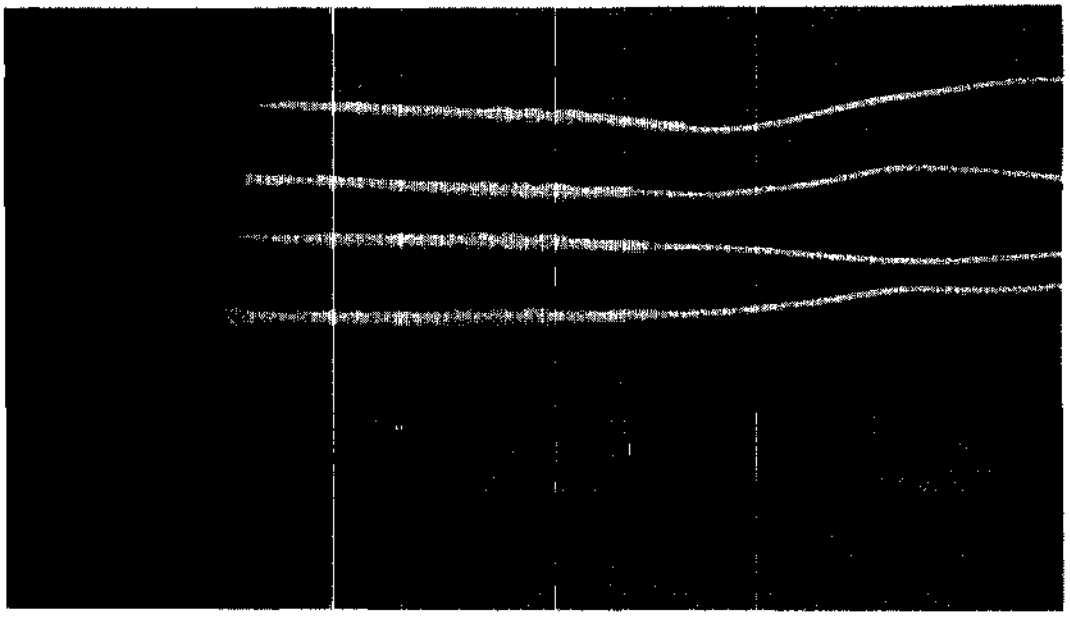

Figure 13. Miniature Boron Ionization Chambers

control unit, were encoded by an internal binary encoding circuit to yield a single unique voltage for a given state. Thus, a given switch had associated with it a certain voltage, and the sums of the various voltages gave a unique status voltage. This status voltage was then transmitted to the computer. A table of the voltage weights associated with each function of the control unit is shown in Table 1. As an example, a voltage of -6.41 volts indicates that the gripper is engaged, the rod is full out, and also stopped. The other analog information transmitted to the computer was the position of the control rod as determined by the potentiometer located on the extension rod of the Link and Instrumentation Unit. For a given position, a unique voltage between zero and -10 vDC resulted. This position voltage and the status voltage were input to the computer from two BNC jacks on the remote monitoring unit.

Table 1. Weighting Values for the Experimental Status

Function Switch	Voltage When Closed
Gripper engaged	-5.000
Full in	-2.500
Full out	-1.250
Insert	-0.620
Withdraw	-0.310
Stop	-0.160

The final function of the control unit was to provide visual output on the status of the system to the operator and experimenter. The states of the various microswitches and switches were indicated by neon lights. The voltage to the solenoid and the position of the control rod were obtained from voltage meters. The same information, except for solenoid voltage, was duplicated on the remote unit at the computer.

Nuclear Instrumentation System

When the NTG was used to shut down the GTRR the neutron flux was monitored at six different locations. Five miniature, non-gamma-compensated, boron-10 ionization chambers were used in and near the core while a gamma-compensated fission chamber (part of the GTRR instrumentation) was located in the graphite reflector. In addition, miniature, gamma-sensitive units were used on occasion to monitor the gamma background and flux.

The miniature detectors were less than 5/16 inch in diameter and two inches long. The chambers were connected to 1/8 inch diameter, coaxial cable with miniature fittings. The detectors were then covered with heat shrink tubing and sealed with epoxy so as to be usable in a water environment. The detectors were supplied by Reactor Controls, Inc., Oak Ridge, Tennessee. A photograph of the miniature, boron chambers is shown in Figure 13.

The current from the miniature detectors, which ranged from 8×10^{-9} amp to 4×10^{-4} amp in these experiments, was input to Reactor Controls, model E-908 current electrometers. These electrometers were capable of outputing a voltage of zero to +10 vDC which is linearly or

logarithmically proportional to the input current. The linear ranges were capable of measuring from 1×10^{-10} amp to 10×10^{-3} amp.

There were two logarithmic ranges which could be adjusted for different current ranges. Both logarithmic ranges were set for four decades of input current, from 4×10^{-8} amp to 4×10^{-4} amp on the high range, and from 4×10^{-9} amp to 4×10^{-5} amp on the low range. The significant kinetics data were anticipated to extend over three decades of input current, and the electrometers were thus adjusted to match this range as nearly as possible in order to maximize the data resolution. A photograph of the electrometers is shown in Figure 14.

The fission chamber was part of the GTRR flux monitoring system and consisted of a General Electric Model 5467870G11 detector connected to a General Electric Model 534E7452G3 picoammeter.

The output of both the electrometers and the picoammeter were sent, by way of coaxial cables, to the data acquisition system described later.

It was mentioned before that two tubes were placed outside the shroud of the control rod in order to provide dry locations for two detectors next to the control rod. Two other detector holders were constructed to provide access to other core locations. These two holders were essentially identical, although one was designed to fit into fuel lattice sites and therefore required a plenum plug to seal off the coolant flow. The other holder was designed to fit into core lattice extension sites in the D_2O reflector and had no plenum plug, since such sites do not have forced cooling. Each holder was a one inch diameter, dry, aluminum tube, sealed at the lower end, which was inserted along the axis

Figure 14. Current Electrometers and Power Supply

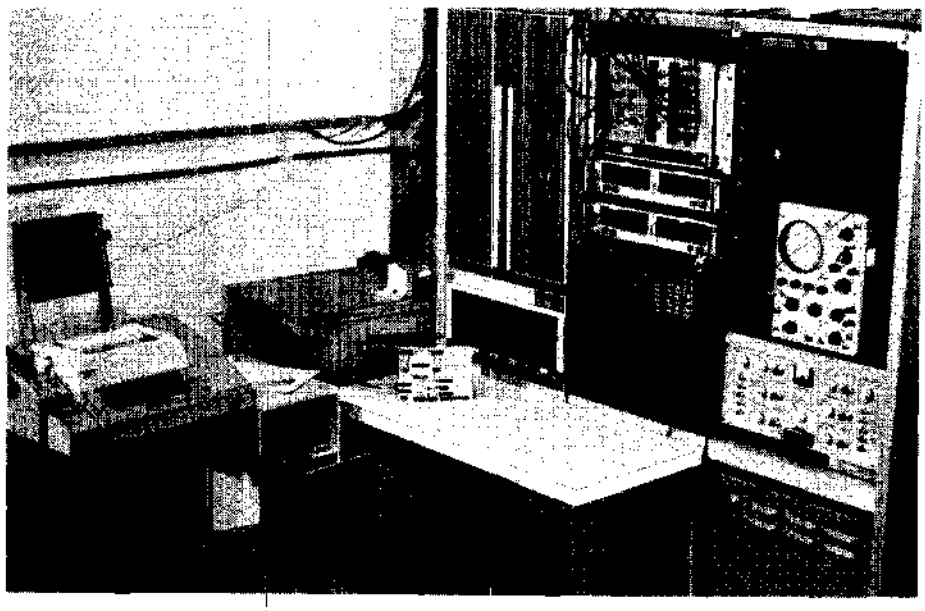

Figure 15. MASTER PDP-8 Computer with Interface

of a standard lower top shield plug. The tube was welded to a flange which was bolted to the top of the shield plug with an "O" ring to provide a helium seal. The detector holders were easily lowered, using standard GTRR procedures, into the core. The detectors were then placed in the holders and positioned at various depths throughout the core.

Data Acquisition System

The purpose of the data acquisition system was to monitor the state of the experiment, that is, the six detector voltages, the status signal, and the position of the control rod, every five milliseconds and then to record this data on magnetic tape for later analysis. The system included two Digital Equipment Corporation PDP-8 computers, a quartz crystal clock, a multiplexing sample-and-hold device, an analog-to-digital converter, a transmission line, and magnetic tape drive. Figure 16 is a block diagram of the system.

The experiment was under control of a PDP-8/I computer located on the reactor floor. This computer will be referred to as the MASTER. Another computer, a PDP-8, hereafter called the SLAVE, was connected to the MASTER by a transmission line and was located outside the containment building. Its purpose was to store data received and write it on magnetic tape on command from the MASTER.

In conjunction with the PDP-8/I was an interface unit which actually collected the data. When a comparator ascertained that the one-microsecond quartz clock had marked off five milliseconds, a signal was output to the sample-and-hold multiplexer. This electronic switching device then read, in some preset sequence, the eight signals discussed previously. Each

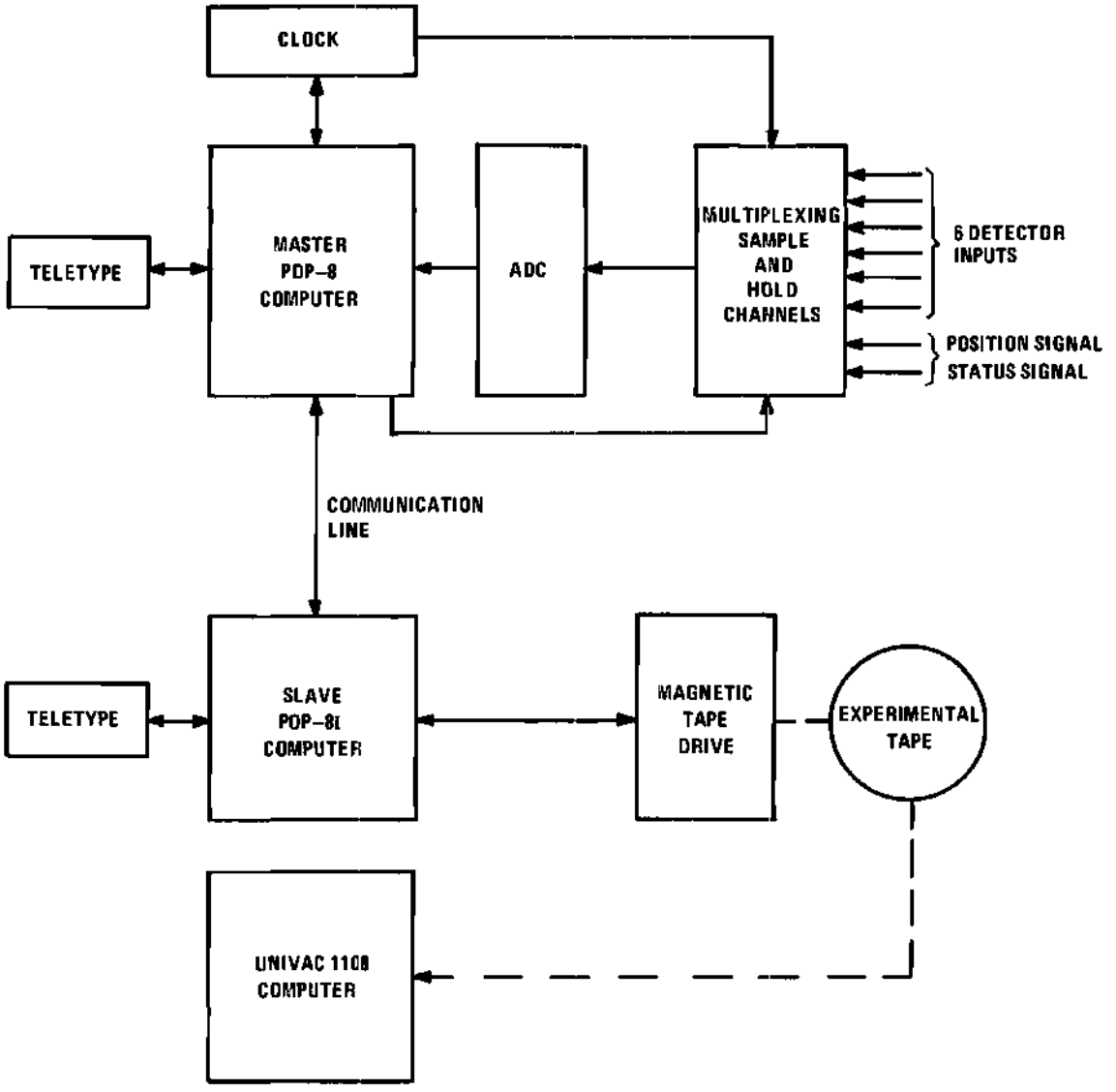

Figure 16. Block Diagram of the Data Acquisition System

signal was, in turn, input to an analog-to-digital converter (ADC) in order to digitize the voltage to some proportional number between zero and 4095.

There were three types of input to the sample-and-hold device. The six channels used for detector output could invert, bias, and amplify the signal. However, four of these did this on command and held the voltage until the ADC was ready. The other two sampled on command and immediately sent the voltage to the ADC. The third type of sample-and-hold input, used for the status and position signal, could not invert or bias the signal, but could attenuate it. These two inputs also sampled on command and sent their signal to the ADC immediately. Figure 15 is a photograph of the MASTER computer system, while Figure 17 is a photograph of the SLAVE system including the magnetic tape drive.

The output of the ADC was then sent via a high speed transmission line to the SLAVE computer, which buffered the data until it transferred it to magnetic tape on command from the MASTER. The magnetic data tape could subsequently be read on the SLAVE computer or on a Univac-1108 computer which was also available at Georgia Tech.

Further information on the computers and standard peripheral equipment is contained in reference 52.

Data Tape Format

A single magnetic tape had the capability of storing many experiments. However, a new tape was used for each day's experiments in order to minimize any data losses. The format of the tape was very simple. Each experiment was separated by an end-of-file (EOF) mark from other

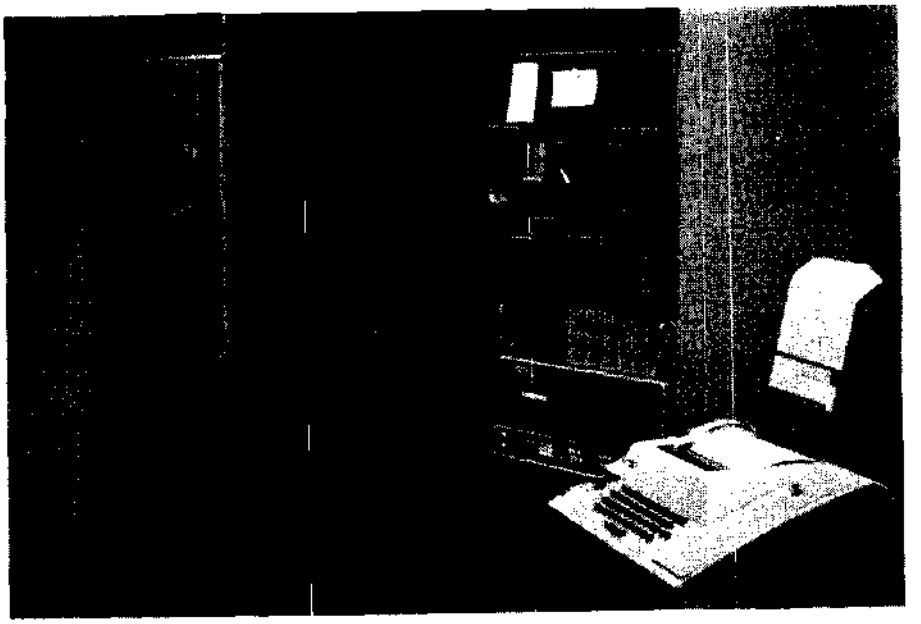

Figure 17. SLAVE PDP-8/I Computer with Magnetic Tape Drive

Figure 18. Hydraulic Cylinder Unit in Central Fuel Element Position

experiments; the PDP-8 and Univac-1108 could accurately position the tape to any EOF mark and thus to any given experiment. Between file marks were groups of data in records, or blocks. A record, or block, consisted of 1,200 words; while a single word was a 12 bit number representing a single datum point, that is, a number between zero and 4095.

A block of 1,200 words was composed of 100 sets of data. A data set consisted of the experiment identification number, a low and high precision counter which indicated the number of data sets taken since the program was initiated, the eight channels of data, and a checksum, which was the negative sum of the other 11 numbers. This checksum was used to verify that no data were lost in transmission. When 100 of these data sets were stored in the SLAVE, the MASTER instructed it to transfer the data to the tape and write an end-of-record mark. At the end of the experiment an EOF mark was written. A new experiment could then be written on the tape.

Data Acquisition Software

Two programs were necessary for the experiment. One ran on the MASTER computer while the other ran on the SLAVE. Both programs were written in Program Assembly Language (PAL) described in reference 53. Figures 19 and 20 are flow charts of the MASTER and SLAVE programs, respectively.

The MASTER program had a preset data acquisition interval of five milliseconds. When initiated, the experiment identification number was input from the teletype. In addition, an experiment description could be typed on the teletype, but this information was not written on the data

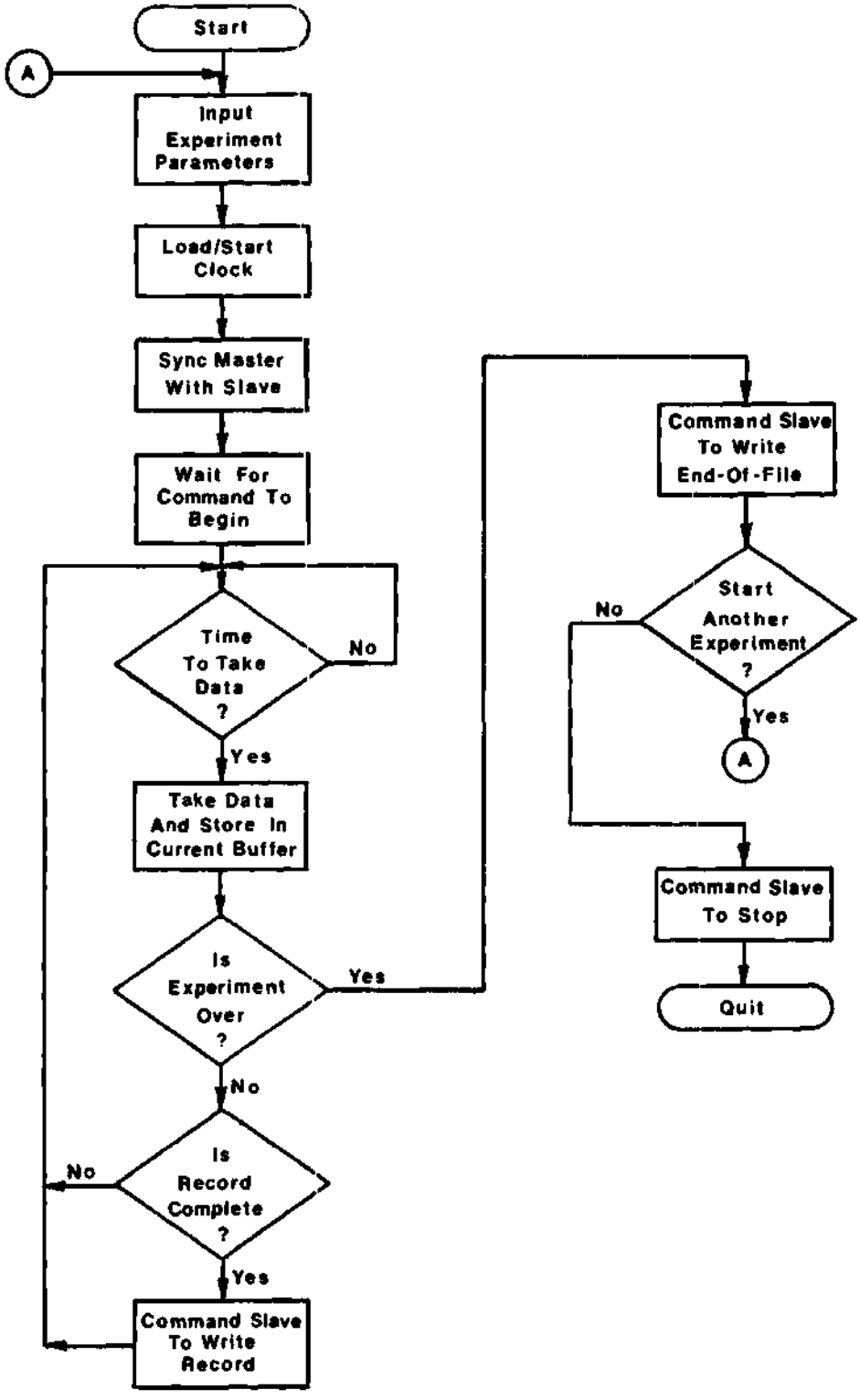

Figure 19. Flow Chart of the MASTER Program

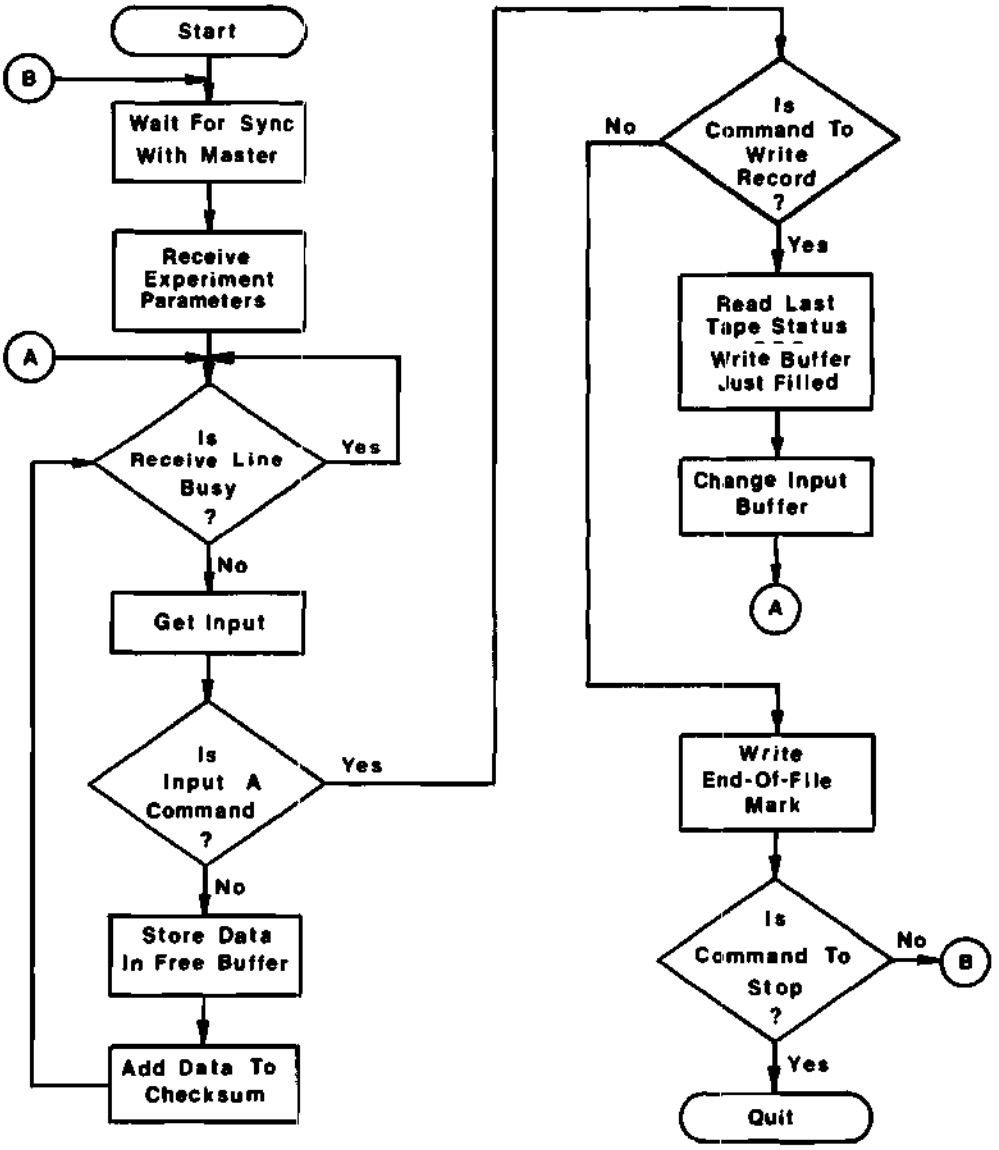

Figure 20. Flow Chart of the SLAVE Program

tape. Upon close of the description, a verification of the computer interface operation was typed. At this point the actual data acquisition was started by loading the computer switch register with a zero. The data were then taken and transmitted to the SLAVE at the specified rate. When a block was filled, the MASTER instructed the SLAVE to write the block. At the end of the experiment the operator loaded a one into the computer switch register; data acquisition ceased, and an EOF mark was written. By changing the switch register again another experiment could be written or the SLAVE computer halted.

CHAPTER III

EXPERIMENTAL PROCEDURES AND RESULTS

Kinetics experiments were undertaken on the GTRR in two, one-week increments with two weeks intervening. Various core configurations and detector positions were investigated. The procedures used in those experiments and representative results will be covered in this chapter.

Reactor Core Configurations

As mentioned previously, the GTRR core has 19 fuel element locations, but in the present experiments only 17- and 18-element configurations were investigated. In all experiments the NTG Control Rod Assembly was inserted into V-10, the central fuel position. As discussed previously, this research concerned only two-dimensional models, and it was necessary to use the NTG rather than the GTRR shim-safety blades to generate two-dimensional transients. With the NTG inserted in the central position there was only axial and radial spatial dependence.

The 18-element configuration was investigated first. Detectors were located in the V-10 location and also in a detector holder in the core lattice extension site, V-23, located in the D_2O reflector. A 17-element configuration was also studied with detectors loaded into a detector holder located in V-18. Figure 21 illustrates the relative locations of the various vertical positions described.

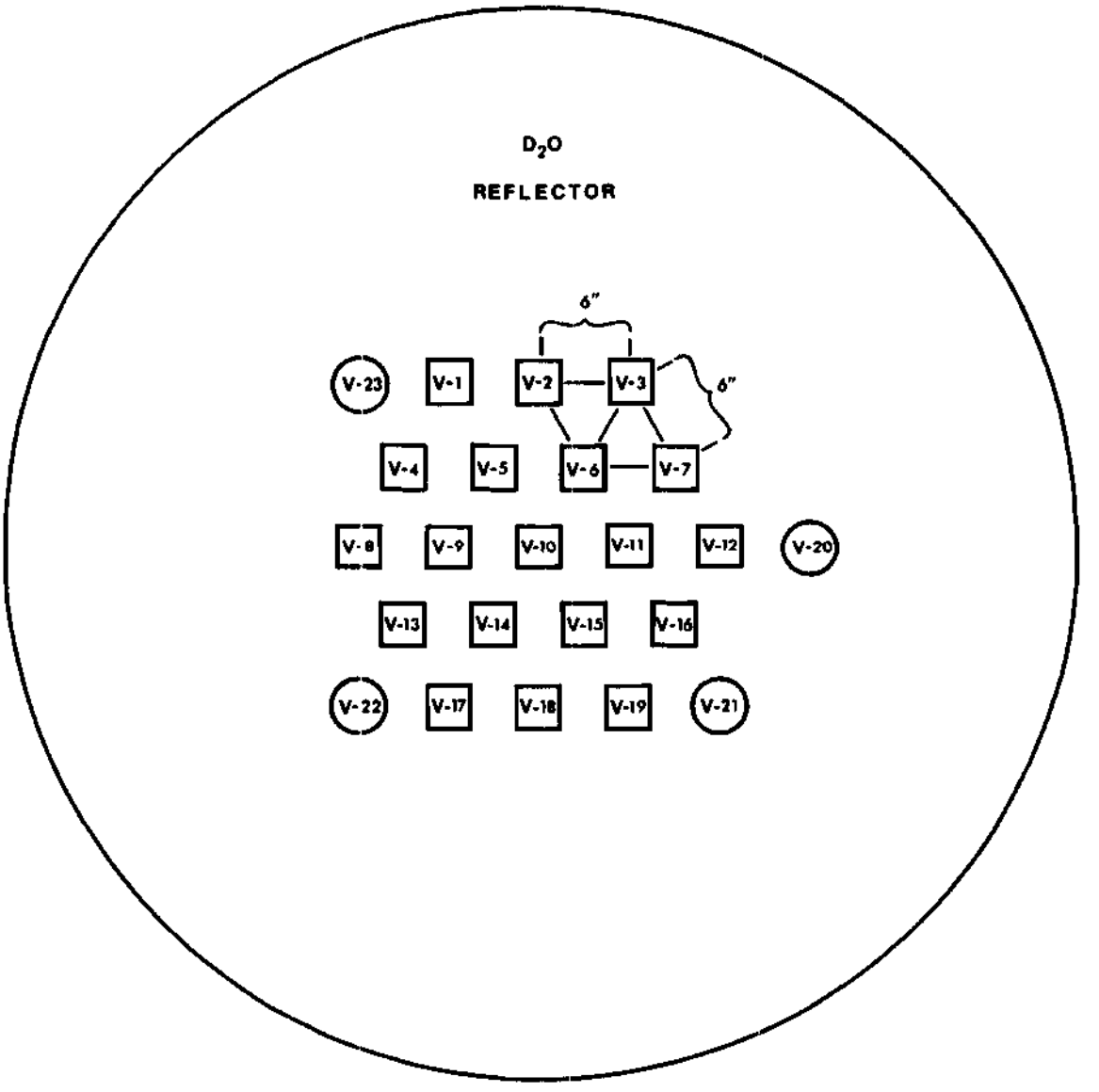

KEY

V-1 Through V-19 Fuel Element Positions

V-20 Through V-23 Core Lattice Extension Sites

V-10 Location Of NTG And Detectors 1 And 2

V-23 Location Of Detectors 3 And 4

Figure 21. Location of GTRR Vertical Access Positions

Since the GTRR core was near end-of-life, the shim-safety blades were banked at approximately 26° for the 18-element core and at approximately 35° for the 17-element core. In both these positions the blades have less than two percent $\Delta k/k$ available. Thus, the flux shape is essentially unperturbed by the shim-safety blade positions.

Since feedback effects were not to be considered in the analytical model, the power level was kept fairly low. Maximum cooling flow was also desirable in order to further minimize temperature effects. Therefore, a power level of 50 kilowatts was chosen to minimize feedback and temperature effects, and also because the detection system operated in a linear fashion up to this power level. However, this power was sufficiently high to observe significant transient effects over nearly three decades. The detection system was therefore adjusted to respond over four decades to closely match the expected range of transient effects so as to obtain maximum resolution.

Experiment Preparation

The preparation of the experiment was relatively complicated due to the necessity of combining into a single experimental system two computers, eight data channels, the NTG system, the reactor, and the reactor control system. Therefore, experimental preparation generally required a full day.

Prior to the actual equipment setup, the fuel was rearranged in the reactor to provide the necessary penetrations to the core. After inserting the detector holders and the NTG Control Rod Assembly, the detectors were loaded into position. Two sheets of heavy-gauge polyethylene

were then laid over a square wooden frame, ten feet long on a side, on the reactor top. The purpose of the plastic and wooden frame was to insure that no oil from a leak in the hydraulic system could enter the core tank and contaminate the heavy water.

The Link and Instrumentation Unit bolted to the hydraulic cylinder was then inserted through the plastic into V-10. The unit was bolted to the reactor face, and the plastic securely sealed with masking tape. The valve platform was located nearby on a wooden stand with the hydraulic pump unit located off the reactor top. A wooden platform was provided on the reactor top to allow temporary storage of the assembled hydraulic cylinder and Link and Instrumentation Unit while fuel was rearranged, or for adjustments of instrumentation. Figure 18 shows the hydraulic cylinder in place with the plastic protective covering.

Following the placement of the NTG, the control unit was placed in the control room. The unit was then connected to the interlocking circuitry, the hydraulic pump unit, the hydraulic cylinder, and the remote monitoring unit located at the computer.

The detectors were connected to the electrometers whose output was then fed into the computer sample-and-hold unit. Power to all units, with the exception of the hydraulic pump unit, was provided from the computer supply in order to eliminate the ground loops common to such extended electrical systems.

With the connecting of the transmission line between computers, the equipment was ready for calibrations and final adjustments.

Experimental Procedures

For each of the core configurations employed it was necessary to obtain axial flux shapes, for each of the vertical positions used, following experimental preparation. This procedure consisted of placing one of the detectors in each vertical experimental position at the core mid-plane. The other detector was then traversed through the core in three inch increments while reading both detector currents simultaneously from the electrometers with digital voltmeters. These values were then normalized to the detector at the core mid-plane. This procedure was also utilized with gamma detectors to obtain axial gamma distributions. The procedure was first performed with the NTG control rod fully withdrawn and the GTRR critical at 50 kilowatts. The procedure was next repeated for the NTG control rod 50 percent and then 100 percent inserted. In these situations it was not desirable (and not possible due to the interlock) to use the GTRR shim-safety blades to maintain criticality as this would have perturbed the flux shapes. All readings were made after the prompt drop to insure that the neutron distribution was stable, although decreasing in magnitude. The detector at the core mid-plane provided the normalization for all traversals.

At the start of each day's experiments all equipment was turned on and examined for any obvious malfunctions. The GTRR cooling system was adjusted to give maximum cooling, and the NTG control rod was withdrawn from the core. The detectors were then positioned at the core mid-plane in preparation for the calibration procedure.

The calibration procedure allowed a given digital output number

from the computer to be associated with a detector current reading and, hence, to the reactor power from known electrometer behavior and reactor power instrumentation. Prior to the power calibration it was necessary for each data channel to have its input amplified and/or biased so the expected input range of data signals would be within the zero to 4095 output capability of the analog-to-digital converter.

The signals used during this part of the calibration were produced from a constant current source within the electrometers. Thus, by changing the linear current scales, output to the ADC of 0.0, 0.1, 1.0, and 10.0 volts could be obtained. After biasing and/or amplification, samples were taken at the experimental data acquisition interval of five milliseconds on each data channel, for each test voltage. This provided a calibration of the logarithm of detector current versus ADC output. The electrometers were capable of very accurately producing the logarithm of a given current.

Once this procedure was completed the reactor power was increased in a series of steps to 50 kilowatts. At each step the power was maintained as steady as possible, and the data acquisition system was then used to obtain digital output proportional to both the linear detector signal and its logarithm. This was done for each pair of detectors in the core. The linear signal was later used to calculate the power associated with the logarithmic signal for a given detector. Table 2 represents the ADC output for the various test voltages for neutron data channel one for June 8, 1971. The results of a linear least squares fit are also shown. A plot of a typical reactor power versus ADC output

calibration curve for the same date and channel is shown in Figure 22.

Table 2. Results of Test Voltage Calibration of Channel One for June 8, 1971

Test Voltage	ADC Value	Least Squares Fit
0.0	48	48.27
0.1	88	88.75
1.0	453	451.69
10.0	4081	4081.12

After the calibration was completed, the reactor was placed on automatic control, and the 50 kilowatt level maintained for at least 1,800 seconds. This allowed all shorter-lived delayed neutron precursors to build to saturation. The longer-lived groups, notably the photoneutron groups typical of a heavy water moderated reactor, were not fully saturated, but this was not significant for the fast transients studied.

During the buildup time, the electrometers and computers were prepared and the detectors positioned. During most experiments there were two detectors in each vertical position. One was always left at the core mid-plane, while the other was positioned above or below the mid-plane at some integral number of three inch increments.

When the buildup time was nearly complete, the pump unit was turned on with the control unit in a "stop" mode. Proper system pressure was verified, and notations of experiment I.D., insertion time, valve settings, shim blade positions, core temperatures, buildup time, detector locations and readings, and scale settings were made on a pre-prepared experiment log sheet. The automatic control system was turned off, and the

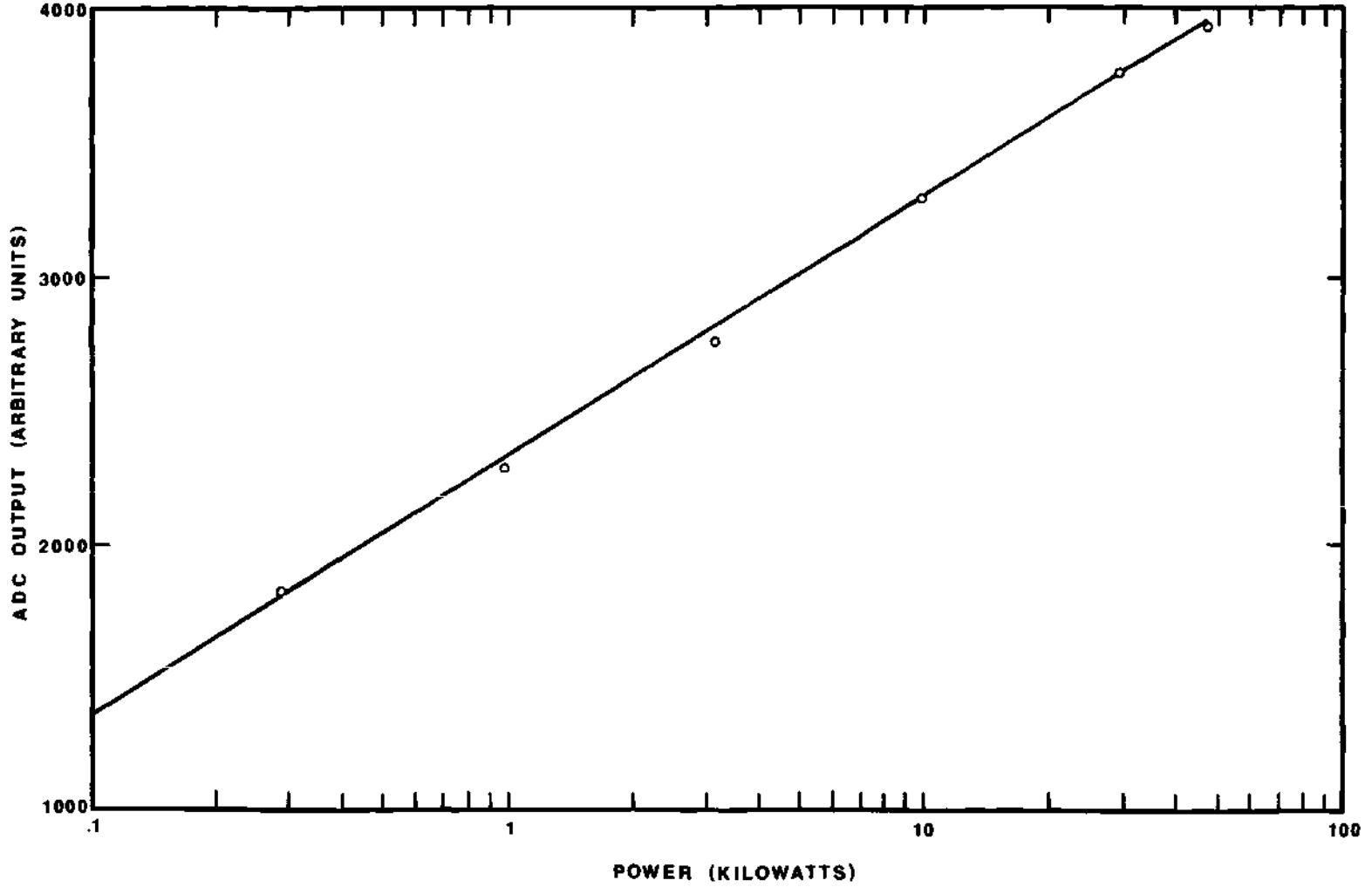

Figure 22. Reactor Power Versus ADC Digital Output for Channel One for June 8, 1971

experimenter then sat at the MASTER computer and started the data acquisition system by changing a sense switch. Approximately two seconds later, on a voice command to the reactor operator, the control unit switch was turned to "down," which sent the NTG rod into the core. Data were taken until reactor power fell below 100 watts, a power below which no significant fast transient effects occurred. At this point, the shim blades were dropped into the core and the computer stopped. The experimenter determined whether to run another experiment or stop for the day, and signaled the computer accordingly. If another experiment were to be run the withdrawal of the NTG control rod was then initiated.

Data Reduction

Three programs were written for handling the experimental data recorded on the magnetic tape. The first was written in FOCAL[52] and ran on the SLAVE computer. This program sampled the data and checked for possible errors in transmission from the MASTER computer. The program was run at the end of the day, and the output was typed on the teletype for a record of the day's experiments. This enabled the experimenter to ascertain if the experimental system had run properly.

A second program was written in FORTRAN-V for the Univac-1108. This program combined several days' experimental tapes onto one tape.

The final program was written in FORTRAN-V, also, for the Univac-1108. This program analyzed the kinetics data, using the calibration data, to provide the average detector current and reactor power along with the detector current for each detector. The time from the start of insertion of the control rod, rod position, and the ADC value associated

with each data channel were also printed out. Finally, the fractional change in current for each detector and the ratio of all fractional changes to all others were output. The program could average over any number of data sets and scan different intervals of the data. In general, averages were taken over ten data sets, or 50 milliseconds, in order to eliminate a small 60 cycle oscillation noted in the data. The oscillation caused less than a 0.5 percent change in the flux level.

Results

The plots of the axial neutron flux for V-10 and V-23 are shown in Figures 23 and 24. Note that the axial scale represents the distance below the reactor top, the reference point used in the experimental measurements. On this scale the core mid-plane (the normalization point) is located at 12 feet, while the top of the heavy water reflector is around nine feet. No data is presented below the core mid-plane in Figure 24 since the detector holder for that position did not extend into that region.

Note that the shape in V-10 in Figure 23 with the NTG rod full out did not appreciably differ from that with the NTG rod full in. However, with the rod 50 percent inserted there was a pronounced skewing of the shape toward the bottom of the reactor due to the presence of the strongly absorbing rod in the upper half of the core.

During the course of the experiments two runs were made with a 17-element core configuration, and with insertion times and detector positions similar to those of Weaver's[49] experiments on the GTRR. This was done to check the reproducibility of the experiments and to give an

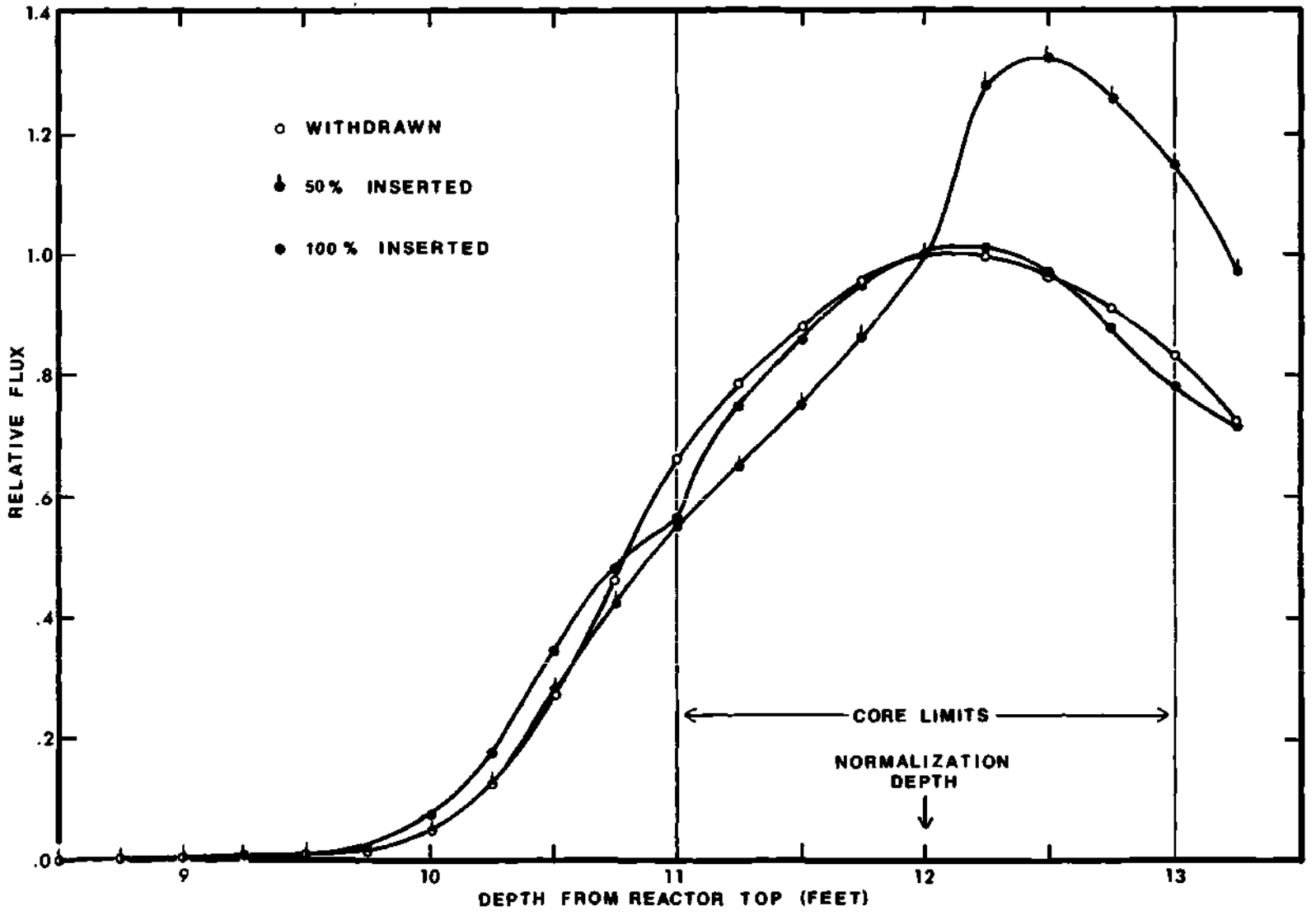

Figure 23. Experimental Axial Flux Distribution for V-10

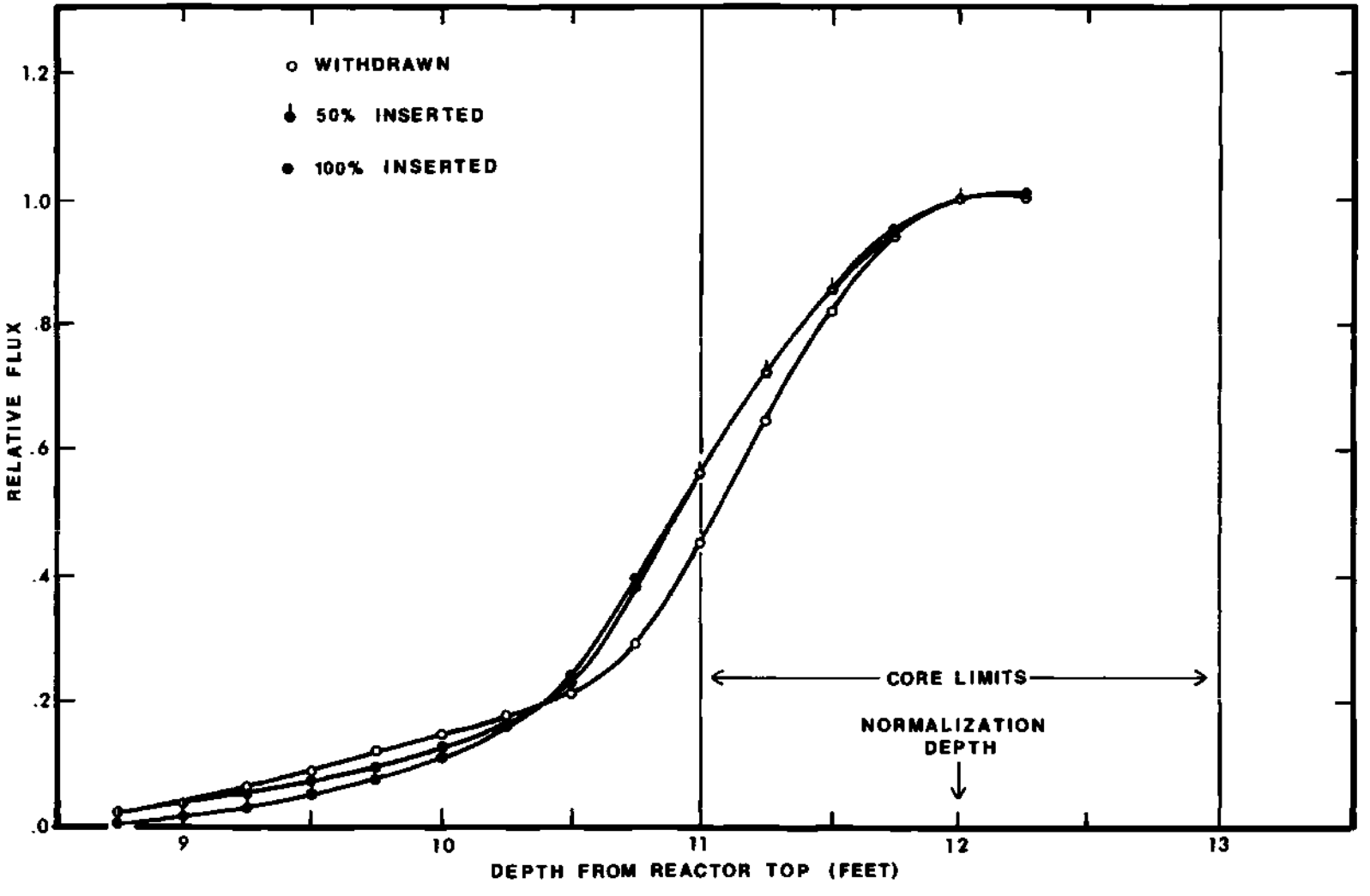

Figure 24. Experimental Axial Flux Distribution for V-23

indication of any significant nuclear changes in the reactor. Analysis of the detector positioned nine inches above the core mid-plane, for Weaver's 2.2 second experiment and a present experiment with very nearly the same insertion time, shows the two runs to be essentially identical. They differed by less than five percent in magnitude throughout most of the experiment. At one point where the rate of change in power was most rapid, the difference momentarily reached nine percent, but was within the accuracy to which the flux could be measured. The accuracy of the experiments will be discussed later. Other detector positions yield similar results for both runs.

It was not possible to obtain experimental measurements of the radial distribution of the flux. However, the ratio of the flux in V-23 to that in V-10 provides an indication of this distribution. The ratios are presented in Table 3 for the NTG rod withdrawn and 100 percent inserted.

Table 3. Radial Flux at the Core Mid-Plane

	Flux Relative to V-10	
Configuration	V-10	V-23
NTG Rod Withdrawn	1.00 ± .02	0.52 ± .02
NTG Rod 100% Inserted	1.00 ± .03	0.89 ± .05

Figure 25 shows the fractional change in detector current, or relative flux, versus time for the detectors in V-10 and V-23. The experiment

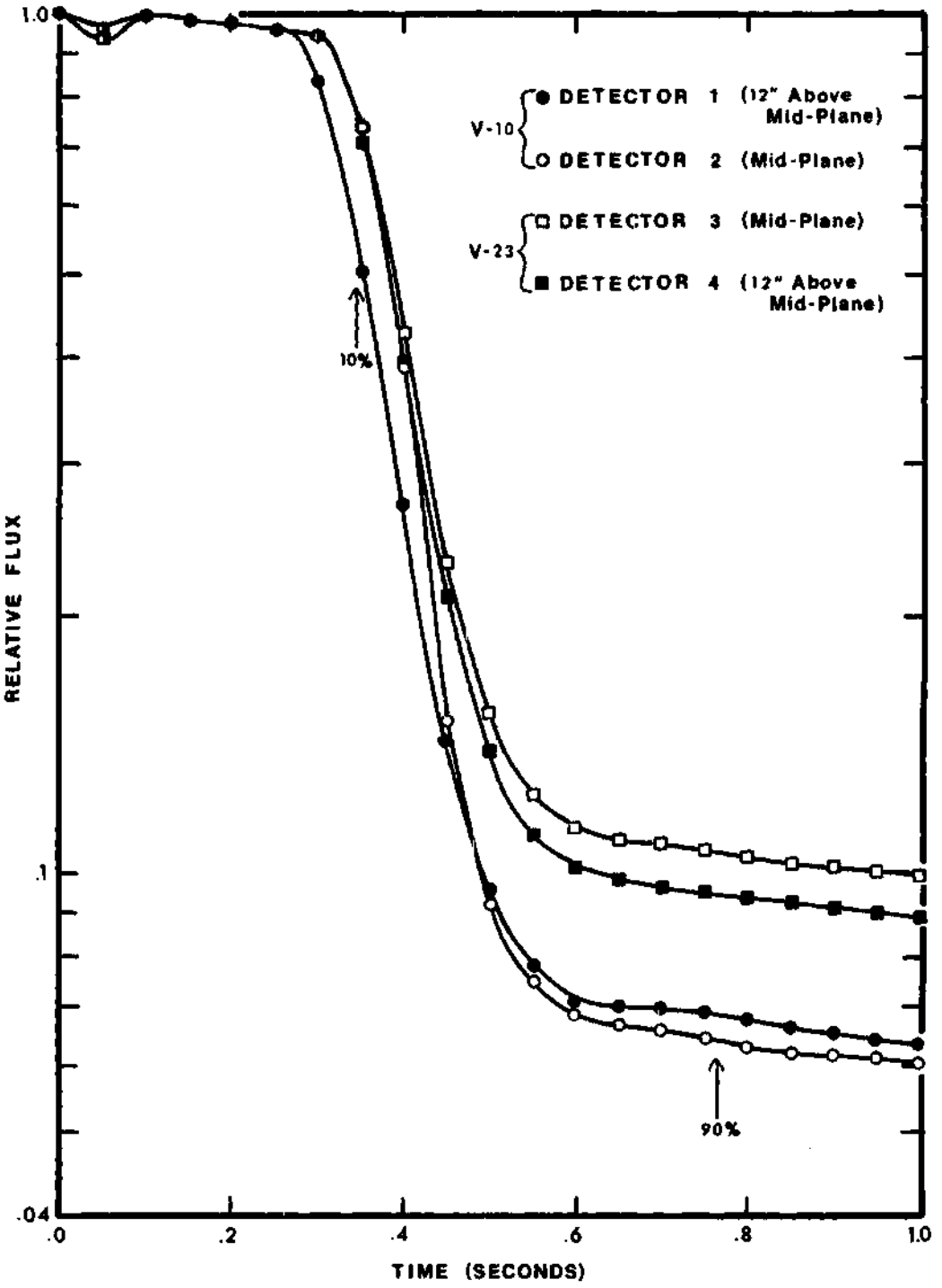

Figure 25. Results of Experiment 202

represented in number 202, which inserted the rod as fast as possible, 1.35 seconds for the full 30 inches of travel, and 0.422 second from 10 percent inserted to 90 percent inserted. The results shown are typical of the other experiments.

In Figure 25, the detectors in V-10, that is, detectors 1 and 2, demonstrate typical spatial effects. The drop in neutron population created by the NTG rod being inserted is first noted by detector 1. This detector is located 12 inches above the core mid-plane and is nearer to the rod. Detector 2, located at the mid-plane, does not significantly detect this drop in magnitude until several milliseconds later when the rod is further inserted. The relative fluxes then converge to the same value, cross over, and then diverge. The fact that the ratio of the relative flux for both detectors is not constant is indicative of the spatial dependence of the flux.

After the rod is fully inserted, the two detectors respond to the asymptotic decay in the flux with the same period. The relative flux is now determined by the axial flux shape. The detectors in V-23 also illustrate similar spatial dependence, but to a lesser degree since they are farther from the perturbing rod.

Tabular results of the fractional changes in detector current, or relative flux, versus time and rod position of the eight experiments performed on the 18-element GTRR core are given in Appendix B. Appendix B also presents the power history of the GTRR and other experimental parameters on the days of the experiments, and a discussion of the errors associated with the experimental system.

Table 4 presents a summary of the eight experiments in order of increasing insertion times. In all experiments two detectors were placed at the core mid-plane for each position. Thus, only the data for these two detectors is presented for comparison. The times noted are differences and not elapsed times since the delay in initiating rod movement was not constant.

Table 4. Fractional Changes and Partial Times of Experiments for Various Percentages of Rod Insertion

Experiment I. D.	Fractional Change (V-10 Core Mid-Plane) 10%	50%	90%	Fractional Change (V-23 Core Mid-Plane) 10%	50%	90%	Time for 10% to 50% Insertion (Seconds)	Time for 10% to 90% Insertion (Seconds)
101	.48331	.08067	.06166	.70292	.13847	.10339	.195	0.411
202	.77714	.08789	.06378	.77461	.14691	.10577	.177	0.422
103	.75660	.08221	.06045	.75885	.14335	.10525	.191	0.439
204	.82871	.08888	.06369	.82687	.14696	.10473	.178	0.446
203	.84360	.10707	.05595	.83352	.16830	.09287	.527	1.149
205	.91331	.10963	.05629	.90275	.17017	.09364	.606	1.190
102	.81256	.09873	.04896	.83895	.16850	.09019	.638	1.334
201	.80116	.11004	.05369	.78934	.17038	.08878	.720	1.527

CHAPTER IV

SPATIALLY DEPENDENT KINETICS ANALYTICAL METHODS

A detailed presentation and development of both the space-time and adiabatic equations, in two-dimensional, cylindrical geometry, solved by the multigroup, kinetics analysis program KINET is given by Weaver.[49] The assumptions used, handling of boundary conditions, and the development and testing of the program are also discussed. The purpose of this chapter, therefore, will not be to redevelop those equations, but to provide an illustrative presentation of the space-time or standard method and the adiabatic approximation. This should be useful in considering the limitations and relationships involved in the methods, along with the comparisons of experimental data with the space-time and adiabatic simulations in the following chapter.

Space-Time or Standard Methods

Space-time or standard methods commonly refer to application of approximate, finite-difference techniques to multigroup, multi-dimensional diffusion theory. They are also called "exact" methods on occasion, but this will be seen to be an inaccurate description. For such methods, spatially and temporally continuous equations which represent neutron behavior, within the limitations of diffusion theory, are discretized with respect to space and time and solved by digital computers. The method of discretization involves assumptions and approximations resulting in a

large set of coupled equations which must be solved iteratively.

In addition to the error introduced by discretization, there is also error associated with the approximations necessary to account for the behavior of delayed neutrons. Machine errors, such as the accumulation of truncation errors, further worsen the situation, as do problems of solution stability and convergence. Even diffusion theory has recently been questioned as to its accuracy for space-dependent kinetics calculations.[54] Thus, in the end, it is obvious that the many sources of error in this approach lead to a result which is far from "exact." However, the method is most often the one chosen as a standard of comparison.

As an illustrative example of the technique, the finite-difference approach will be applied to develop the one-dimensional, multigroup kinetics equations. In this development, the essential details of the approach will not be overshadowed by mathematical minutiae.

Consider first, the one-dimensional, multigroup diffusion equation for the g^{th} energy group,

$$\frac{1}{V_g}\frac{\partial \phi_g(x,t)}{\partial t} = D_g(x,t)\frac{\partial^2 \phi_g(x,t)}{\partial x^2} - \Sigma_{ag}(x,t)\phi_g(x,t) \qquad (1)$$

$$+ \sum_{\substack{g'=1 \\ g'\neq g}}^{G} \Sigma_{g'g}(x,t)\phi_{g'}(x,t) - D_g(x,t)B_g(x,t)^2\phi_g(x,t)$$

$$+ \chi_g \frac{(1-\beta)}{k} \sum_{g'=1}^{G} \nu\Sigma_{fg'}(x,t)\phi_{g'}(x,t) + \sum_{i=1}^{I} f_{ig}\,\lambda_i\,C_i(x,t),$$

with the time rate of change of the precursors represented as

$$\frac{\partial C_i(x,t)}{\partial t} = \frac{\beta_i}{k} \sum_{g'=1}^{G} \nu\Sigma_{fg'}(x,t)\phi_{g'}(x,t) - \lambda_i C_i(x,t) \qquad (2)$$

The definitions of the parameters follow:

V_g is the group neutron velocity,

$\phi_g(x,t)$ is the neutron flux at position x and time t, for energy group g,

$D_g(x,t)$ is the diffusion coefficient for group g,

$\Sigma_{ag}(x,t)$ is the absorption cross section,

G is the total number of neutron energy groups,

$\Sigma_{g'g}(x,t)$ is the scattering cross section from group g' to group g,

$B_g(x,t)^2$ is the buckling for group g,

χ_g is the fraction of neutrons born of fission into group g (assumed independent of the energy of the neutron causing the fission),

β is the delayed neutron fraction (assumed constant),

k is an eigenvalue introduced for mathematical convenience,

$\nu\Sigma_{fg'}(x,t)$ is the fission cross section for group g',

I is the total number of delayed neutron groups,

f_{ig} is the fraction of delayed neutrons born in group g from delayed neutron group i,

λ_i is the decay constant for delayed neutron group i (assumed constant),

$C_i(x,t)$ is the concentration of the delayed neutron precursors at position x and time t, and

β_i is the delayed neutron fraction for the i^{th} delayed group (assumed constant).

Note that the derivation also assumes no external neutron sources.

In the subsequent discussion, the dependence on position and time of the various parameters listed above will not be explicitly noted in order to simplify the notation.

Now defining

$$\tau_{g'g} \equiv \Sigma_{ag} + D_g B_g^2 - \Sigma_{g'g}$$

as the total removal cross section, equation 1 can be simplified to

$$\frac{1}{V_g}\frac{\partial \phi_g}{\partial t} = D_g \frac{\partial^2 \phi_g}{\partial x^2} - \sum_{g'=1}^{G} \tau_{g'g}\phi_{g'} \qquad (3)$$

$$+ \chi_g \frac{(1-\beta)}{k} \sum_{g'=1}^{G} \nu\Sigma_{fg'}\phi_{g'} + \sum_{i=1}^{I} f_{ig}\lambda_i C_i .$$

Equation 3 is simply a neutron balance equation for the g^{th} energy group at some position x and time t. The term on the left represents the time rate of change of the neutron population. The first term on the right represents the leakage, the second is the total removal term, while the third and last terms represent production sources due to fission and delayed neutrons, respectively.

Figure 26 represents the one-dimensional grid over which the continuous equations will be integrated to yield an approximate set of coupled equations, G+I equations for each gridpoint. The n^{th} gridpoint will be represented as x_n, and ϕ_g^n will be the flux at that point. The distance between point x_n to x_{n+1} is h_n, and the gridpoints need not be equally spaced. The flux is considered constant over each half-interval to the

left and right of a gridpoint, and the nuclear properties are considered constant between gridpoints. It is important to note that in finite-difference methods the flux is calculated only at the gridpoints. The boundary conditions at either end are zero flux or zero slope.

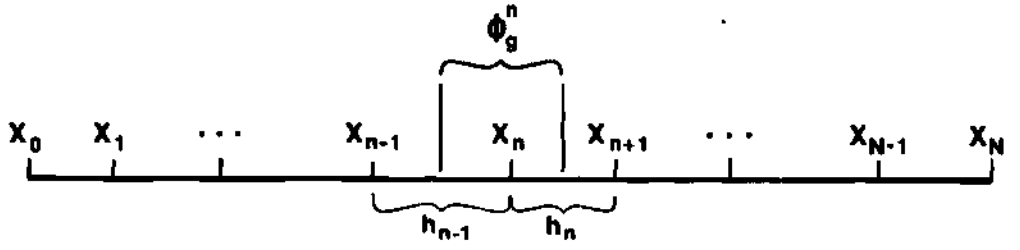

Figure 26. One-Dimensional Grid with Interval of Integration

Equation 3 will now be integrated, with respect to x, from point $x^- = x_n - (h_{n-1}/2)$ to point $x^+ = x_n + (h_n/2)$. This integration can be thought of as combining the infinite number of equations for each point on the interval into one, weighted equation valid only at the single gridpoint. Consider integration of the total removal cross section term as typical of all terms of the type $\Sigma(x,t)F(x,t)$; the approximation to the integral will then be a weighted sum of terms,

$$\int_{x_n^-}^{x_n^+} \tau_{g'g}^n \phi_g^n, \, dx = \left(\frac{h_{n-1}}{2} \tau_{g'g}^{n-1} + \frac{h_n}{2} \tau_{g'g}^n\right)\phi_{g'}^n \, .$$

All similar terms will be represented in this fashion. The leakage term presents a different situation due to its second derivative. First, represent the integral of the leakage as the weighted sum of each half-

interval,

$$\int_{x_n^-}^{x_n^+} D_g^n \frac{\partial^2 \phi_g}{\partial x^2}\, dx = \frac{h_{n-1}}{2} D_g^{n-1} \left(\frac{\partial^2 \phi_g^n}{\partial x^2}\right) + \frac{h_n}{2} D_g^n \left(\frac{\partial^2 \phi_g^n}{\partial x^2}\right). \tag{4}$$

As an approximation for the second derivatives, consider the Taylor series expansions[23] for ϕ_g^{n-1} and ϕ_g^n. That is,

$$\phi_g^{n-1} = \phi_g^n - (h_{n-1}) \frac{\partial \phi_g^n}{\partial x} + \frac{(h_{n-1})^2}{2} \frac{\partial^2 \phi_g^n}{\partial x^2}$$

and

$$\phi_g^{n+1} = \phi_g^n + (h_n) \frac{\partial \phi_g^n}{\partial x} + \frac{(h_n)^2}{2} \frac{\partial^2 \phi_g^n}{\partial x^2}.$$

Combining the equations will yield an identity with one side being equal to the right-hand side of equation 4. Applying this result to equation 4 allows the integral of the leakage term to be approximated by

$$\int_{x_n^-}^{x_n^+} D_g^n \frac{\partial^2 \phi_g^n}{\partial x^2}\, dx = \left(\frac{D_g^{n-1}}{h_{n-1}}\right)\phi_g^{n-1} + \left(\frac{D_g^n}{h_n}\right)\phi_g^{n+1} - \left(\frac{D_g^{n-1}}{h_{n-1}} + \frac{D_g^n}{h_n}\right)\phi_g^n.$$

The integral of equation 3 is now represented by

$$\frac{1}{V_g}\left(\frac{h_{n-1}}{2} + \frac{h_n}{2}\right)\frac{\partial \phi_g^n}{\partial t} = \left(\frac{D_g^{n-1}}{h_{n-1}}\right)\phi_g^{n-1} + \left(\frac{D_g^n}{h_n}\right)\phi_g^{n+1} - \left(\frac{D_g^{n-1}}{h_{n-1}} + \frac{D_g^n}{h_n}\right)\phi_g^n \tag{5}$$

$$- \sum_{g'=1}^{G} \left(\frac{h_{n-1}}{2} \tau_{g'g}^{n-1} + \frac{h_n}{2} \tau_{g'g}^n\right)\phi_{g'}^n + \chi_g \frac{(1-\beta)}{k} \sum_{g'=1}^{G}$$

$$\times \left(\frac{h_{n-1}}{2} \nu\Sigma_{fg'}^{n-1} + \frac{h_n}{2} \nu\Sigma_{fg'}^n\right)\phi_{g'}^n + \sum_{i=1}^{I} f_{ig} \lambda_i \left(\frac{h_{n-1}}{2} + \frac{h_n}{2}\right) C_i^n.$$

Integration of the precursor equation is carried out in like fashion to yield

$$\left(\frac{h_{n-1}}{2} + \frac{h_n}{2}\right) \frac{\partial C_i^n}{\partial t} = \frac{\beta_i}{k} \sum_{g'=1}^{G} \left(\frac{h_{n-1}}{2} \nu\Sigma_{fg'}^{n-1} + \frac{h_n}{2} \nu\Sigma_{fg'}^{n}\right)\phi_{g'}^{n} \qquad (6)$$

$$- \lambda_i \left(\frac{h_{n-1}}{2} + \frac{h_n}{2}\right) C_i^n.$$

The development to this point has taken the diffusion equation, which is continuous in time and space, and created a set of equations, still continuous in time, but now discontinuous in space. Thus, for N gridpoints, the original G+I continuous, coupled equations are now represented by (G+I) X N spatially discontinuous, but still coupled, differential equations.

A method for solving the time dependence of this large set of equations must now be undertaken, and finite-difference[23] schemes are most common. A simple finite-difference approach is to use the first order slope over the time interval as an approximation to the time derivative. Theta weighting will also be used to allow later flexibility in choosing a method, ranging from fully explicit to fully implicit, of solving for the time dependence. Theta-weighting assigns one method a weight of θ and the other a weight of $(1-\theta)$, and then combines both weighted methods into a single general equation. The choice of θ then allows flexibility in the choice of methods or combination of methods.

The explicit method (also known as the Euler method) solves the equation for the flux at some future time H using only terms known for the

present time 0. The general equation, assuming a time step of Δt, is

$$ {}^{H}\phi_g = {}^{O}\phi_g + \Delta t \; f({}^{O}\phi_g, {}^{O}C_i). $$

Implicit methods of solution have the general form

$$ {}^{H}\phi_g = {}^{O}\phi_g + \Delta t \; f({}^{H}\phi_g, {}^{H}C_i). $$

This type of solution requires that all fluxes at the future time be solved for simultaneously.

Let the time derivative in equation 5 be represented as

$$ \frac{\partial \phi_g^n}{\partial t} = \frac{{}^{H}\phi_g^n - {}^{O}\phi_g^n}{\Delta t}, $$

where

${}^{H}\phi_g^n$ is the value of the flux for group g, at point n at some future time H,

${}^{O}\phi_g^n$ is the value of the flux at the present time 0, and

Δt is the difference in time between 0 and H.

The right-hand side of equation 5 will be denoted as the weighted sum of the expression evaluated at time 0 and time H. The weighting will be θ and $(1-\theta)$. Therefore, the theta-weighted equations for the flux are

$$ \frac{1}{V_g}\left(\frac{h_{n-1}}{2} + \frac{h_n}{2}\right)\left(\frac{{}^{H}\phi_g^n - {}^{O}\phi_g^n}{\Delta t}\right) = \theta\left\{\left(\frac{{}^{H}D_g^{n-1}}{h_{n-1}}\right){}^{H}\phi_g^{n-1} + \left(\frac{{}^{H}D_g^{n}}{h_n}\right){}^{H}\phi_g^{n+1}\right. \tag{7} $$

$$ \left. - \left(\frac{{}^{H}D_g^{n-1}}{h_{n-1}} + \frac{{}^{H}D_g^{n}}{h_n}\right){}^{H}\phi_g^n - \sum_{g'=1}^{G}\left[\left(\frac{h_{n-1}}{2}\,{}^{H}\tau_{g'g}^{n-1} + \frac{h_n}{2}\,{}^{H}\tau_{g'g}^{n}\right)\right.\right. $$

(continued)

$$- \chi_g \frac{(1-\beta)}{k} \left(\frac{h_{n-1}}{2} {}^{H}\nu\Sigma_{fg'}^{n-1} + \frac{h_n}{2} {}^{H}\nu\Sigma_{fg'}^{n} \right) \Big] {}^{H}\phi_{g'}^{n}$$

$$+ \sum_{i=1}^{I} f_{ig} \lambda_i \left(\frac{h_{n-1}}{2} + \frac{h_n}{2} \right) {}^{H}C_i^n \Big\}$$

$$+ (1-\theta) \left\{ \left(\frac{{}^{O}D_g^{n-1}}{h_{n-1}} \right) {}^{O}\phi_g^{n-1} + \left(\frac{{}^{O}D_g^{n}}{h_n} \right) {}^{O}\phi_g^{n+1} - \left(\frac{{}^{O}D_g^{n-1}}{h_{n-1}} + \frac{{}^{O}D_g^{n}}{h_n} \right) {}^{O}\phi_g^{n} \right.$$

$$- \sum_{g'=1}^{G} \left[\left(\frac{h_{n-1}}{2} {}^{O}\tau_{g'g}^{n-1} + \frac{h_n}{2} {}^{O}\tau_{g'g}^{n} \right) \right.$$

$$- \chi_g \frac{(1-\beta)}{k} \left(\frac{h_{n-1}}{2} {}^{O}\nu\Sigma_{fg'}^{n-1} + \frac{h_{n-1}}{2} {}^{O}\nu\Sigma_{fg'}^{n} \right) \Big] {}^{O}\phi_g^{n}$$

$$+ \sum_{i=1}^{I} f_{ig} \lambda_i \left(\frac{h_{n-1}}{2} + \frac{h_n}{2} \right) {}^{O}C_i^n \Big\} \; .$$

The precursors are again handled in a like fashion, except that θ is taken to be $\frac{1}{2}$. This prevents further mathematical confusions from introducing a separate theta-weighting, and since $\theta = \frac{1}{2}$ yields the most accurate results, it can be readily applied to the simpler precursor equations. The precursor equations are now

$$\left(\frac{h_{n-1}}{2} + \frac{h_n}{2} \right) \left(\frac{{}^{H}C_i^n - {}^{O}C_i^n}{\Delta t} \right) = \tfrac{1}{2} \left[\frac{\beta_i}{k} \sum_{g'=1}^{G} \left(\frac{h_{n-1}}{2} {}^{H}\nu\Sigma_{fg'}^{n-1} + \frac{h_n}{2} {}^{H}\nu\Sigma_{fg'}^{n} \right) {}^{H}\phi_{g'}^{n} \right. \qquad (8)$$

$$- \lambda_i \left(\frac{h_{n-1}}{2} + \frac{h_n}{2} \right) {}^{H}C_i^n \Big] + \tfrac{1}{2} \left[\frac{\beta_i}{k} \sum_{g'=1}^{G} \left(\frac{h_{n-1}}{2} {}^{O}\nu\Sigma_{fg'}^{n-1} + \frac{h_n}{2} {}^{O}\nu\Sigma_{fg'}^{n} \right) {}^{O}\phi_{g'}^{n} \right.$$

$$- \lambda_i \left(\frac{h_{n-1}}{2} + \frac{h_n}{2} \right) {}^{O}C_i^n \Big] \; .$$

This equation must now be solved for ${}^{H}C_i^n$ in terms of ${}^{O}C_i^n$, ${}^{O}\phi_g^n$, and ${}^{H}\phi_g^n$, which can then be used to eliminate the unknown precursor terms in the flux equation. Thus,

$$ {}^{H}C_i^n = \frac{(2 - \lambda_i \Delta t)}{(2 + \lambda_i \Delta t)} {}^{O}C_i^n + \frac{\theta \, \Delta t \, \beta_i}{k \left(\frac{h_{n-1}}{2} + \frac{h_n}{2}\right) (2 + \lambda_i \Delta t)} \tag{9} $$

$$ \times \sum_{g'=1}^{G} \left(\frac{h_{n-1}}{2} {}^{H}\nu\Sigma_{fg'}^{n-1} + \frac{h_n}{2} {}^{H}\nu\Sigma_{fg'}^{n}\right) {}^{H}\phi_{g'}^{n} + \frac{(1-\theta) \, \Delta t \beta_i}{k \left(\frac{h_{n-1}}{2} + \frac{h_n}{2}\right) (2 + \lambda_i \Delta t)} $$

$$ \times \sum_{g'=1}^{G} \left(\frac{h_{n-1}}{2} {}^{O}\nu\Sigma_{fg'}^{n-1} + \frac{h_n}{2} {}^{O}\nu\Sigma_{fg'}^{n}\right) {}^{H}\phi_{g'}^{n} \, . $$

When equation 9 is substituted into equation 7, the result can be now rewritten with all known terms; that is, the terms evaluated at time 0 on one side, and all unknown terms, those evaluated at time H, on the other side. To further simplify notation let

$$ H_n \equiv \left(\frac{h_{n-1}}{2} + \frac{h_n}{2}\right) $$

$$ {}^{O}F_{g'}^{n} \equiv \left(\frac{h_{n-1}}{2} {}^{O}\nu\Sigma_{fg'}^{n-1} + \frac{h_n}{2} {}^{O}\nu\Sigma_{fg'}^{n}\right) $$

$$ {}^{O}T_{g'g}^{n} \equiv \left(\frac{h_{n-1}}{2} {}^{O}\tau_{g'g}^{n-1} + \frac{h_n}{2} {}^{O}\tau_{g'g}^{n}\right) $$

and

$$ {}^{O}L_g^n \equiv \left(\frac{{}^{O}D_g^{n-1}}{h_{n-1}}\right) {}^{O}\phi_g^{n-1} + \left(\frac{{}^{O}D_g^{n}}{h_n}\right) {}^{O}\phi_g^{n+1} - \left(\frac{{}^{O}D_g^{n-1}}{h_{n-1}} + \frac{{}^{O}D_g^{n}}{h_n}\right) {}^{O}\phi_g^{n} $$

with similar equations for time H. The flux equation with only flux terms

as unknowns is,

$$\frac{1}{V_g} {}^{H}\phi_g^n - \frac{\Delta t\ \theta}{H_n}\left\{{}^{H}L_g^n - \left[\sum_{g'=1}^{G} {}^{H}T_{g'g}^n - \chi_g \sum_{g'=1}^{G} \frac{(1-\beta)}{k} {}^{H}F_{g'}^n\right.\right. \tag{10}$$

$$\left.\left. - f_{ig} \sum_{g'=1}^{G} \sum_{i=1}^{I} \frac{\Delta t\ \lambda_i\ \beta_i}{k(2 + \lambda_i \Delta t)} {}^{H}F_{g'}^n\right] {}^{H}\phi_{g'}^n\right\} = \frac{1}{V_g} {}^{O}\phi_g^n$$

$$+ \frac{\Delta t(1-\theta)}{H_n}\left\{{}^{O}L_g^n - \left[\sum_{g'=1}^{G} {}^{O}T_{g'g}^n - \chi_g \sum_{g'=1}^{G} \frac{(1-\beta)}{k} {}^{O}F_{g'}^n\right] {}^{O}\phi_{g'}^n\right\}$$

$$+ \frac{\Delta t\ \theta}{H_n}\left(f_{ig} \sum_{g'=1}^{G} \sum_{i=1}^{I} \frac{\Delta t\ \lambda_i\ \beta_i}{k(2 + \lambda_i \Delta t)} {}^{O}F_{g'}^n \phi_{g'}\right)$$

$$+ \Delta t\ f_{ig} \sum_{i=1}^{I} \left(\frac{(2 + \lambda_i \Delta t)(1 - 2\theta)}{2 + \lambda_i \Delta t}\right) \lambda_i\ {}^{O}C_i^n\ .$$

Equation 10 now represents (G+I) X N coupled equations, discontinuous in both space and time, which must be solved for each time step. Once ${}^{H}\phi_g^n$ is obtained, the precursors are updated using equation 9. While the number of equations has been greatly increased, the solution is now tractable because the discontinuous equations can be readily programmed for digital computers, whereas solution of the continuous equations in closed form is impractical for all but the simplest cases.

The initial estimates of ${}^{O}\phi_g^n$ and ${}^{O}C_i^n$ for the solution of equation 10 are derived from statics calculations. The statics equations are equations 5 and 6 with the time derivatives set equal to zero.

If the gridpoint under consideration is an endpoint, the boundary conditions must be applied. For such points all cross sections are set

to zero with the result that only leakage is of concern. Thus, equation 10 can be written as

$$- {}^{H}\phi_{g}^{n} + {}^{H}L_{g}^{n} = 0 ,$$

where ${}^{H}L_{g}^{n}$ represents the leakage term involving the fluxes on the left and right of the considered point. If zero flux is the required boundary condition, then the leakage is required to equal zero, causing the flux to automatically be set to zero. For zero slope, the coefficients of the flux terms in the leakage are set so that the central term, the one involving ${}^{H}\phi_{g}^{n}$, has a coefficient at one and is equal to the appropriate flux to the left or right, causing an approximation of zero slope.

The solution of equation 10 in an implicit method requires ${}^{H}\phi_{g}^{n}$ at each time step. Thus, when solving for a particular group flux, the ${}^{H}\phi_{g}^{n}$'s are considered to be known and the latest value for each is used. This is done until all groups have been updated, and new values for all group fluxes are known. The new group fluxes are then compared to the past set and some convergence criteria evaluated.

The choice of θ will determine the exact mode of solution. A θ of zero reduces the equations to fully explicit. This type of solution is fastest but requires very small time steps, on the order of the prompt neutron lifetime, to produce stable solutions. While each step is fast, the great number of required steps for practical problems results in long computation times. Fully implicit solutions are produced from a $\theta = 1$. These type schemes are stable for any time step, but are subject to truncation error. The use of longer time steps allows shorter computation

times. Using a $\theta = \frac{1}{2}$ provides stable solutions, which would be expected to take longer than fully implicit, and have the least error, but such solutions tend to oscillate about the exact solution. Yasinsky[22] suggests using $\theta = 1$ for subcritical transients and $\theta = \frac{1}{2}$ for supercritical transients.

In review, it should be obvious that standard methods require many assumptions and approximations in their development; even the initial theory is itself an approximation. However, the predictions of such methods are expected to yield reasonable results and are, thus, extensively used as standards although a limited amount of work has been done to justify this type of activity.

Adiabatic Approximation

The development and discussion of the adiabatic approximation in this section is similar to that of Ott and Meneley.[7] This development places the scheme in proper perspective with reference to the earlier discussions of standard methods, and also to a series of similar type approximations known as the quasistatic family of approximations. The adiabatic approximation is frequently considered an extension of point kinetics; and, indeed, it was first developed by Henry[3] in the course of a new point kinetics derivation as discussed in Chapter I.

This derivation has as its goal the conversion of the Boltzmann transport equation, or its approximate form, the multigroup diffusion equation, into standard point kinetics formulation without approximation. The form of the diffusion equation used here will be

$$\frac{1}{V}\frac{\partial \Phi(\vec{r},E,t)}{\partial t} = (-T + F_p)\ \Phi(\vec{r},E,t) + S_d[\Phi(\vec{r},E,t')], \tag{11}$$

where

T is the removal and scattering operator,

F_p is the prompt fission operator,

$\Phi(\vec{r},E,t)$ is the total flux at position r, energy E, and time t,

$S_d[\Phi(\vec{r},E,t')]$ is the delayed neutron operator, as a function of the total flux at some earlier time t', and

V is the neutron velocity.

The desired point kinetics formulation is

$$\frac{d\phi(t)}{dt} = \frac{\rho(t) - \beta(t)}{\Lambda(t)}\ \phi(t) + \sum_{i=1}^{I} \lambda_i\ C_i(t) \tag{12}$$

and

$$\frac{dC_i(t)}{dt} = \frac{\beta_i(t)}{\Lambda(t)}\ \phi(t) - \lambda_i\ C_i(t) \tag{13}$$

where

$\rho(t)$ is the time dependent reactivity, and

$\Lambda(t)$ is the time dependent prompt generation time.

The other parameters have been previously defined.

This result was obtained by first taking the total flux, defined above, and factoring it into a time-dependent amplitude function and a position-, energy-, and time-dependent shape function; that is

$$\Phi(\vec{r},E,t) = \phi(t)\ \psi(\vec{r},E,t). \tag{14}$$

It is immediately obvious that the time-dependent amplitude is

similar to the flux in the point kinetics representation of equations 12 and 13. Point kinetics, therefore, only predict the amplitude of the neutron population, as is commonly known. The amplitude function is expected to have the main time dependence of the total flux, while the shape function will include only the spatial time dependence.

Since the amplitude function must have the bulk of the time dependence for the point kinetics equations to be valid, Henry[3] proposed a normalization constraint on the spatial function as follows:

$$\frac{d}{dt}\int\int\int \frac{\psi^*(\vec{r},E,t_o)\ \psi(\vec{r},E,t)}{V}\,d\vec{r}\,dE = 0\ ,$$

where $\psi^*(\vec{r},E,t_o)$ is the time-independent, adjoint flux evaluated prior to the transient. Due to the definition of the adjoint flux[1] the integral is proportional to the resultant power. Thus, by forcing the spatial component of the power to be constant in time, the amplitude function carries the bulk of the time dependence. However, the constraint does allow the shape function to vary with time as long as the normalization is satisfied. This is the advantage of this method over conventional point kinetics where the shape function is always constant in time.

Using the constraint and the factored total flux, the Boltzmann transport equation can be recast into the form of equations 12 and 13, with each of the parameters defined in terms of the adjoint shape function, the shape function, the amplitude function, and other variables. In the limit of point kinetics, the parameters reduce to the accepted forms.

If only the amplitude of the reactor behavior is required, the point kinetics equations, 12 and 13, can be solved quite readily. Spatial

dependence evaluation requires an equation for the spatial shape which is coupled to the point kinetics equations. The common form of the adiabatic approximation, outlined in the introduction, merely uses static flux shapes, calculated for different steady states of the reactor, to define the spatial dependence. Thus, it should be obvious that higher orders of the adiabatic approximation, the quasistatic equations, are available, depending on the degree of approximation of the coupled spatial equation.

The spatial equation can readily be obtained by substituting the factored flux, equation 14, into equation 11, the multigroup diffusion equation. Dividing the result by the amplitude function yields the spatial equation, which is coupled to the amplitude, or point kinetics, equations. Thus,

$$\frac{1}{V}\left[\frac{d\phi(t)}{dt}\cdot\frac{\psi(\vec{r},E,t)}{\phi(t)}+\frac{\partial}{\partial t}\psi(\vec{r},E,t)\right]=\left[-T+F_p\right]\psi(\vec{r},E,t) \qquad (15)$$

$$+\frac{S_d[\phi(t')\ \psi(\vec{r},E,t')]}{\phi(t)}\,.$$

The degree to which the various terms in this equation are considered determines the order of the adiabatic approximation. Typically, the amplitude equation is solved for many time steps before the spatial equation, with its much slower time rate of change, is used to update the spatial portion of the solution.

If the equation is solved with all terms included, but with the time derivative of the shape function replaced with a difference approximation, the result is very nearly that of a standard method. This is due

to the fact that equations 12, 13, and 15 are merely another form of the multigroup diffusion theory equations. This, then, represents the highest order adiabatic solution, which can approach the standard solution to any desired degree depending on the time step used in the difference approximation of the spatial time derivative.

The next lower order approximations assume that the time derivative of the shape is negligible with respect to the time derivative of the amplitude function. Thus, the term is set equal to zero, and the resulting equation is solved for the spatial dependence. This type of solution, along with the previous one, is a quasistatic solution.

If the shape of the delayed neutron distribution is assumed to be that of the prompt neutrons, and if both the time derivatives of the shape and amplitude are neglected, the adiabatic approximation results. The spatial equation with these assumptions included is

$$\left[- T + \frac{1}{k} F_p\right] \psi(\vec{r},E,t) = 0 \qquad (16)$$

which, with the inclusion of the eigenvalue, merely represents a statics calculation.

The delayed neutron holdback effect, discussed in Chapter I, is now seen to result from the neglect of the delayed neutron shape. This approximation has been shown to be responsible for the major portion of the error of the adiabatic approximation.[32,33]

Finally, the static shape equation, equation 16, can be solved prior to any calculation of the amplitude equations, for the expected set of reactor compositions, to yield spatial shapes which can be used to

later update amplitude parameters. There is no feedback to the spatial equation from the amplitude predictions; and the result is the simplest type of adiabatic approximation.

If the spatial equation is not considered in any fashion, then the result is, of course, the amplitude equations alone or point kinetics. This is, therefore, the very lowest order adiabatic approximation. At the other extreme, exact methods can readily be considered as the highest order adiabatic approximation.

Of course, other less obvious choices for approximating the spatial equation can result in "partial order" approximations. For example, the program KINET utilizes the lowest order approximation; that is, decoupled statics calculations to provide input parameters for the amplitude calculations. At the same time, the statics calculations include higher order approximations, such as corrections for the difference in the shape of the delayed neutrons from the prompt neutron distribution.

The solution of the adiabatic approximation requires, as do the standard methods, further approximations of the time derivatives so as to proceed to a set of equations solvable on a digital computer. Finite-difference is the analytical technique generally used to solve the equations, and is, therefore, applicable to both methods under consideration in the chapter.

In summary, this chapter has shown the two methods of concern in this dissertation are actually different orders of approximation of spatially-dependent, multigroup diffusion theory. The relationship of the two is now evident, so that experimental results and comparisons presented in the next chapter can be seen in better perspective.

CHAPTER V

COMPARISON OF ANALYSIS WITH THE GTRR EXPERIMENTAL RESULTS

The results of the two-dimensional, multigroup program KINET,[49] employing the methods discussed in Chapter IV, are presented in this chapter. The program was used to provide both statics and kinetics simulations of the experimental data.

Statics Calculations

It has been suggested by various authors[39,40,48] that the accuracy of analytical kinetics results are very dependent on the ability of the model to predict the static flux shapes and the multiplication of the reactor. This was verified on the GTRR by the experiments of Weaver,[49] who suggested that the model then used to represent the GTRR be further improved before proceeding with kinetics studies. As a result, a great deal of time was devoted to investigation of numerous ways to improve the GTRR model.

The basic model used was the eight-region, cylindrical model discussed in reference 55. The overriding consideration in the various investigations of the statics model was to represent, as accurately as possible, the actual physical dimensions, geometry, and known nuclear properties of the GTRR. Only if this was done could the kinetics results be considered valid.

The first step was to attempt a mockup of the ten-element, cold,

clean GTRR, which was known to be critical with all shim blades full out. The core region of the basic model was replaced with a three-region model representing one, central, homogenized fuel element surrounded by a pure, heavy water moderating region, with a third concentric region consisting of nine, homogenized fuel elements. This concentric core model arose naturally from the coarse lattice spacing of the GTRR and the cylindrical nature of the reactor.

The concentric core model was also desirable in order to provide a heavy water region in which to simulate the experimental core detector locations. The previous model assumed the V-10 detectors to be more nearly surrounded by fuel instead of moderator, as they actually were.

In order to further represent the core's physical dimensions more accurately, the GTRR structure was investigated for the various experimental configurations undertaken. As a result, the region boundaries were redefined, and the mesh spacing used in the computer calculations were designed so as to conform with these boundaries and the actual experimental detector locations. More accurate atom densities were also obtained for cross section calculations. Figure 27 represents an R-Z cross section of the geometric model of the ten-element mockup of the GTRR.

In this model, region one is the homogenized axial fuel element, and region nine is the homogenized fuel ring containing nine fuel assemblies. Region ten is the pure heavy water ring in which the V-10 detectors are located. Region four represents the graphite reflector, while the remaining regions are composed of varying amounts of heavy water, moderator, and aluminum from other core structures. Region two is not represented, as it is used as a dummy region for internal calculations in the

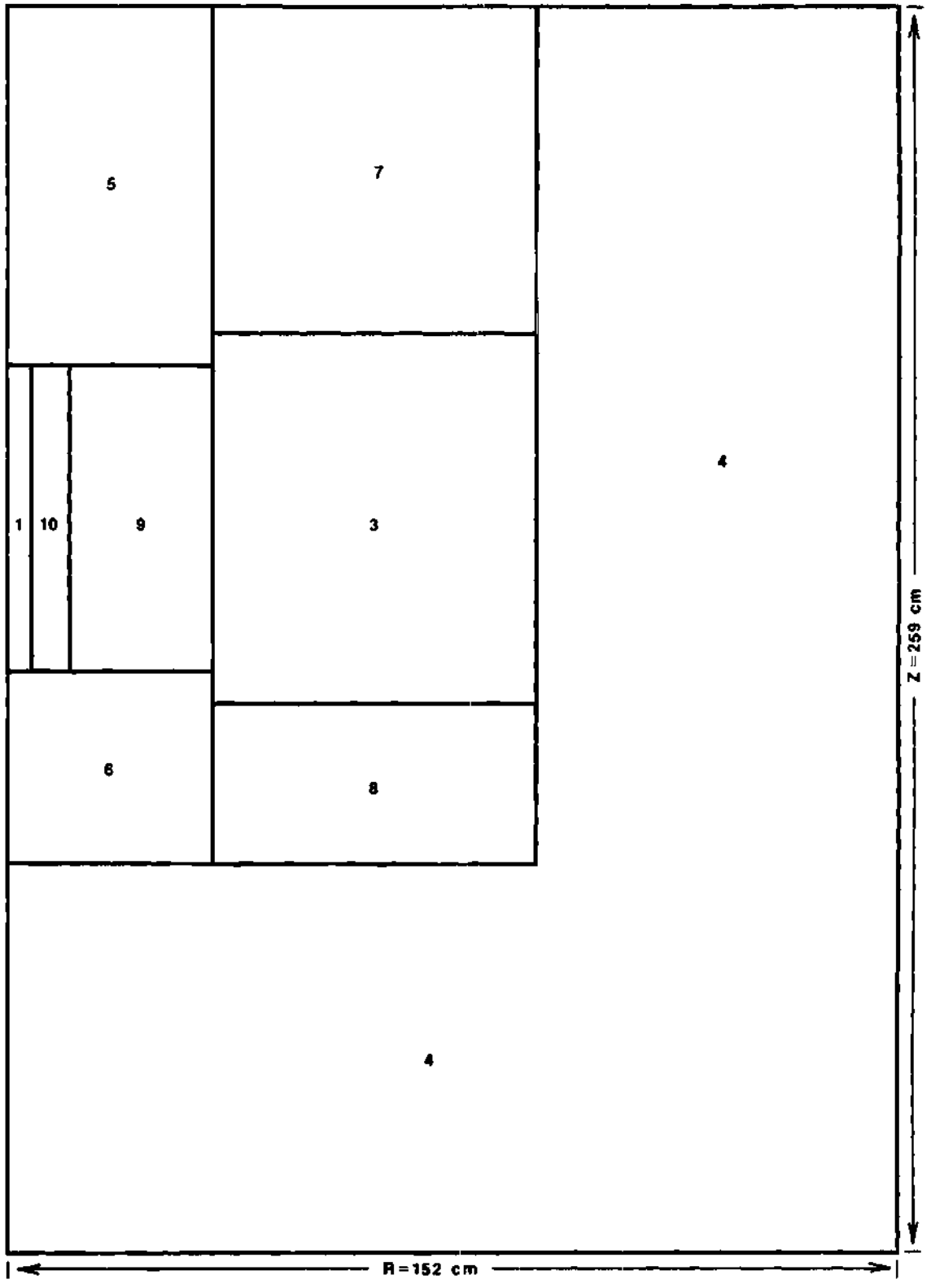

Figure 27. R-Z Cross Section of the Ten-Element GTRR Mockup

analysis program.

The cross sections for the regions differing from those used previously were then calculated using their atom densities and the fast and thermal cross section programs FORM[56] and TEMPEST,[57] which have been modified to run on the Georgia Tech Univac-1108 computer. The most recent microscopic cross sections available in the program libraries were used. Several check runs were made to verify previously accepted GTRR cross sections. As a result of this work, most region cross sections were updated.

The ten-element mockup of the initial GTRR criticality yielded a k-effective of 1.1045. The fission cross sections were then divided by this factor to force criticality. The axial flux shapes were compared to those measured on the ten-element critical GTRR, and were found to agree to within five percent in the fuel region and 10 percent in the reflector. Radial flux shapes were not measured and no comparisons were possible. The ten-element model cross sections are shown in Table 5.

A model of the 18-element core configuration used in the experiments was then prepared. This model was similar to the ten-element model, except that a four-region representation of the NTG Control Rod Assembly, with the control rod withdrawn, was placed in the central fuel element site. The 18 fuel elements were homogenized into a single, annular ring beyond the moderator ring. The new fuel region and the NTG cross sections were also calculated using FORM and TEMPEST. The k-effective from the ten-element mockup of the known critical GTRR was used to "correct" the fission cross sections in the 18-element model.

Table 5. Ten-Element Model Region Cross Sections

Region Number	D_1 (cm)	D_2 (cm)	$\Sigma_{1\to 2}$ (cm^{-1})	Σ_{a_1} (cm^{-1})	Σ_{a_2} (cm^{-1})	$\nu\Sigma_{f_1}$ (cm^{-1})	$\nu\Sigma_{f_2}$ (cm^{-1})
1	1.4647	1.0000	1.722×10^{-3}	1.649×10^{-3}	3.623×10^{-2}	2.223×10^{-3}	6.987×10^{-2}
3	1.4507	0.8657	7.772×10^{-3}	1.690×10^{-4}	7.855×10^{-4}	0.0	0.0
4	1.1113	0.8620	2.338×10^{-3}	0.0	2.587×10^{-4}	0.0	0.0
5	1.3240	0.8389	9.198×10^{-4}	1.680×10^{-4}	3.260×10^{-4}	0.0	0.0
6	1.3403	0.8574	8.872×10^{-3}	1.760×10^{-4}	6.573×10^{-4}	0.0	0.0
7	1.3366	0.8534	8.944×10^{-3}	1.740×10^{-4}	5.849×10^{-4}	0.0	0.0
8	1.3455	0.8635	8.770×10^{-3}	1.790×10^{-4}	7.599×10^{-4}	0.0	0.0
9	1.3421	0.8604	8.595×10^{-3}	5.280×10^{-4}	9.459×10^{-3}	5.410×10^{-4}	1.818×10^{-2}
10	1.3124	0.8258	9.438×10^{-3}	1.620×10^{-4}	8.160×10^{-5}	0.0	0.0

Two different 18-element models were studied, and the evaluation of those models relied extensively on the various statics measurements reported in Chapter III. The first had two concentric fuel rings with the inner ring having six homogenized fuel elements, and with the outer ring having 12 elements. However, this model yielded radial flux values inconsistent with those actually measured and was subsequently rejected.

The 18-element model eventually used was one in which the 18 elements were homogenized into one annular fuel ring. This ring was later divided into upper and lower portions to provide means to account for the uneven axial fuel burnup experienced in the GTRR. A statics calculation with the NTG control rod representation and 18 elements yielded a k-effective of 1.0802. This is about what was expected with the excess reactivity of 18 elements in a cold, clean core with the NTG control rod assembly in place.

Figure 28 is an R-Z cross section of the 18-element model. In this model, region one represents the pure heavy water ring with regions 16 and 17 representing the fuel regions. Regions 9 through 12 are a model of the NTG Control Rod Assembly. Nine is the plenum plug region; ten is the shroud and moderator; 11 is the control rod, shroud, and moderator; and 12 is the drive rod, shroud, and moderator. The other regions are as described for the ten-element model. Regions 2, 13, 14, and 15 are dummy regions used in the analysis program.

It was determined from shim blade calibration curves that the average 26.5° banked position of the shim blades during the experiments accounted for about 1.6 percent $\Delta k/k$. Thus, a poison search was carried out to calculate the amount of absorber to be placed in the regions in

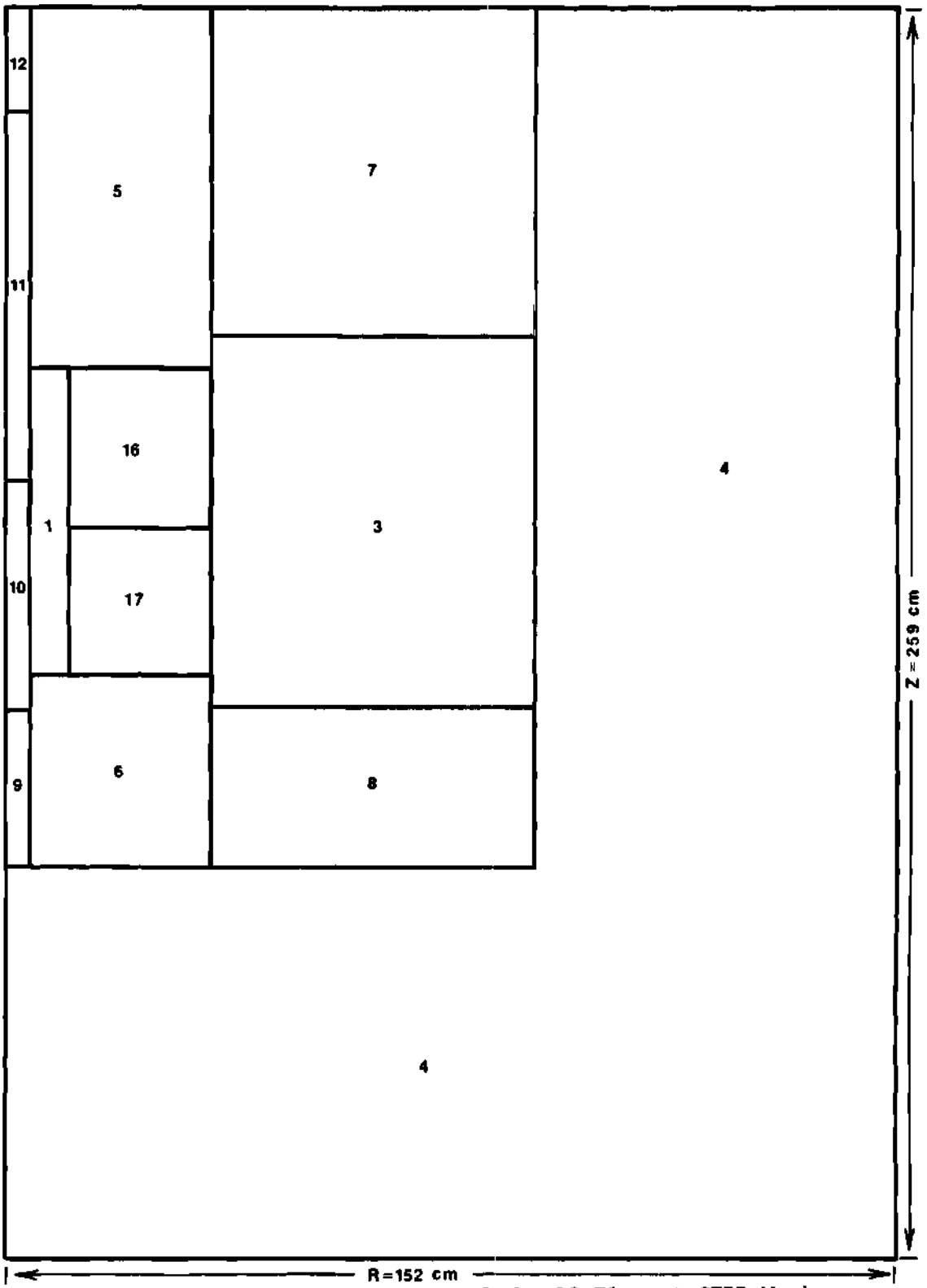

Figure 28. R-Z Cross Section of the 18-Element GTRR Mockup with NTG Control Rod Partially Inserted

which the shim blades are located in order to represent this amount of reactivity. Prior models had placed the blades in the region directly over the core, region five, yet Figure 1 reveals that the shim blades are also partially located in the outer reflector regions. This was accounted for in the model by increasing absorption in regions five and seven.

A calculation was now made with the shim blades included, which now predicted a k-effective of 1.0575. This amount of excess reactivity was concluded to be held down by burnup and fission product poisons. Since the reactor was operated at about 21°C for all experiments, temperature effects would be negligible. In addition, all experimental measurements were performed at power levels of 50 kilowatts, or less, after the reactor had been shut down from its one megawatt level for at least 100 hours. Thus, xenon poisoning would be negligible with the bulk of fission product poisons being attributable to samarium and other long-lived or permanent poisons. Samarium would be peaking in concentration at about that time. After considering a reactivity inventory, based on estimates of reactivity obtained from the safeguards reports on the GTRR,[50,55] the excess reactivity of the model was considered to have about 40 percent of its total held by fission product poisons and 60 percent by burnup. Previous models assumed only burnup.

It was mentioned earlier that uneven axial burnup had been experienced in the GTRR. This resulted from the banked shim blades being within the upper half of the core during the earlier power history. The core was, therefore, divided into two equal upper and lower portions so that this axial non-uniformity could be taken into account. The axial distribution was assumed to have about 55 percent of the total burnup in the

lower portion with 45 percent in the upper portion. No attempt was made to model the radial distribution of burnup. This probably does not introduce any significant error since the continual shifting of fuel elements in the course of the GTRR's normal experimental program has caused that distribution to be essentially uniform.

The burnup and poison factors were applied to the fission and absorption cross sections for the two fuel regions, and a final statics calculation obtained. This model now represents a critical, 18-element core with an NTG control rod in place, banked shim blades, burnup and fission product poisons. The cross sections for this model are shown in Table 7.

After modeling the critical 18-element reactor, calculations were made with the NTG control rod represented as being 50 percent and 100 percent inserted to obtain analytical flux shapes. The axial shapes are shown for V-10 and V-23 in Figures 29 and 30. Table 6 represents the analytical results for the radial flux ratios.

Table 6. Analytical Radial Flux at Core Mid-Plane

Configuration	Flux Relative to V-10	
	V-10	V-23
NTG Rod Withdrawn	1.00	0.61
NTG Rod 100% Inserted	1.00	1.22

Table 7. Eighteen-Element Model Region Cross Sections

Region Number	D_1 (cm)	D_2 (cm)	$\Sigma_{1\to2}$ (cm^{-1})	Σ_{a_1} (cm^{-1})	Σ_{a_2} (cm^{-1})	$\nu\Sigma_{f_1}$ (cm^{-1})	$\nu\Sigma_{f_2}$ (cm^{-1})
1	1.3124	.8258	9.438×10^{-3}	1.620×10^{-4}	8.160×10^{-5}	0.0	0.0
3	1.4507	.8657	7.772×10^{-3}	1.690×10^{-4}	7.855×10^{-4}	0.0	0.0
4	1.1130	.8620	2.338×10^{-3}	0.0	2.587×10^{-4}	0.0	0.0
5	1.3278	.8439	9.111×10^{-3}	8.485×10^{-4}	1.966×10^{-3}	0.0	0.0
6	1.3463	.8643	8.755×10^{-3}	1.792×10^{-4}	7.768×10^{-4}	0.0	0.0
7	1.3366	.8534	8.944×10^{-3}	5.620×10^{-4}	1.889×10^{-3}	0.0	0.0
8	1.3455	.8635	8.770×10^{-3}	1.790×10^{-4}	7.599×10^{-4}	0.0	0.0
9	1.6328	1.2870	3.385×10^{-3}	4.810×10^{-4}	9.669×10^{-3}	0.0	0.0
10	1.3470	.8651	8.740×10^{-3}	1.790×10^{-4}	7.919×10^{-4}	0.0	0.0
11	.8895	.5455	3.402×10^{-3}	5.746×10^{-3}	9.609×10^{-2}	0.0	0.0
12	1.1525	.7602	7.462×10^{-3}	1.311×10^{-3}	2.307×10^{-2}	0.0	0.0
16	1.3736	.8965	7.772×10^{-3}	8.890×10^{-4}	1.830×10^{-2}	9.210×10^{-4}	3.030×10^{-2}
17	1.3736	.8965	7.772×10^{-3}	8.930×10^{-4}	1.838×10^{-2}	9.150×10^{-4}	3.010×10^{-2}

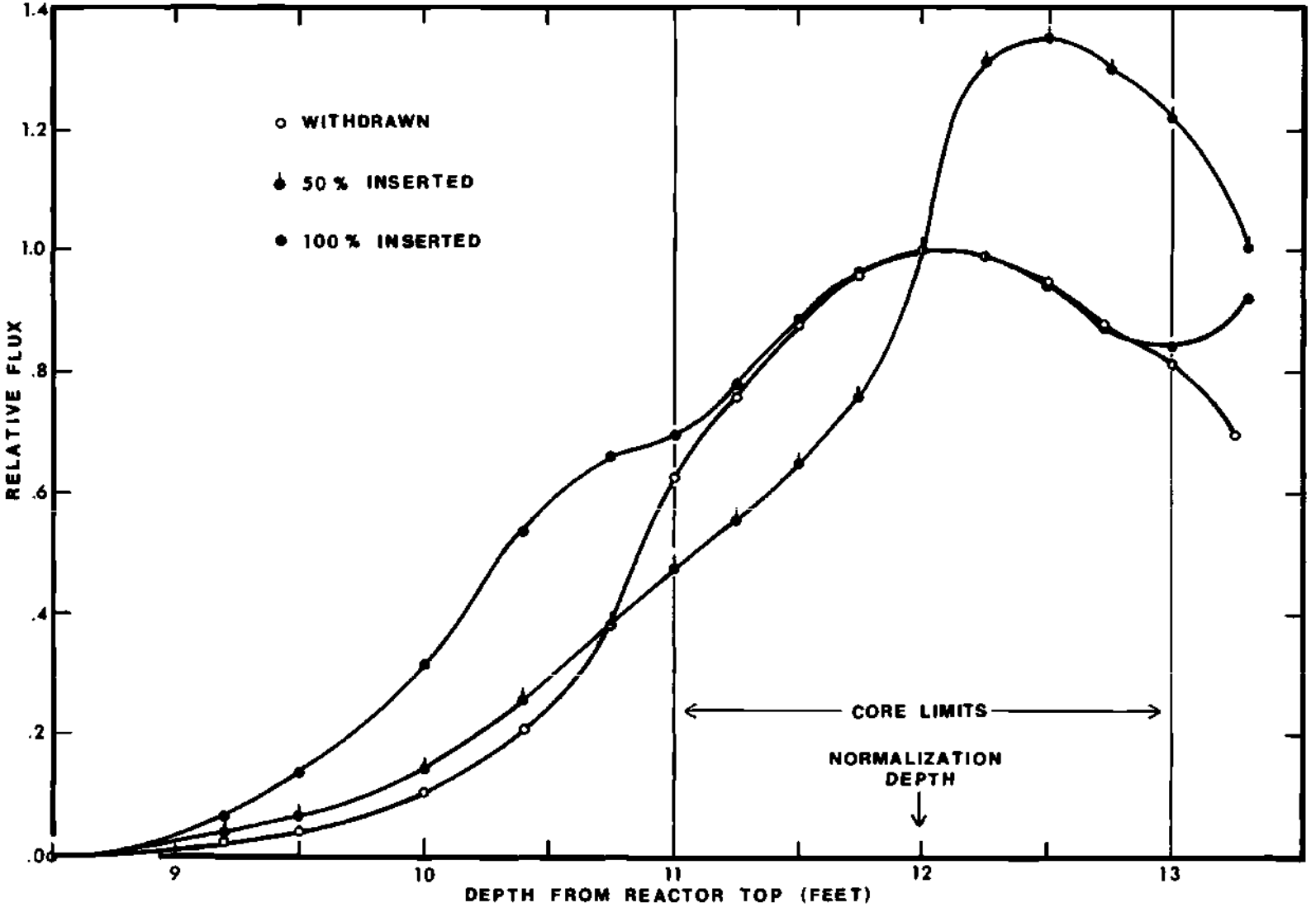

Figure 29. Calculated Axial Flux Distribution for V-10

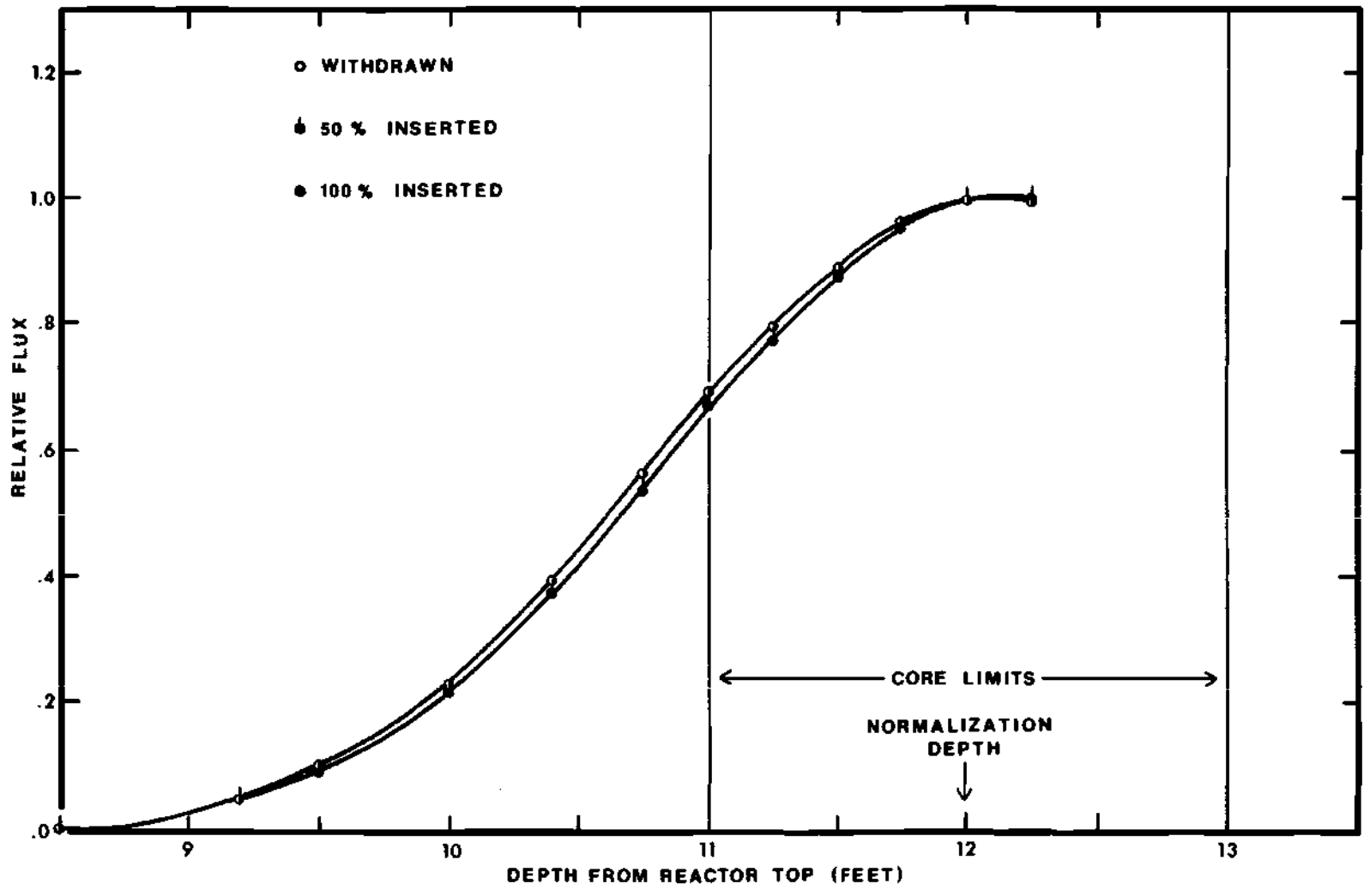

Figure 30. Calculated Axial Flux Distribution for V-23

Comparison of Statics Calculations with Experiment

With respect to the major features, the analytical statics flux shapes agreed well with the experimentally measured shapes. Comparison of Figures 23, 24, 28, and 29 verifies this. In particular, the agreement in the core, the area of greatest importance in this work, was better than that in the reflector regions. This is expected since diffusion theory is less valid for regions with large flux gradients, such as a reflector. For example, in the analytical shape for the fully inserted rod, the strong thermal absorption of the rod gives rise to thermal peaking in the reflectors. This effect was not noted experimentally, although for the V-10 position, a small change in the gradient was seen where such peaks would be expected.

Specifically, the V-10 shapes for the critical reactor agree to within five percent in the core and about 15 percent in the near reflectors. Comparisons at distances greater than about one foot from the core are not significant due to the low flux levels there. When the NTG rod is 50 percent and 100 percent inserted, the deviation between the shapes in the core is greater: 13 percent and 25 percent, respectively. These deviations occur at the core extremities. The difference between the shapes in the reflector for the 50 percent inserted case was less than 10 percent, while the thermal peaking noted earlier for the full in case gave rise to about a 70 percent deviation in the reflector.

Since V-23 is actually a position in the reflector, the agreement of analysis with experiment is not as good as for V-10. For the region between the axial limits of the core, the deviation is about 25 percent for the 50 percent and 100 percent inserted situations, and about 55 per-

cent with the rod fully withdrawn. The region corresponding to the upper reflector exhibits a 70 percent deviation one foot above the core, for all rod positions.

The V-23 analytical shapes indicate the analysis program was more insensitive to the perturbation of the NTG control rod than was experimentally observed. Analytically, the insertion of the rod led to negligible differences in the three shapes, while there were small, but definite, changes noted in the experiment.

Examination of Tables 3 and 6 for the radial flux values at the core mid-plane shows a 17 percent difference in the values for the fully withdrawn rod, and a 37 percent difference for the fully inserted values. However, due to the large gradients involved, the analytical values can be made to agree to within 10 percent if the positioning error of the detectors is taken into account. The analytical values presented in Table 6 correspond to those at the expected detector positions. Appendix B discusses the error in positioning the detectors and the subsequent errors in the measured flux levels.

The analytical model better predicts the static flux shapes than did previously used models. The agreement in the reflectors was especially improved, as was the radial agreement. Considering the limitations of diffusion theory in the reflector regions, the statics flux shapes were found to be acceptable for the kinetics calculations. The kinetics results presented in the next sections illustrate how the degree of agreement of statics calculations with experiment affects the accuracy of kinetics simulations.

Along with the flux shape calculations, the ability of the statics

model to predict reactor multiplication must also be taken into consideration. Experimental evidence of this aspect of an experiment is difficult to obtain, however. The most reasonable approach was to assess the accuracy of the predictions of the NTG control rod worth. Inverse kinetics calculations can be used to obtain experimental values of reactivity since time rates of change in the flux are available from kinetics experiments. In fact, this was done by Weaver[49] for his series of experiments on the GTRR using the same NTG control rod. Using experimental data with insertion times ranging from 2.2 seconds to 312 seconds, Weaver obtained rod worths of 5.4 percent $\Delta k/k$, for the longest insertions, to 7.9 percent $\Delta k/k$ for the shorter insertions. Based on these calculations, Weaver's total rod worth of 8.2 percent $\Delta k/k$, as determined from the analysis program, appeared to be verified on the assumption that the data from short insertions would yield more accurate reactivity estimates.

However, inverse kinetics, which is derived from point kinetics, also suffers from its limitations. Thus, it is more reasonable to assume that the 312 second insertion experiment actually yields a more accurate rod worth estimate since point kinetics would be more correct in predicting the response of such a non-severe transient. It was, therefore, assumed that the 5.4 percent $\Delta k/k$ value was more realistic, and some confirmation of this rod worth was sought.

Initial confirmation was obtained from the statics calculations which had predicted a total rod worth of about 4.5 percent $\Delta k/k$. The change in the model which was primarily responsible for the difference in worths was the decrease in size of the control rod region. The previous models had assumed an eight centimeter radius region over which the control

material was homogenized. Since a two inch diameter stainless steel rod is effectively a black absorber, the large area of homogenization used previously did not correctly account for the self-shielding present in such a rod.

In the present model the stainless steel was homogenized over a smaller diameter in order to more accurately account for the self-shielding. Still, the 4.5 percent $\Delta k/k$ value was somewhat low compared to the experimental value of 5.4 percent $\Delta k/k$. The absorption cross sections for the NTG control rod were increased to yield a total rod worth of about 5.6 percent $\Delta k/k$, more nearly matching the experimental value determined from inverse kinetics. Increasing the total rod worth further would result in the static flux shapes being in much worse agreement with the actual shapes. The previously discussed agreement with experiment of the static flux shapes supports the lesser rod worth utilized in this model.

The final confirmation of the need for a decreased rod worth was provided by the kinetics simulations which were subsequently performed. The calculated asymptotic flux levels, which are dependent partially on the reactivity of the perturbation, are in good agreement with the observed values. Greater reactivity worth would have resulted in increased flux depression and would have led to unreasonable kinetics simulations of the asymptotic decay.

Because programs used in reactor design typically employ much finer mesh spacings than are utilized in the present work, it was decided to double the number of grid points in the fuel, moderator, and control rod regions on the model as a test of the accuracy of the model. Statics calculations were made as described above, and the results were then com-

pared to the previously obtained static flux shapes.

In the situation with the control rod represented as withdrawn, there was negligible difference between the two calculations. For the case where the rod was 50 percent inserted, there were very small improvements in the magnitude of the flux in the upper and lower portions of both the V-10 and V-23 axial flux shapes. The magnitude of the flux at the peak was unaffected. The calculations with the rod fully inserted evidenced no improvement in the V-10 shape, and a less than six percent improvement in radial flux ratio at the core mid-plane.

The finer mesh also proved to have little effect on the rod reactivity. The total worth was unchanged, while the value at the one-half inserted position was within one percent of the previous value.

Kinetics Calculations

Following the analysis of the static behavior of the GTRR, simulations of the transient behavior were undertaken with the two-dimensional code KINET. Appendix C lists in tabular form the various mathematical controls used and tabular summaries of the simulations of the kinetics experiments discussed here. Figure 31 represents the results of a typical kinetics simulation, experiment 202 in this case, using the space-time, or standard, method. As noted previously, the elapsed time from 10 percent to 90 percent insertion was 0.422 second for this experiment. The 10 percent and 90 percent positions are indicated on the figure.

The delayed neutron parameters used were those of Keepin, Bernstein, and Ergen[58] hereafter referred to as the KBE parameters. Due to program array storage limitations, only the first 12 of the groups were

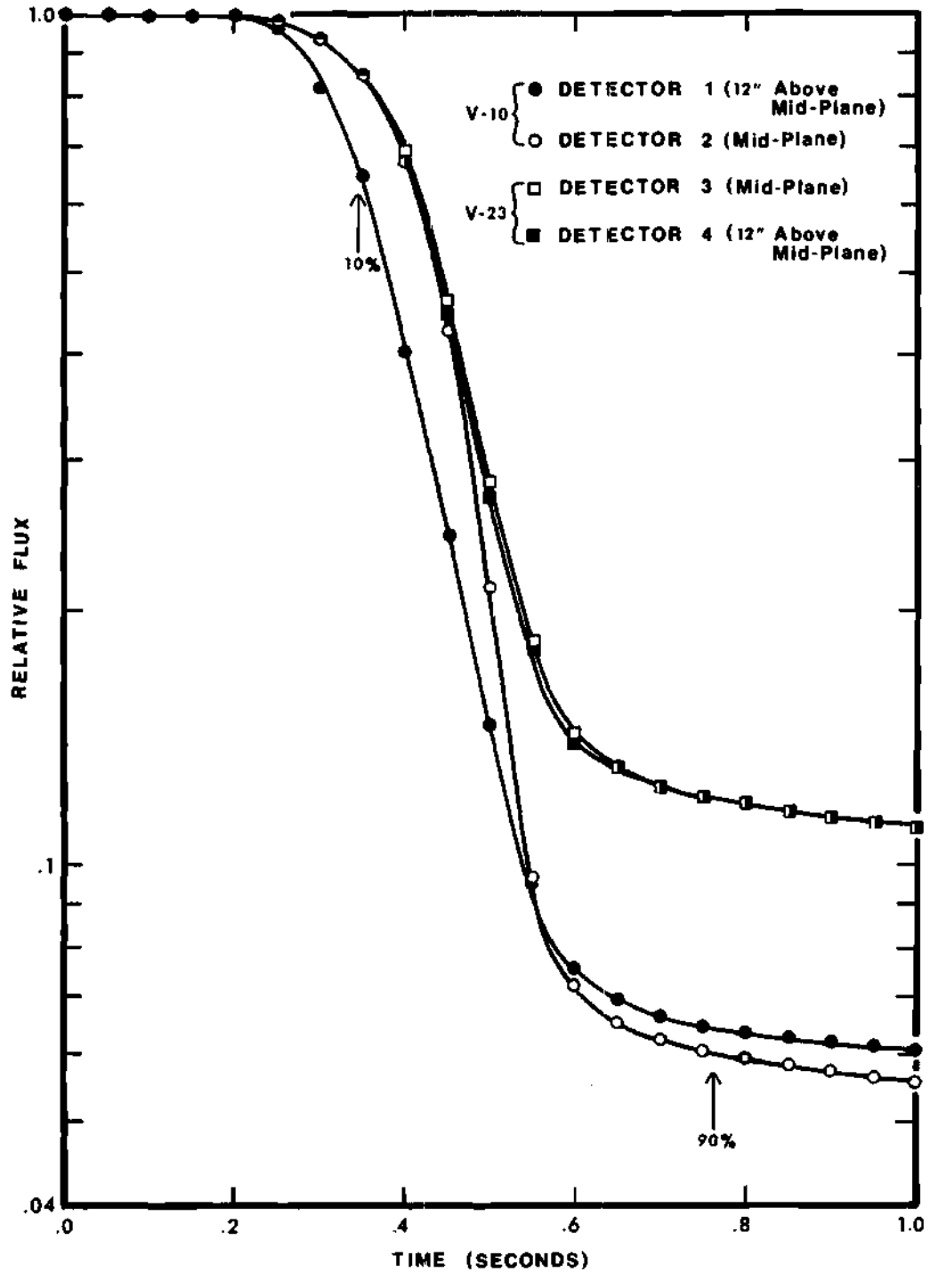

Figure 31. Results of Kinetics Simulation of Experiment 202

used. Since the three groups neglected have a total abundance of only 3.9×10^{-6}, or less than 0.05 percent of the total, and have half-lives in excess of 29,000 seconds, their omission was not considered significant in the present work which deals only with the first few seconds after the initiation of a subcritical transient. Table 8 lists the 15 groups of KBE delayed neutron parameters.

The KBE parameters were measured experimentally by irradiating small samples of U-235, and then rapidly transporting them to nearby detectors for counting. The results were presented as relative abundances, that is, β_1/β. This method does not include the effectiveness of the neutrons in producing fissions, which is of course dependent on the particular reactor being used. In general, the fission delayed groups have an effectiveness greater than 1.0 for any enriched reactor, such as the GTRR, while the photoneutron groups have an effectiveness less than 1.0.

Graham[59] has measured effective delayed neutron groups for the GTRR, but not the total effective delayed neutron fraction. However, his measurements indicated the average abundance weighted effectiveness for all groups to be about 1.0, which led to an effective delayed neutron fraction about that of the KBE groups, that is, 0.00755. Graham also notes that a similar value was calculated for the MITR, a reactor very similar to the GTRR. This value was therefore used in the present work. Table 8 reflects this by presenting absolute abundances rather than relative abundances. Further discussion of the Graham parameters will be presented in the next section on kinetics comparisons.

Included in Table 8 are nine groups of photoneutrons. These photoneutrons arise in significant amounts in a heavy water reactor since

Table 8. Delayed Neutron Parameters of Keepin, Bernstein, and Ergen

Group	Type	β_i	$\lambda_i (sec^{-1})$
1	Fission	1.70×10^{-4}	3.87
2	Fission	8.38×10^{-4}	1.40
3	Fission	2.66×10^{-3}	3.11×10^{-1}
4	Photo	6.54×10^{-4}	2.77×10^{-1}
5	Fission	1.23×10^{-3}	1.15×10^{-1}
6	Fission	1.39×10^{-3}	3.17×10^{-2}
7	Photo	2.05×10^{-4}	1.69×10^{-2}
8	Fission	2.48×10^{-4}	1.27×10^{-2}
9	Photo	7.04×10^{-5}	4.81×10^{-3}
10	Photo	3.38×10^{-5}	1.50×10^{-3}
11	Photo	2.08×10^{-5}	4.28×10^{-4}
12	Photo	2.36×10^{-5}	1.17×10^{-4}
13*	Photo	3.25×10^{-6}	4.37×10^{-5}
14*	Photo	1.03×10^{-7}	3.36×10^{-6}
15*	Photo	5.03×10^{-7}	6.24×10^{-7}

*Not used in present work.

fission product gamma rays, with energies in excess of 2.23 MeV, can undergo gamma-neutron interactions in the deuterium present.[60] Kinetically, the photoneutrons thus produced behave in the same way as the fission group delayed neutrons; but the photoneutrons do tend to have longer half-lives and smaller abundances. The primary difference in their behavior lies in the fact that the photoneutron-producing gammas have a large mean free path, and consequently, the photoneutrons are not necessarily born at the site of the precursor as with fission groups. Thus, the distribution of photoneutrons can have a different shape from both fission group delayed neutrons and prompt fission neutrons. Although such shape differences can be a consideration in kinetics work,[7] the effect is minimized here by the large volume of homogenization used in the model, and by the fact that the total abundance of photoneutrons comprises less than 14 percent of all delayed neutrons.

The group velocities used in the kinetics work were 2.020×10^8 centimeters per second for the fast group, and 2.484×10^5 centimeters per second for the thermal group. The latter velocity is the average velocity of a Maxwellian distribution of thermal neutrons at 21 degrees Celsius.

For each simulation, the buildup times noted prior to each experiment and the rod positions versus time obtained from the data were input to the program. A minor difficulty encountered with the rod position data was a slight retrograde motion of the control rod, initially, due to the slow opening of one of the solenoid valves. With respect to the reactor flux levels the motion was not very evident, but it did present a problem in representing the first few milliseconds of rod motion.

This was later overcome by a smoothing procedure, which removed the motion and yet maintained the proper flux response for the initial movement of the rod.

Comparison of Kinetics Calculations with Experiment

At this point it is important to digress and consider that the subcritical transients being studied in this research are both severe and rapid. The discussion of space-time experiments in the Introduction revealed that a limited amount of research of this nature has been undertaken. Most previous experiments designed expressly for the investigation of spatial dependence have involved slow, non-severe transients. In addition, attempts to draw conclusions on the adequacy of calculational models are frequently based on comparisons of the asymptotic decay region. This research is thus an endeavor to ascertain the validity of models on transients that are inherently difficult to calculate, but which more nearly represent the operational transients expected in power reactors. As will be pointed out subsequently, the models under consideration calculate the asymptotic response quite well with little difficulty.

With respect to comparisons, the general agreement of the space-time kinetics simulation of the slower experiments with the experimental results presented in Chapter III is fairly good. The final asymptotic decay is accurately represented with the magnitudes of the relative flux in V-10 being within 10 percent of the experimental values. The spatial changes evident in V-10 during the experiment are also noted in the space-time prediction.

The simulation does fail to adequately resolve the final magnitudes

of the two detector responses in V-23, but shows some slight evidence of the spatial change seen in the experiment.

As discussed in the section on the statics results, the degree of agreement of the statics calculations with experiments leads directly to similar degrees of agreement in the kinetics simulations with experiment. Therefore, it is interesting to note that the lack of success of the simulation in predicting the V-23 detector responses can be directly attributed to the lack of spatial changes in the statics model V-23 flux shapes discussed earlier. Recall that the full out and 100 percent inserted shapes show no change and this result, therefore, gives rise to the lack of resolution between the detectors in the kinetics simulation. However, there is a slight spatial change noted in the V-23 simulation and referring to the statics shape it is seen that there was, indeed, a slight variation noted for the 50 percent inserted shape. Likewise, the success in predicting the obvious spatial changes evident in the responses of the V-10 detectors is also due to the generally good agreement of the V-10 flux shapes with experiment.

One method of assessing the adequacy of the simulation in the region where the flux level is decaying rapidly is to plot the ratio of the analytical solution to experimental results versus the depth of the control rod. A good simulation should give ratios near unity. Such a plot for detector 2, located in V-10 at the core mid-plane, for three different experiments with different rates of insertion is shown in Figure 32. The results represent typical behavior of all the detectors, but detector 2 shows the largest deviation.

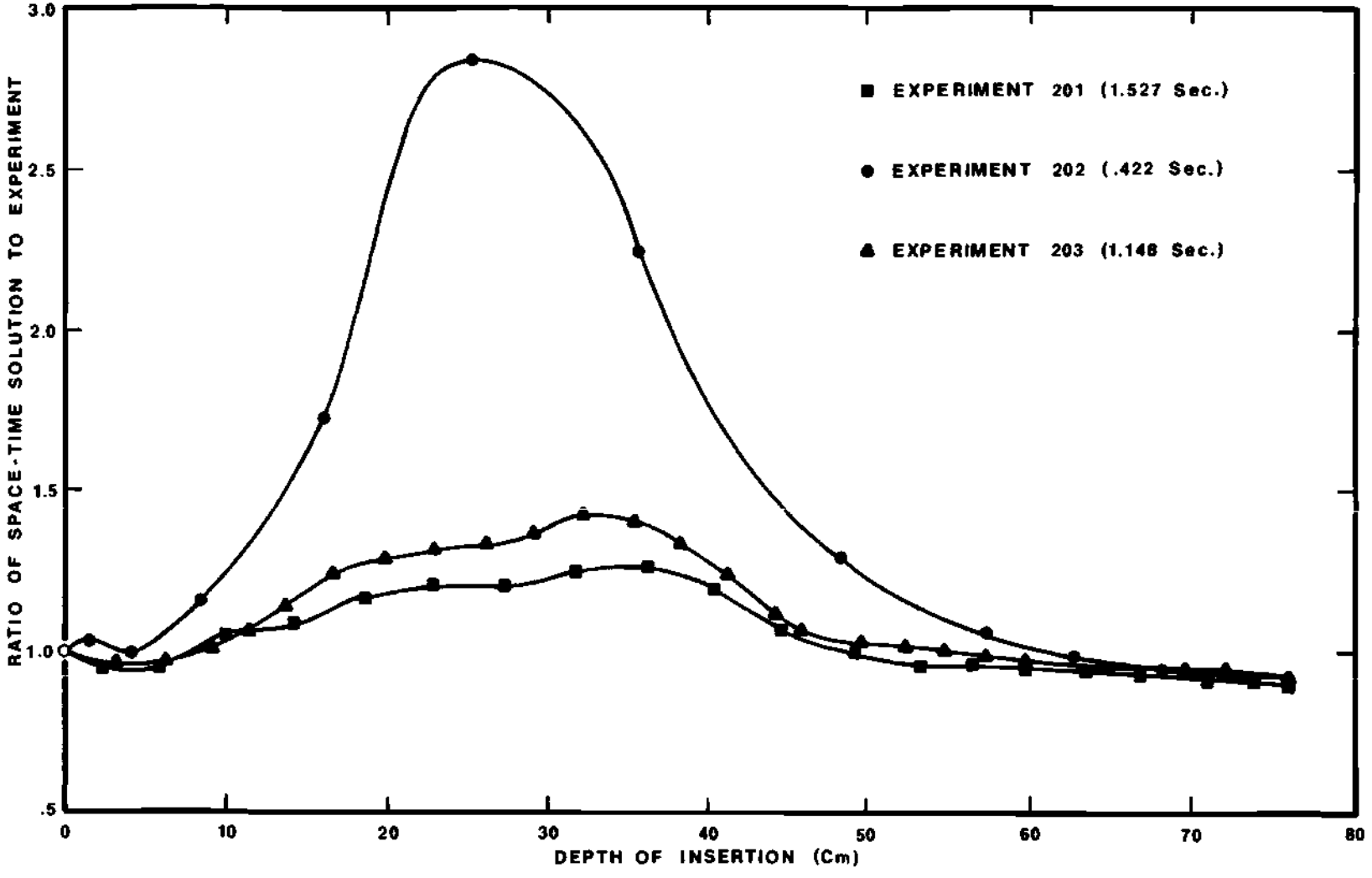

Figure 32. Ratio of Analytical Kinetics Solution to Experimental Results Versus Depth of Rod at the Core Mid-Plane in V-10

Figure 32 demonstrates a trend of deviation which appears dependent on the rate of reactivity insertion. This dependence on the rate of insertion of reactivity was noted in the results of Weaver,[49] but was not obvious at that time since the results of these faster experiments were not available. These curves show that for the fastest reactivity insertion, the kinetics simulation is in significant error with respect to the experiment. This result is totally unexpected on the basis of the slower experiments.

The degree of disagreement manifest for experiment 202 could possibly have been the result of poor convergence in the analysis program KINET. In order to verify convergence, a point kinetics program was written, and the results compared to the results of an adiabatic prediction of the same experiment. A point kinetics prediction provides the maximum expected deviation from experiment. If the point kinetics results were in some reasonable agreement with the average thermal flux as calculated by the adiabatic approximation rather than agreeing with the space-time prediction, it could be concluded that the convergence was acceptable.

The point kinetics results were first matched to the slowest experiment in order to calculate an appropriate neutron lifetime. Experimental rod positions and rod worths obtained from the statics calculations were used. The results of a point kinetics simulation of this experiment showed a deviation from the adiabatic calculation of the average thermal flux of less than 13 percent throughout the transient. The asymptotic decay region was matched within a few percent. After verifying the slower insertion experiment a prediction of the fast experiment was made with

point kinetics. In this case, the agreement was within 10 percent and the asymptotic region was matched very well. Due to the excellent agreement encountered it was concluded that the space-time results could be considered reasonable and the convergence correct.

Once the convergence question was resolved, physical considerations necessary to explain the space-time deviation from experiment were investigated. Because the space-time prediction of the asymptotic decay region magnitudes were reasonable, it was assumed that the effective delayed neutron fraction and the total NTG rod worth were sufficiently accurate. Altering either of these parameters can cause a lesser deviation in the prompt drop region, but will also destroy the agreement noted in the portion of the transient following the prompt drop. Point kinetics simulations with such changes verified this behavior.

Based on these considerations, and the fact that the effect apparently was rate dependent, the rod worth during the transient was investigated. As mentioned in the discussion on statics, the total rod worth was matched to that predicted from an inverse kinetics calculation of a long insertion experiment. However, when a series of statics runs was made with the NTG rod representation at various depths, the rod worths calculated were lower than those of the inverse kinetics calculation for the same depth of insertion, while the total worth was similar.

As a test, another point kinetics prediction of experiment 202 was made with the reactivity of the rod adjusted to match the results of the inverse kinetics calculation. The point kinetics results in the prompt drop region were significantly improved with respect to the experimental

response of detector 3, the detector which most nearly matches the average reactor response as determined by the linear reactor channel. The asymptotic decay region was unaffected. The representation of the rate of insertion of rod reactivity thus proves to be a significant source of error for the very fast insertion experiments. Improving the statics model to better represent the rod reactivity versus time with a greater accuracy should succeed in improving the space-time results.

Several studies of the effects of slight changes in model parameters were next undertaken to determine the effect on the space-time predictions. The parameters examined included the theta weighting, the time step, the effective delayed neutron fraction, the choice of delayed neutron groups, and the thermal group neutron velocity.

In all space-time simulations, the value of theta was chosen to be one, as suggested in Chapter IV; thus, the iterative scheme was fully implicit. A sample calculation with a theta of 0.5, resulting in the Crank-Nicholson algorithm of iteration, yielded a solution which exhibited an indication of oscillation about the fully implicit solution while remaining within five percent of that solution. The major difference was a significant increase in the amount of time necessary to solve the problem.

A theta of zero was not investigated as a fully explicit scheme is generally conceded to be unstable for all but extremely small time steps. Therefore, the expenditure of a significant amount of computer time was not deemed advisable.

Next, a series of calculations investigating the effect of the time step was made. All simulations of experiments used a time step of 0.001 second. Thus, a simulation using a time step of one-half as large

was made to see if improvement in the solution was possible. A time step of 0.005 second was then utilized to investigate a possible worsening of the simulation. This is a common manner of investigating the adequacy of the time step used in analyses.

In both situations, the results were essentially identical with the time step of 0.001 second. The greatest difference was less than one percent at the point where the flux gradient with time was steepest. Consequently, a time step of 0.001 second is quite adequate to represent the transient.

Decreasing the effective delayed neutron fraction in a simulation should lead to a greater fractional change during the course of the transient. A sample calculation, employing an effective delayed neutron fraction decreased 10 percent from the value of 0.00755 used for the GTRR, leads to the expected result: the fractional changes are decreased by 10 percent for all detectors shortly after the initiation of the transient. Therefore, the value of the delayed fraction used, that is, 0.00755, results in an accurate representation, especially in the asymptotic region, and can be considered adequate for the present work.

In line with investigations of the delayed neutrons, a simulation of experiment 202 was made with a set of delayed neutron parameters obtained from experiments on the GTRR by Graham.[59] This eight-group set of parameters is shown in Table 9.

In comparing the space-time prediction made with the Graham parameters to a prediction using the KBE groups discussed earlier, it is noted that the former results in only a slight lag during the severe portion of the transient. However, in the asymptotic decay region the Graham param-

eters cause the simulation to yield a magnitude about eight percent greater than do the KBE groups, which have been seen to yield reasonable results. This would appear to further verify the choice of the KBE groups for this work, even though the Graham parameters were derived from work on the GTRR.

Table 9. Delayed Neutron Parameters of Graham

Group	β_i	$\lambda_i (sec^{-1})$
1	4.741×10^{-3}	2.37×10^{-1}
2**	2.356×10^{-3}	3.33×10^{-2}
3	3.692×10^{-4}	8.33×10^{-3}
4	2.628×10^{-5}	8.89×10^{-4}
5	1.676×10^{-5}	3.03×10^{-4}
6	2.416×10^{-5}	1.09×10^{-4}
7*	3.010×10^{-6}	4.54×10^{-5}
8*	1.140×10^{-5}	5.94×10^{-7}

*Photoneutron parameters.

**Mixed group, approximately 30% photoneutron.

Finally, a kinetics simulation was performed with the thermal velocity increased by 10 percent in order to examine the effects on the transient. This amount of deviation from the value used would be difficult to justify except by hypothesizing a non-Maxwellian distribution of thermal neutrons, which is unlikely in the case of the well-thermalized neutrons expected in the heavy water moderated GTRR. Nonetheless, it is interesting and useful to note the magnitude and consequences of such a

change. Such an increase would be expected to cause a perturbation to be propagated more rapidly and not affect the final magnitudes. The results of the calculation did indeed confirm this. The fractional changes during the most severe portion of the transients were increased by about 2.5 percent. The solution then rapidly converged to the former solution, and the decay following full insertion of the rod was identical with the solution obtained with the proper thermal velocity. The effect of even such a large error in the thermal velocity is seen to be nearly negligible.

Adiabatic Approximation Simulations

Following the space-time calculations, simulations of the experiments were made using the full adiabatic approximation. The tabular results of these simulations are presented in Appendix C.

A typical adiabatic simulation predicted, as did the space-time simulation, the same general spatial features seen in the experimental data and described for the space-time calculation. The important difference between the space-time and adiabatic simulation is the evidence of the delayed neutron holdback effect. During the course of the prompt drop in the transient, the adiabatic calculation lags the space-time calculation considerably. This effect was discussed in earlier chapters, and is the principal objection to the adiabatic method. Figure 33 presents the ratio of the space-time solution to the adiabatic solution versus the depth of the control rod for detector two, for experiments 201 through 203. This detector was located at the core mid-plane of V-10. The figure illustrates the typical delayed neutron holdback effect expected of the adiabatic approximation. The two slower experiments exhibit a maximum devia-

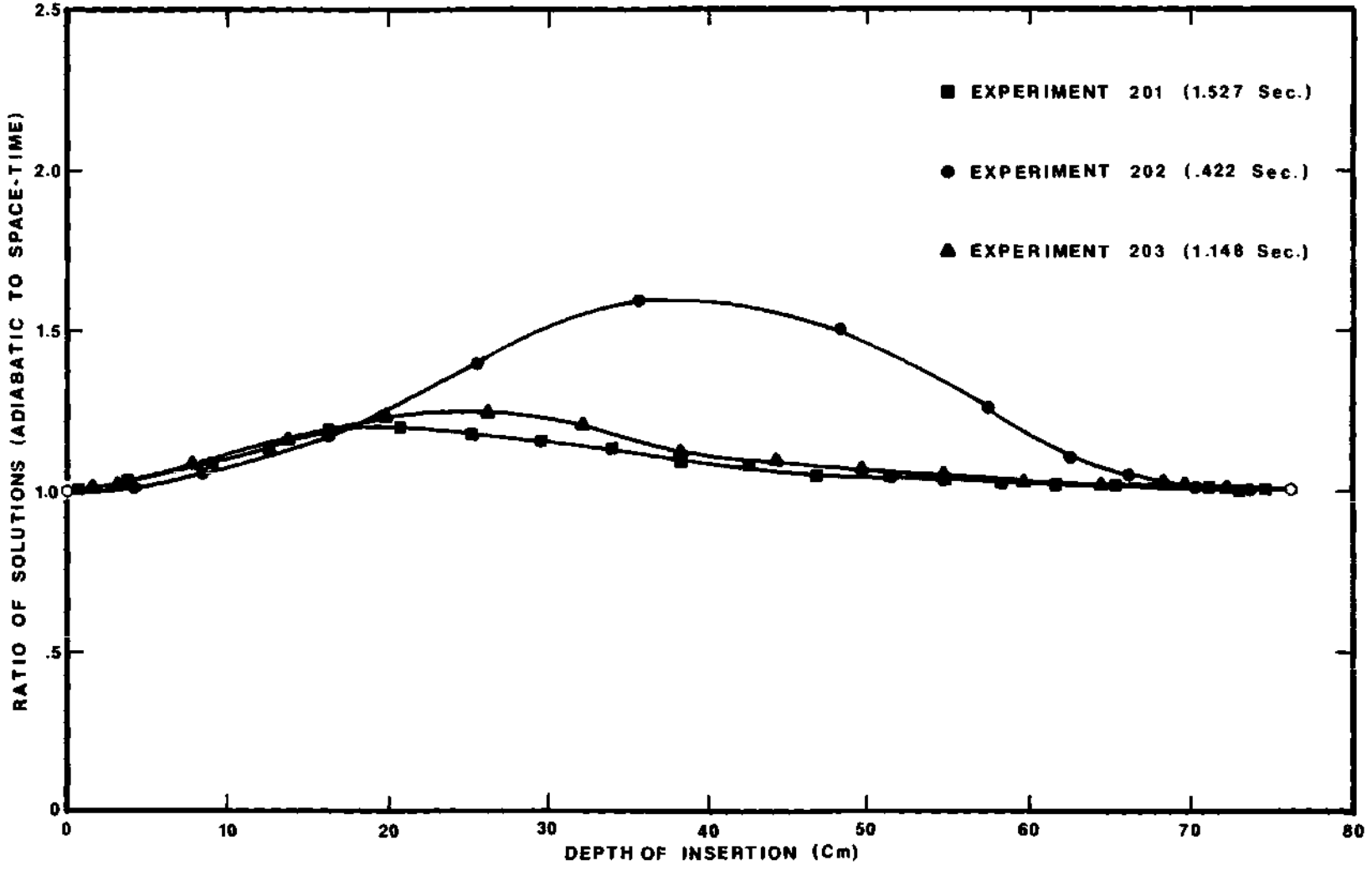

Figure 33. Ratio of Space-Time Kinetics Solution to Adiabatic Kinetics Solution Versus Depth of Rod at the Core Mid-Plane in V-10

tion from the space-time solution, due to the holdback effect, of less than 25 percent. This represents the largest deviation of any detector, for those experiments. Weaver reports for his fastest experiment, 1.34 seconds from 10 percent insertion to 90 percent insertion, a deviation of about 28 percent at the core mid-plane in V-23. The experiment 203 simulation, 1.15 seconds through the core, exhibits a deviation at the same point of about 25 percent. The maximum deviation, for the simulations of the fastest experiment, is 60 percent which again represents the maximum deviation expected in the core region. Therefore, the simulations of experiment 202 demonstrate a 140 percent increase in deviation over experiment 203 while there was less than a 65 percent decrease in the insertion time.

It should also be noted that while adiabatic simulations of the experiments produced disagreements with the space-time solutions of as much as 60 percent, it can be seen from Figure 33 that by the time the rod is fully inserted the two results are in excellent agreement. This agreement also extends to the decay occurring after rod motion is complete.

Mixed-Methods Calculations

Following the adiabatic simulations, a series of simulations suggested by Weaver as having possible economic benefits was undertaken for the faster insertions used in the present work. These predictions involved the "mixed-methods" approach in which the fast group is treated adiabatically while the thermal group is treated with a space-time approach. The tabular results of the mixed-methods calculations on experiments 201 through 203 are also given in Appendix C.

The previous studies had shown the mixed-methods approach to be as accurate as a full space-time approach alone for both energy groups, and for the fastest experiments undertaken. The costs in computer time were essentially equal, with the mixed-methods requiring slightly more time. The same results were noted in the present faster experiments with the differences between methods being negligible. There was no delayed neutron holdback effect in either energy group. The computer time necessary was, again, about equal.

The results discussed above do not seem to present any economic benefits, but the studies have so far been only on two-group models. It is expected that for more than two groups substantial savings could be effected by the mixed-methods approach.

CHAPTER VI

CONCLUSIONS AND RECOMMENDATIONS

In summary, the purpose of the present work was to provide an extension of experimental data on a realistic, essentially two-dimensional reactor to which analytical methods could be compared, and to make an assessment of two of those methods. In Chapter I, it was noted that many authors have cited the need for such experiments and assessments, with respect to space- and time-dependent reactor kinetics.

The kinetics experiments designed especially for the study of spatial dependence have usually been on simple assemblies and involved only slow, non-severe transients. In addition, the comparisons of model calculations with experimental results concentrated on the asymptotic decay region. Due to the limited nature of the experiments, the necessary assessments of the validity of kinetics approximations are made by comparisons to finite-differenced, multigroup diffusion theory calculations. But even these standard methods of calculation, which require many assumptions to generate the discontinuous set of equations required for solution by computer, need verification.[39,40] The results of the investigations reported here provide an initial answer to some of the questions which have been raised, with respect to spatially-dependent kinetics calculational methods. The faster insertions undertaken, and the development of an excellent fast data acquisition system, mean that useful data to which analytical comparisons can be made are now available for the prompt drop

and subsequent rapid decay portion of subcritical transients. This part of the transient has not, until now, been considered in great detail. The conclusions and recommendations which, therefore, are derived from the results presented earlier follow.

Conclusions

Much has been said when reporting experiments involving spatially-dependent kinetics of the need for an accurate statics model.[19] Indeed, this was found to be true in the work of Weaver on the GTRR, and once again, the results presented earlier in this dissertation illustrate and confirm this fact. However, the faster and more severe transients which were studied provide some qualifications to that general statement depending on the severity of the transient, or the portion of the transient under study.

If the transient is not too severe, if only the asymptotic decay portion is to be examined, or if relative spatial changes are desired, the accuracy of the statics model need not be particularly stringent. As long as the model predicts the shape to within 10 or 15 percent of the actual shape in the fuel region, and to within 25 or 30 percent in the reflector, it can still be expected to provide calculations of kinetics behavior (of the nature outlined above) with similar errors. This degree of error is typically acceptable from the standpoint of a design calculation. Thus, for less severe transients, obtaining a very precise statics model is probably less important than having a well-defined concept of the degree and nature of the statics model's inaccuracies. This is due to the fact that corrections to the transient behavior are readily inferred from

the known inaccuracies of a statics model. This was demonstrated in Chapter V when the kinetics simulation's deviations from experiment were shown to directly follow from the known deviation in the statics model from experiment.

Thus, much useful kinetics information can still be obtained from a model which only approximately predicts statics behavior. This is particularly true if the degree of error in the statics model is well known.

When dealing with severe transients generated by moderate-to-large reactivities being inserted quickly, the statics model must be appreciably better than discussed above if the prompt drop portion of the transients is to be accurately calculated. This criterion results from the need for accurate predictions of the reactivity versus time. The kinetics results have shown that for the fastest reactivity insertions the errors in the shape (and hence the reactivity) lead to significantly large errors in calculating the time dependence of the flux. This effect was not expected on the basis of the results of the slower insertions. A trend toward this result was noted in the previous work on the GTRR after the faster experiments undertaken had provided positive evidence. This type of deviation due to a reactivity discrepancy is not so readily assessed as is the error due to the statics flux shape differences noted for the less severe transients. Thus, the deviation must be accounted for beforehand by a statics model which accurately predicts subcritical reactor multiplications, especially as a function of time.

In the experiments performed, it was discovered that approximately -5.6 percent $\Delta k/k$ inserted faster than 1.15 seconds led to the type of behavior outlined above. However, it is interesting to note that ex-

tremely fast insertions more nearly approaching that of a step-insertion would not be expected to exhibit this behavior, because such insertions are more easily modeled, and have little or no reactivity time dependence. In fact, step-insertions are frequently used in simplifying problems. Therefore, the effect discussed occurs only for large, moderately-fast insertions of negative reactivity such as would be expected with control rods used in emergency shutdown situations.

If the error due to this flux shape-reactivity phenomenon is applicable in a large positive transient, then its significance in an accident analysis is obvious. A large, fast, positive ramp might have its total energy release predicted with a large error, and the time at which negative feedback effects were calculated to play a significant part in the accident might be grossly in error.

The model used in this work predicted the experimentally known shapes quite reasonably. Diffusion theory proved, once again, to be adequate, although it very possibly was the cause of the underestimated reactivity noted for the partial shapes. This was attributed to the large absorption of the control rod. Indeed, diffusion theory has as one of its assumptions that the flux be slowly varying with position which implies that the absorption cross sections should be small.[2] The fact that the flux is strongly dependent on position in the reflectors is probably the major cause of the analytical differences from experiment which were noted in those regions.

Since FORM and TEMPEST use only the atom densities and microscopic cross sections along with various assumptions of the type of moderation, more sophisticated programs employing flux weighting or other schemes

should be used to generate cross sections. In the present model, an improvement in cross sections would probably result in a significant improvement in the statics model.

To recapitulate the conclusions of the statics work, statics modeling is definitely important, but blind striving for an exact representation of static behavior may be unproductive. Accurate and usable kinetics results are still obtainable if the deficiencies of the statics model are known, or if less severe transients, or the asymptotic portion of a transient, are to be predicted.

The use of finite-difference solutions of multi-dimensional, multigroup diffusion theory has long been considered as a standard for assessments of other kinetics methods. Nonetheless, the equations still are only approximate and there is a need to justify these methods for realistic reactors.

The standard, or space-time, results presented in Chapter V generally predict overall spatial features quite well for a two-dimensional, heterogeneous reactor. The source of the disagreements with experiment has been identified and represents only refinements of physical parameters and modeling. The various parametric studies described in Chapter V verify that the mathematical model is operating correctly and that the mathematical controls are appropriate. The expected results for given changes in important physical parameters were also observed. Under the circumstances, the finite-difference approach applied to diffusion theory does appear to adequately predict reactor response given correct physical parameters and a well-defined statics model.

Having accepted the results of the space-time simulations as reasonable, comparisons of the adiabatic simulations to the space-time model can then be considered valid. Therefore, the comparison presented in Chapter V illustrates that the adiabatic model can be expected to give errors in the flux level of no more than 25 percent for insertions as fast as 1.15 seconds. This degree of error may be acceptable in design work. The spatial effects are predicted quite well, and the asymptotic region is essentially unchanged from space-time results. The savings in computer time of the adiabatic method could easily offset the loss of exactness since the adiabatic calculation required only one-half the time of the space-time method. For large insertions, with speeds beyond 1.15 seconds, the error may be unacceptably large, even with the apparent economic savings. In all situations though, the prediction of spatial changes was adequate and the asymptotic region well modeled.

In short, the adiabatic model can provide desirable economic benefits with acceptable error for predictions of slow, and even moderately-fast, large reactivity transients. For faster transients, other methods may be necessary if information other than relative spatial changes and the long term response is necessary.

An interesting extension of the adiabatic approximation is the novel "mixed-methods" approach of Weaver. This method of treating those groups expected to respond quickly to perturbations, generally the fast groups, with adiabatic approximations, and the thermal groups with full space-time methods, yields results as accurate for all energy groups as a full space-time treatment. The earlier work had shown this result to be true up to, and including, the fastest insertions undertaken. Applying

the mixed-methods to the insertions presented here demonstrates that it is as accurate as the full space-time method for speeds up to three times faster than had been previously attempted. The only drawback for two-group calculations is that calculation time is comparable to a full space-time prediction. However, the mixed-methods scheme is expected to show only a linear increase in time necessary for more than two groups, due to the rapid calculation of the adiabatic groups, while a full space-time approach goes as the square of the number of groups.

Recommendations

Considering that an excellent experimental device, a computerized, high-speed data acquisition system, and a two-dimensional, multigroup program are available for producing, recording, and analyzing subcritical transients in the GTRR, it is recommended that further uses be investigated for this system. The development of the entire system has required a great deal of time; it has been tested extensively and has proven to be reliable. With minor modifications, possible uses of the experimental system include: generating three-dimensional, spatial kinetics data; producing desired power histories under computer control; generating and collecting effective delayed neutron data for both fission and photoneutron groups, including those with the shortest half-lives; and developing calibration procedures for control rods. The system undoubtedly could be used for still other investigations and should be seriously considered for future investigations on the GTRR.

The analysis program, KINET, should prove useful for carrying out numerical studies for the GTRR. Both the kinetics and statics portions of

the program could be advantageous in evaluating the response of the reactor in experimental situations, and, perhaps, for design or safety studies.

With reference to the results presented in this dissertation, the relationship between the statics results and kinetics results discussed should be further pursued. On the GTRR, this would require devising some method for safely instrumenting fuel elements in order to obtain flux measurements axially next to the fuel elements and radially through the core while maintaining a full symmetrical complement of fuel elements. The NTG could then be used to generate various subcritical spatial shapes with data being taken rapidly by computer. Thus, a great deal of statics data could be obtained with which to compare kinetics results to better define the relation of statics results to kinetics results. An excellent time for this type of work would be during low power operation of the new five megawatt core anticipated for the GTRR.

The degree and sources of errors in kinetics results for given ambiguities in the rate of rod insertion should certainly be given consideration. Reactors are generally not designed with step-insertion methods of control; thus, the effect noted earlier should be examined to discover its effect in both fast, positive, and negative transients. This type of disagreement is a potential source of serious error in safety calculations for such types of transients for the reasons outlined earlier.

Finally, it is highly recommended that the mixed-methods approach should be further investigated. Various test cases involving a range of reactor types and conditions should be numerically studied for multigroup situations with this scheme to acquire exact evaluations of its accuracy

and its potential economic benefits. The availability of a program at Georgia Tech using this scheme, and also with options for two other standard analytical techniques, provides excellent opportunities for performing many of these studies here.

APPENDICES

APPENDIX A

DESCRIPTION OF THE HYDRAULIC DRIVE

There were several safety criteria set forth by the Atomic Energy Commission which affected the design and operation specifications of the NTG. For the Hydraulic Drive these include:

1. The maximum rate of adding positive reactivity will be 0.025 percent $\Delta k/k$ per second,

2. The fixed orifices controlling the withdrawal of the control rod should be redundant, such that a failure of one will not lead to an increase in addition of positive reactivity,

3. The fixed orifices should have provisions for monitoring possible component failure.

The operation of the Hydraulic Drive will be described below with reference to the above mentioned criteria.

The insertion or withdrawal of the NTG control rod is dependent on the states of four solenoid valves designated SV1 through SV4 on Figure 7. When the system is turned on, the motor and pump unit supply oil to the de-energized solenoid valves. In their normal de-energized states, the valves function as shown on the diagram. Thus, oil flows through SV1, SV2, and SV3 to charge the two and one-half gallon accumulator to about 600 psi. An accumulator merely consists of a piston backed by nitrogen gas under pressure, so that as oil flows into the accumulator, the nitrogen increases in pressure as the piston is forced back. The accumulator is then fully

charged when the nitrogen pressure equals system pressure. The pressure of the accumulator is monitored on gauge G1. In this configuration, oil can only charge the accumulator. Oil is prevented from reaching the cylinder by the pilot-operated check valve V1. A pilot-operated valve opens only when oil pressure is applied to the pilot line, which is not done in this case since valve SV1 links the pilot line directly to the reservoir.

The insertion speed is determined by two valves, V2 and V3. V2 is a small flow control valve used for slower insertions. With V3 closed and V2 opened to various degrees, and with pressures ranging from 200 to 600 psi, insertion speeds from 0.93 inch per second to 18.4 ips are possible.

When V2 is closed, V3 is used for high speed insertions. V3 provides speeds from 48.0 ips at 200 psi, to the maximum of 100 ips, at about 610 psi.

In order to insert the control rod, valves SV1 and SV2 are energized. This switches incoming oil pressure to the pilot-operated check valve V1, thus opening it, and at the same time ceases applying pressure to the accumulator. The check valves V4 and V5 prevent oil from returning down their respective lines. The oil under pressure in the accumulator is now able to go directly to the top of the cylinder through check valve V3, forcing out the drive rod. The oil forced from the bottom of the cylinder now flows through check valve V7 and valve SV2 to the reservoir.

The withdrawal speed of the cylinder is determined by the valves V8 and V9. The oil, on withdrawal, is forced to pass through these valves and by the check valves V6 and V7. These redundant and independent valves

maintain the preselected rate of positive reactivity insertion at safe levels. Pressure drops and, therefore, any possible component failures are monitored by gauges G1, G2, and G3. Gauge G4 is used to monitor system pressure.

On withdrawal, valves SV1, SV3, and SV4 are energized. This allows the pilot-operated valve V1 to remain open so the oil can return to the accumulator. SV4 is closed, thereby preventing loss of oil to the reservoir. SV3 diverts incoming oil to the bottom of the cylinder forcing the piston to withdraw the drive rod. After withdrawal, the solenoid valves are de-energized and the accumulator recharges.

APPENDIX B

EXPERIMENTAL RESULTS

Table 12 presents a summary of the various reactor parameters, as noted prior to each experiment on an experimental log, while Table 13 identifies the experimental detector positions. Figure 34 represents the reactor power history, in histogram form, for the two days of the reported experiments. Tables 14 through 21 comprise tabular summaries of the NTG control rod position and fractional changes in detector current for each neutron detector versus time. These tables summarize the 18-element core experiments. The relative value of the flux at each detector position initially can be inferred from the axial flux traverses and radial flux ratios presented in Chapter V. The errors in these results will now be discussed.

Consider first, the error in the axial flux shapes and radial flux ratios. The axial flux shapes were all obtained in the same fashion. One detector was positioned at the core mid-plane, and the other traversed axially while the voltage readings of the electrometers were obtained with digital voltmeters. The principal source of error in these measurements arises from the positioning of the detectors accurately in both the radial and axial directions. The errors of the detectors and electrometers are small compared to the positioning errors; the inaccuracies in the detection system will be further discussed in the section with the kinetics portion of the experiments.

It is estimated that the error in positioning the detectors in the axial direction is approximately plus or minus one-half inch. This was due to the visual means of positioning the detectors, and the fact that the detector cables were not perfectly straight at all times. This discrepancy will give rise to varying errors in the measured flux, which will depend on the flux gradient at the detector location. Thus, at the core mid-plane, a one-half inch positioning error gives rise to only one percent error in the flux level, while at the core boundaries, the regions with the steepest gradients, the error is about 10 percent.

The radial positioning error depends on the type of detector holder. The holder in V-10 had a small diameter and was constrained by a plenum plug so the radial error was less than plus or minus one-fourth inch. The holder in V-23 had no plenum plug to constrain the end, and had a larger inside diameter. The error there was about plus or minus one inch. The resulting error in the V-10 measured flux is negligible with the NTG rod withdrawn since the flux is essentially flat in that region. When the rod is inserted the error could be as large as five percent due to the increased radial flux gradient. The positioning error at V-23 accounts for approximately a three percent error in the measured flux at that position whether the NTG rod is withdrawn or extended.

Leaving one detector at the core mid-plane was necessary to provide a normalization point for the detector which was being traversed. Using standard means of combining error such as those discussed by Bevington,[61] the percentage errors in the axial flux shapes are summarized in Table 10.

Table 10. Percentage Errors in Axial Flux Shapes

Rod Position	V-10		V-23	
	Core Mid-Plane	Core Limits	Core Mid-Plane	Core Limits
Withdrawn*	± 1.5%	± 3.3%	± 4.4%	± 12.5%
50% Inserted	± 2.3%	± 13.0%	± 4.4%	± 12.5%

*100% inserted shape is essentially the same as the withdrawn shape and the errors are similar.

The radial flux ratios are subject to the same position errors previously discussed. While the ratios for the NTG rod withdrawn were directly measured, as above, the inserted ratios were obtained from kinetics data and have the additional error due to the data acquisition system. The errors in the radial measurements are given in Table 11. The errors of the data acquisition system will be discussed later, but are included in the radial error estimates.

Table 11. Percentage Errors in Radial Flux Ratios at Core Mid-Plane

Rod Position	Flux Relative to V-10	
	V-10	V-23
Withdrawn	± 1.5%	± 3.4%
100% Inserted	± 3.2%	± 5.2%

The data acquisition system used in obtaining the flux levels during the kinetics experiments has sources of inaccuracy in addition to the de-

tector positioning errors discussed. These include statistical neutron level fluctuations, electrometer noise, non-logarithmic response, and ADC errors. Errors in the calibration procedure used to associate a power, or detector current, to a digital output further complicate the question of errors.

As discussed in Chapter III, care was taken to perform the experiments at power levels where detector response was linear. The power level from which the subcritical transients were initiated was, therefore, 50 kilowatts. The detector response was quite linear throughout this region until the power decreased to below about one kilowatt. Below this point the gamma background increased in proportion to the neutron level and caused departure from linear behavior. Above one kilowatt, the region of interest in the experiments, the gamma background was completely negligible in comparison to other errors.

Statistical fluctuations in neutron population near the detector and random noise in the electrometers were responsible for an error with a standard deviation of less than 0.1 percent, respectively. Prior to the experiments the electrometers were adjusted so as to respond logarithmically over four decades of linear input. During the course of calibrating the electrometers it was determined that the output was logarithmically proportional to the input to within 0.4 percent. The ADC unit provided the last major source of error in the series of components comprising a detector channel. Analyzing the response of the ADC to known input voltages, a variation of less than plus or minus four was found in about 65 percent of the tests, regardless of the voltage input. This corresponds to an error in the worst case of approximately 0.4 percent. Thus, the

total error in determining a digital output proportional to the neutron flux surrounding the detector is approximately 0.6 percent. The detector positioning error causes a much larger uncertainty in relating the digital output to a proportional neutron flux. The result for a typical neutron detection channel is a range of errors from approximately 2 to 13 percent, depending on detector location and flux shape during the subcritical transient.

In Chapter III the reactor power calibration procedure was explained. The purpose of the procedure was to provide means of associating a digital output to a given reactor power, as determined by the reactor linear power channel. For a given power, as determined by the reactor channel, the power as determined from the ADC output generally varied by about two percent. Figure 22 shows the deviation in the power calibration points. Since the final result was to be relative to the initial power, the total error in calculating the fractional change in power could be as much as 18 percent depending on detector position and the flux gradient. The power calibration also has the inherent problem of trying to relate kinetics responses of a subcritical transient to the static responses of a critical reactor. Since only the fractional change is of concern, the power calibration scheme was replaced with one which associated a detector current, which has been seen to be very proportional to the neutron flux, with the digital output. Table 2 shows that the digital output is quite linear with respect to test voltage inputs with the error being less than one percent. While the error is only slightly better than with the power calibration, the current calibration scheme is simpler since fewer points are required; and since the error in associating a detector current with

the flux about the detector is quite small, the current calibration procedure provides a better idea of how the local flux is responding to a perturbation than does a power calibration. Therefore, the maximum error in fractional change in current, or flux, for a detector located at the axial boundaries of the core, would be approximately 18 percent and less than five percent for detectors located at the mid-plane.

The final consideration of error in the experimental system is the accuracy of the NTG control rod position. This position must be correctly known to provide reactivity estimates for the theoretical analysis. The cable and pulley system described earlier for position indication was photographically verified to be quite accurate. Voltage output was proportional to the position of the rod with less than one percent error, while the ADC error of plus or minus four is of the same magnitude. The total error in ascertaining the rod position with the data acquisition system was, therefore, a maximum of about one percent throughout the rod motion.

Table 12. Reactor Conditions Prior to Kinetics Experiments

Experiment I.D.	Shim Blade Position (degrees)				Regulating Rod Position (inches)	Core D_2O Temperature (°C)
	1	2	3	4		
101	26.5	26.6	26.6	26.6	6.25	20.3
102	26.6	26.9	26.8	26.9	4.00	21.1
103	26.2	26.0	26.0	26.0	7.40	20.8
201	26.0	26.5	26.9	27.1	4.25	20.6
202	26.4	26.5	26.5	26.5	5.85	20.2
203	26.5	26.5	26.5	26.5	3.65	20.7
204	26.6	26.6	26.6	26.6	6.10	21.0
205	26.7	27.1	27.2	26.9	3.00	21.2

Table 13. Experimental Detector Positions

Experiment I.D.	Detector Positions with Respect to Core Mid-Plane (inches)			
	1 (V-10)	2 (V-10)	3 (V-23)	4 (V-23)
101	+ 9	0	0	+ 9
102	+ 9	0	0	+ 9
103	- 6	0	0	- 6
201	- 6	0	0	- 6
202	+ 12	0	0	+ 12
203	+ 12	0	0	+ 12
204	+ 6	0	0	+ 6
205	+ 6	0	0	+ 6

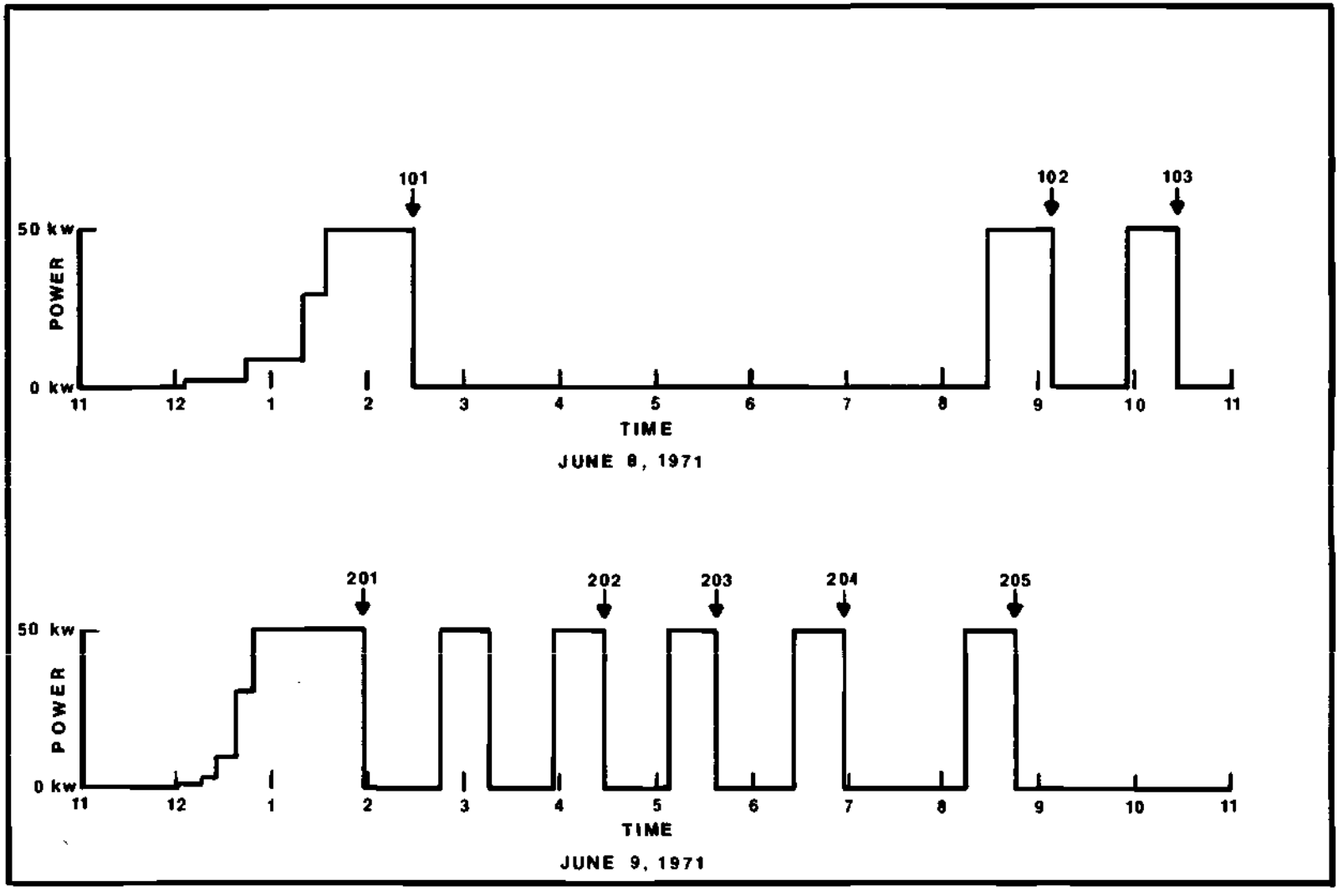

Figure 34. Power Histogram for June 8 and 9, 1971

Table 14. Representative Results of Experiment 101. A 1.35 Second Insertion

Time (sec)	Depth (cm)	Fractional Changes for Detectors 1	2	3	4
.00	.00	1.00000	1.00000	1.00000	1.00000
.05	.71	1.00836	1.00382	.99494	.99878
.10	2.37	.98992	.98443	.98825	.98695
.15	3.72	.96928	.96784	.97139	.97067
.20	2.75	.96397	.96010	.96429	.96130
.25	2.10	.96047	.95569	.95965	.95842
.30	2.74	.92896	.87623	.92570	.91941
.35	7.28	.69971	.49733	.71771	.68586
.40	15.04	.36197	.24702	.41421	.38653
.45	24.32	.14985	.13081	.22569	.20723
.50	34.15	.09389	.08843	.15240	.13898
.55	43.91	.07501	.07254	.12380	.11302
.60	53.97	.06765	.06577	.11141	.10215
.65	62.67	.06433	.06335	.10650	.09755
.70	66.75	.06293	.06250	.10452	.09600
.75	69.31	.06270	.06143	.10309	.09440
.80	71.02	.06208	.06076	.10234	.09353
.85	71.67	.06085	.06018	.10099	.09231
.90	72.48	.06001	.05948	.09963	.09125
.95	72.51	.05920	.05888	.09818	.08991
1.00	72.68	.05839	.05809	.09693	.08865
1.05	72.96	.05828	.05754	.09615	.08765
1.10	73.27	.05828	.05682	.09521	.08703
1.15	74.15	.05723	.05620	.09417	.08607
1.20	74.27	.05599	.05566	.09301	.08502
1.25	74.55	.05517	.05493	.09183	.08394
1.30	76.25	.05467	.05453	.09105	.08333
1.35	79.41	.05389	.05371	.08977	.08207
1.40	78.53	.05402	.05354	.08935	.08177
1.45	78.30	.05334	.05302	.08866	.08102
1.50	77.40	.05271	.05256	.08777	.08025
2.00	76.14	.04819	.04828	.08069	.07366
2.50	76.15	.04525	.04491	.07517	.06859
3.00	76.17	.04350	.04197	.07028	.06405
3.50	76.17	.03949	.03944	.06608	.06002
4.00	76.18	.03758	.03730	.06254	.05671
4.50	76.19	.03545	.03536	.05933	.05377
4.95	76.19	.03387	.03382	.05696	.05125

Table 15. Representative Results of Experiment 102. A 2.62 Second Insertion

Time (sec)	Depth (cm)	Fractional Changes for Detectors 1	2	3	4
.00	.00	1.00000	1.00000	1.00000	1.00000
.05	.92	1.02823	1.01021	1.00496	1.01131
.10	1.87	1.00131	.98639	.98874	.98097
.15	2.64	.97955	.96688	.98014	.96121
.20	1.91	.97417	.95695	.97454	.95281
.25	1.52	.97327	.95148	.96987	.94559
.30	2.25	.96200	.94107	.95666	.93475
.35	5.38	.81622	.87407	.88877	.84287
.40	9.81	.67503	.74668	.78542	.72404
.45	13.31	.56116	.65528	.68924	.63347
.50	15.13	.43842	.56372	.59569	.54309
.55	16.25	.34687	.47661	.50871	.45953
.60	18.09	.28149	.40178	.43393	.38965
.65	20.31	.23392	.34041	.37221	.33209
.70	22.71	.19861	.28967	.32287	.28569
.75	25.20	.17278	.24826	.28395	.24927
.80	27.72	.14984	.21216	.25165	.22043
.85	30.23	.13316	.17949	.22598	.19665
.90	32.71	.11988	.14708	.20443	.17718
.95	35.15	.10889	.11946	.18660	.16095
1.00	37.56	.09937	.10151	.17153	.14746
1.05	39.92	.09270	.09023	.15859	.13603
1.10	42.22	.08483	.08197	.14757	.12599
1.15	44.50	.07922	.07574	.13808	.11794
1.20	47.01	.07444	.07052	.12963	.11039
1.25	50.77	.07059	.06643	.12289	.10463
1.30	52.34	.06795	.06347	.11755	.10003
1.35	53.81	.06466	.06070	.11246	.09582
1.40	55.48	.06188	.05822	.10811	.09190
1.45	57.27	.06021	.05594	.10400	.08862
1.50	59.08	.05763	.05411	.10053	.08561
1.55	60.92	.05601	.05241	.09753	.08300
1.60	62.76	.05440	.05108	.09493	.08090
1.65	64.59	.05322	.05010	.09293	.07887
1.70	67.94	.05221	.04908	.09043	.07716
1.75	70.98	.05221	.04841	.08921	.07603
1.80	71.40	.05221	.04781	.08821	.07522
1.85	71.31	.05193	.04728	.08735	.07429
1.90	72.21	.05049	.04681	.08633	.07347
1.95	71.98	.04972	.04628	.08537	.07269
2.00	72.47	.04898	.04585	.08457	.07199
2.05	72.46	.04861	.04549	.08388	.07148
2.10	72.56	.04835	.04510	.08307	.07077

Table 15. Representative Results of Experiment 102. A 2.62 Second Insertion (Concluded)

Time (sec)	Depth (cm)	Fractional Changes for Detectors			
		1	2	3	4
2.15	72.75	.04752	.04470	.08231	.07007
2.20	73.01	.04691	.04419	.08145	.06929
2.25	73.27	.04653	.04373	.08065	.06858
2.30	73.57	.04611	.04340	.07999	.06810
2.35	73.87	.04544	.04295	.07928	.06730
2.40	74.19	.04519	.04249	.07848	.06670
2.45	74.52	.04510	.04214	.07785	.06611
2.50	74.83	.04510	.04177	.07718	.06558
2.55	75.14	.04462	.04149	.07665	.06507
2.60	76.22	.04413	.04142	.07600	.06456
2.65	78.16	.04349	.04111	.07524	.06389
2.70	77.98	.04305	.04089	.07495	.06355
2.75	77.25	.04278	.04060	.07431	.06314
2.80	76.82	.04251	.04022	.07386	.06279
2.85	76.57	.04219	.04005	.07333	.06238
2.90	76.43	.04200	.03986	.07291	.06193
2.95	76.34	.04185	.03963	.07240	.06159
3.00	76.28	.04173	.03927	.07190	.06105
3.50	76.20	.03908	.03698	.06765	.05735
4.00	76.20	.03662	.03496	.06384	.05396
4.50	76.21	.03473	.03319	.06047	.05092
4.95	76.21	.03342	.03176	.05770	.04861

Table 16. Representative Results of Experiment 103. A 1.66 Second Insertion

Time (sec)	Depth (cm)	Fractional Changes for Detectors 1	2	3	4
.00	.00	1.00000	1.00000	1.00000	1.00000
.05	1.60	.99871	.99348	.98796	.99433
.10	5.99	.97957	.98504	.98339	.98113
.15	5.94	.97951	.97977	.98075	.97514
.20	4.06	.96889	.97216	.97314	.96684
.25	3.13	.95266	.96070	.95775	.94940
.30	4.01	.94031	.93826	.93799	.92938
.35	8.07	.72939	.73372	.73676	.71930
.40	15.74	.41334	.38290	.42762	.40985
.45	25.04	.20980	.14427	.23194	.21673
.50	34.91	.11776	.08886	.15496	.14174
.55	44.68	.08127	.07225	.12552	.11345
.60	54.57	.07085	.06518	.11274	.10137
.65	61.52	.06880	.06366	.10992	.09829
.70	65.04	.06830	.06263	.10817	.09627
.75	67.41	.06805	.06124	.10640	.09470
.80	69.02	.06659	.06015	.10480	.09312
.85	70.18	.06466	.05944	.10325	.09160
.90	71.04	.06377	.05871	.10182	.09043
.95	71.74	.06291	.05780	.10061	.08900
1.00	72.32	.06200	.05698	.09929	.08781
1.05	72.84	.06109	.05626	.09793	.08671
1.10	73.30	.06021	.05556	.09672	.08565
1.15	73.75	.05949	.05492	.09553	.08465
1.20	74.17	.05900	.05435	.09444	.08360
1.25	74.58	.05879	.05378	.09341	.08272
1.30	74.97	.05795	.05330	.09252	.08163
1.35	75.29	.05632	.05306	.09159	.08083
1.40	75.59	.05581	.05265	.09071	.08001
1.45	75.78	.05525	.05213	.08978	.07931
1.50	75.90	.05505	.05149	.08896	.07849
1.55	75.98	.05474	.05100	.08819	.07777
1.60	76.03	.05435	.05060	.08744	.07716
1.65	76.07	.05351	.05024	.08657	.07647
1.70	76.10	.05307	.04984	.08577	.07570
1.75	76.12	.05283	.04934	.08511	.07509
1.80	76.12	.05235	.04890	.08441	.07452

Table 16. Representative Results of Experiment 103. A 1.66 Second Insertion (Concluded)

Time (sec)	Depth (cm)	Fractional Changes for Detectors			
		1	2	3	4
1.85	76.13	.05188	.04847	.08383	.07377
1.90	76.14	.05126	.04816	.08307	.07290
1.95	76.15	.05098	.04779	.08235	.07242
2.00	76.15	.05098	.04737	.08180	.07183
2.50	76.17	.04717	.04394	.07601	.06664
3.00	76.19	.04404	.04113	.07109	.06215
3.50	76.19	.04116	.03880	.06698	.05854
4.00	76.20	.03893	.03674	.06329	.05531
4.50	76.20	.03730	.03490	.06012	.05222
4.95	76.20	.03530	.03336	.05750	.04974

Table 17. Representative Results of Experiment 201, A 2.63 Second Insertion

Time (sec)	Depth (cm)	Fractional Changes for Detectors 1	2	3	4
.00	.00	1.00000	1.00000	1.00000	1.00000
.05	.86	1.01346	1.01324	1.00593	1.01088
.10	1.85	.98224	1.00079	.98674	.98022
.15	3.24	.97796	1.00103	.99156	.98611
.20	2.28	.96906	.99261	.98457	.97777
.25	2.19	.96458	.98921	.98009	.97262
.30	3.28	.94112	.96792	.95528	.94853
.35	6.24	.87305	.89246	.87909	.86263
.40	7.78	.76018	.79011	.77816	.75368
.45	9.91	.67360	.70369	.69002	.66682
.50	12.87	.59393	.62309	.61176	.58907
.55	14.38	.51543	.54231	.53681	.51422
.60	16.30	.45319	.46936	.46774	.44542
.65	18.42	.39492	.40779	.40962	.38851
.70	20.65	.34623	.35533	.36100	.34112
.75	22.91	.30616	.31140	.32078	.30149
.80	25.16	.27426	.27323	.28735	.26841
.85	27.41	.24651	.23921	.25874	.24152
.90	29.63	.22144	.20773	.23496	.21831
.95	31.84	.20188	.17610	.21459	.19876
1.00	34.02	.18321	.14602	.19739	.18144
1.05	36.17	.16734	.12348	.18230	.16674
1.10	38.31	.15324	.10874	.16911	.15426
1.15	40.42	.14185	.09858	.15758	.14340
1.20	42.47	.12763	.09091	.14775	.13398
1.25	44.54	.11756	.08460	.13920	.12570
1.30	46.55	.10672	.07947	.13192	.11864
1.35	49.14	.09682	.07523	.12523	.11233
1.40	51.94	.08772	.07164	.11964	.10714
1.45	53.27	.08108	.06853	.11466	.10229
1.50	54.78	.07431	.06581	.11005	.09810
1.55	56.42	.07003	.06364	.10605	.09416
1.60	58.19	.06652	.06162	.10257	.09093
1.65	59.91	.06355	.05983	.09934	.08795
1.70	61.70	.06165	.05827	.09677	.08531
1.75	63.47	.05933	.05689	.09428	.08308
1.80	65.27	.05751	.05573	.09203	.08109
1.85	66.90	.05605	.05482	.09030	.07945
1.90	68.14	.05534	.05404	.08923	.07834
1.95	69.12	.05443	.05329	.08820	.07727
2.00	69.94	.05394	.05264	.08700	.07641
2.05	70.60	.05379	.05215	.08623	.07566
2.10	71.17	.05306	.05165	.08539	.07449

Table 17. Representative Results of Experiment 201. A 2.63 Second Insertion (Concluded)

Time (sec)	Depth (cm)	Fractional Changes for Detectors 1	2	3	4
2.15	71.69	.05229	.05121	.08453	.07398
2.20	72.17	.05177	.05068	.08373	.07327
2.25	72.62	.05106	.05026	.08285	.07255
2.30	73.07	.05064	.04982	.08210	.07187
2.35	73.50	.05027	.04940	.08130	.07110
2.40	73.94	.04999	.04904	.08061	.07037
2.45	74.38	.04945	.04864	.07990	.06980
2.50	74.81	.04887	.04832	.07926	.06933
2.55	75.42	.04820	.04817	.07858	.06864
2.60	76.96	.04741	.04792	.07791	.06795
2.65	76.66	.04698	.04755	.07731	.06758
2.70	76.45	.04676	.04720	.07682	.06704
2.75	76.33	.04655	.04680	.07635	.06654
2.80	76.26	.04655	.04658	.07586	.06606
2.85	76.20	.04646	.04625	.07531	.06555
2.90	76.19	.04646	.04604	.07485	.06509
2.95	76.16	.04646	.04567	.07444	.06458
3.00	76.15	.04597	.04529	.07379	.06424
3.50	76.16	.04186	.04257	.06927	.06002
4.00	76.18	.03974	.04009	.06540	.05648
4.50	76.19	.03737	.03792	.06187	.05332
4.95	76.20	.03570	.03636	.05907	.05089

Table 19. Representative Results of Experiment 203, A 2.23 Second Insertion

Time (sec)	Depth (cm)	Fractional Changes for Detectors 1	2	3	4
.00	.00	1.00000	1.00000	1.00000	1.00000
.05	.95	1.00083	.99624	.99663	.99739
.10	1.65	.98351	.99080	.99256	.98804
.15	2.79	.97103	.98224	.98512	.97745
.20	2.07	.96396	.97822	.98066	.97186
.25	1.75	.96042	.97270	.97385	.96414
.30	2.81	.89986	.95931	.95756	.94777
.35	6.09	.70871	.88694	.87852	.85747
.40	9.58	.56120	.77935	.76804	.73876
.45	11.37	.44642	.66080	.65162	.62130
.50	13.88	.35651	.54283	.53869	.50771
.55	16.77	.28501	.44055	.44332	.41406
.60	19.84	.23526	.35925	.36714	.33988
.65	22.99	.19511	.29540	.31012	.28463
.70	26.11	.16627	.24345	.26620	.24251
.75	29.22	.14452	.19706	.23261	.21073
.80	32.28	.12769	.15361	.20612	.18560
.85	35.29	.11328	.12355	.18488	.16558
.90	38.25	.10288	.10630	.16746	.14936
.95	41.15	.09396	.09481	.15319	.13625
1.00	44.08	.08654	.08631	.14134	.12576
1.05	47.22	.08086	.07957	.13171	.11679
1.10	49.86	.07633	.07422	.12381	.10978
1.15	52.32	.07218	.06979	.11706	.10379
1.20	54.81	.06882	.06651	.11161	.09898
1.25	57.38	.06691	.06384	.10652	.09480
1.30	49.84	.06357	.06169	.10263	.09115
1.35	62.30	.06133	.05977	.09922	.08808
1.40	64.73	.05966	.05819	.09656	.08585
1.45	66.70	.05906	.05714	.09490	.08432
1.50	68.13	.05826	.05626	.09348	.08315
1.55	69.22	.05763	.05545	.09212	.08203
1.60	70.10	.05721	.05461	.09097	.08106
1.65	70.78	.05632	.05397	.09000	.08015
1.70	71.35	.05555	.05339	.08904	.07929
1.75	71.88	.05510	.05285	.08811	.07837
1.80	72.36	.05489	.05239	.08721	.07760
1.85	72.80	.05420	.05194	.08636	.07679
1.90	73.24	.05371	.05155	.08544	.07603
1.95	73.67	.05322	.05101	.08464	.07520
2.00	74.09	.05292	.05045	.08381	.07462
2.05	74.51	.05249	.04997	.08314	.07393
2.10	74.93	.05225	.04961	.08239	.07336

Table 19. Representative Results of Experiment 203. A 2.23 Second Insertion (Concluded)

Time (sec)	Depth (cm)	Fractional Changes for Detectors 1	2	3	4
2.15	76.25	.05140	.04928	.08129	.07238
2.20	77.73	.05102	.04919	.08090	.07193
2.25	77.07	.05097	.04874	.08022	.07155
2.30	76.69	.05083	.04830	.07960	.07093
2.35	76.48	.05083	.04788	.07914	.07042
2.40	76.33	.05028	.04758	.07853	.06999
2.45	76.25	.04955	.04736	.07796	.06932
2.50	76.22	.04902	.04700	.07734	.06889
3.00	76.16	.04555	.04380	.07217	.06400
3.50	76.19	.04269	.04124	.06786	.05996
4.00	76.19	.04022	.03913	.06403	.05662
4.50	76.20	.03807	.03712	.06062	.05351
4.95	76.20	.03671	.03547	.05791	.05103

Table 20. Representative Results of Experiment 204. A 1.33 Second Insertion

Time (sec)	Depth (cm)	Fractional Changes for Detectors 1	2	3	4
.00	.00	1.00000	1.00000	1.00000	1.00000
.05	1.90	.99128	.99355	.99014	.98877
.10	4.89	.96660	.98214	.97269	.96839
.15	3.91	.96164	.98134	.97521	.97071
.20	2.80	.95554	.96976	.97053	.96295
.25	3.25	.92562	.94705	.93635	.92802
.30	5.94	.89765	.92748	.92449	.91360
.35	10.16	.58276	.69820	.70347	.67095
.40	17.45	.25416	.35965	.40363	.37368
.45	26.36	.13337	.14487	.22207	.20048
.50	37.04	.09056	.09096	.15027	.13442
.55	46.88	.07405	.07449	.02340	.11007
.60	55.72	.06766	.06776	.11208	.09984
.65	62.40	.05966	.06010	.09784	.09729
.70	65.72	.06464	.06553	.10722	.09511
.75	67.84	.06323	.06423	.10549	.09336
.80	69.30	.06259	.06320	.10391	.09196
.85	70.36	.06186	.06207	.10255	.09060
.90	71.17	.06096	.06124	.10111	.08938
.95	71.82	.06012	.06017	.09969	.08793
1.00	72.39	.05947	.05927	.09835	.08691
1.05	72.88	.05871	.05859	.09726	.08582
1.10	73.34	.05812	.05794	.09602	.08482
1.15	73.77	.05754	.05725	.09487	.08361
1.20	74.18	.05687	.05674	.09394	.08271
1.25	74.58	.05578	.05627	.09290	.08182
1.30	74.98	.05512	.05593	.09189	.08102
1.35	77.65	.05383	.05510	.08993	.07924
1.40	77.16	.05412	.05504	.08989	.07922
1.45	76.73	.05372	.05451	.08897	.07862
1.50	76.48	.05329	.05389	.08824	.07781
2.00	76.15	.05020	.04943	.08113	.07133
2.50	76.17	.04523	.04599	.07559	.06628
3.00	76.19	.04231	.04299	.07068	.06177
3.50	76.20	.03983	.04058	.06653	.05793
4.00	76.20	.03746	.03855	.06284	.05470
4.50	76.20	.03543	.03664	.05964	.05197
4.95	76.21	.03410	.03511	.05785	.04960

Table 21. Representative Results of Experiment 205. A 2.21 Second Insertion

Time (sec)	Depth (cm)	Fractional Changes for Detectors 1	2	3	4
.00	.00	1.00000	1.00000	1.00000	1.00000
.05	.95	1.00677	1.00829	1.00364	1.01054
.10	3.30	.97231	.97595	.96065	.96448
.15	4.76	1.00491	.99321	.98933	.99308
.20	3.20	1.00491	.98892	.98368	.99011
.25	3.83	1.00130	.98239	.97564	.98109
.30	6.34	.96056	.96278	.95531	.05679
.35	8.30	.84245	.88183	.86999	.85823
.40	10.79	.71788	.77098	.76011	.73810
.45	13.51	.59643	.66392	.65429	.63084
.50	15.37	.47371	.55579	.55282	.52826
.55	17.23	.36648	.46010	.46273	.43839
.60	19.61	.28116	.38206	.39060	.36640
.65	22.24	.22473	.31950	.33377	.31083
.70	24.95	.18566	.26827	.28840	.26662
.75	27.74	.15952	.22389	.25311	.23252
.80	30.50	.13938	.18238	.22475	.20511
.85	33.26	.12384	.14616	.20150	.18278
.90	36.00	.11124	.12178	.18252	.16484
.95	38.72	.10087	.10644	.16663	.14961
1.00	41.38	.09350	.09558	.15312	.13729
1.05	44.58	.08586	.08721	.14200	.12700
1.10	49.07	.07987	.08039	.13203	.11804
1.15	53.10	.07539	.07559	.12489	.11137
1.20	55.02	.07201	.07138	.11853	.10559
1.25	56.00	.06823	.06785	.11300	.10051
1.30	57.57	.06530	.06500	.10813	.09624
1.35	59.43	.06295	.06247	.10413	.09252
1.40	61.43	.06136	.06031	.10067	.08949
1.45	63.53	.05915	.05860	.09783	.08688
1.50	66.17	.05765	.05694	.09498	.08427
1.55	70.63	.05672	.05603	.09334	.08293
1.60	70.80	.05635	.05544	.09243	.08205
1.65	70.88	.05538	.05474	.09136	.08117
1.70	71.13	.05488	.05413	.09034	.08017
1.75	71.45	.05418	.05348	.08932	.07928
1.80	71.80	.05378	.05287	.08838	.07853
1.85	72.19	.05378	.05239	.08754	.07764
1.90	72.58	.05378	.05179	.08664	.07684
1.95	72.98	.05349	.05128	.08580	.07617
2.00	73.39	.05258	.05096	.08506	.07539
2.05	73.80	.05106	.05047	.08417	.07462
2.10	74.21	.05031	.05004	.08342	.07395

Table 21. Representative Results of Experiment 205. A 2.21 Second Insertion (Concluded)

Time (sec)	Depth (cm)	Fractional Changes for Detectors 1	2	3	4
2.15	74.62	.04989	.04960	.08268	.07334
2.20	75.79	.04726	.04710	.07756	.06906
2.25	78.93	.04837	.04851	.08033	.07127
2.30	78.20	.04836	.04865	.08063	.07137
2.35	77.37	.04806	.04823	.07995	.07088
2.40	76.89	.04784	.04779	.07935	.07026
2.45	76.59	.04745	.04742	.07879	.06983
2.50	76.41	.04710	.04710	.07819	.06919
2.55	76.31	.04671	.04683	.07771	.06878
2.60	76.25	.04654	.04647	.07705	.06825
2.65	76.22	.04645	.04614	.07660	.06778
2.70	76.20	.04629	.04576	.07604	.06727
2.75	76.19	.04562	.04552	.07548	.06685
2.80	76.18	.04529	.04522	.07499	.06629
2.85	76.18	.04487	.04498	.07446	.06592
2.90	76.17	.04454	.04457	.07405	.06549
2.95	76.17	.04426	.04431	.07366	.06516
3.00	76.17	.04390	.04404	.07318	.06465
3.50	76.19	.04132	.04139	.06871	.06057
4.00	76.20	.03970	.03914	.06487	.05710
4.50	76.20	.03716	.03723	.06149	.05406
4.95	76.20	.03518	.03557	.05876	.05154

APPENDIX C

ANALYTICAL RESULTS

Table 22 summarizes the mathematical controls used in all kinetics simulations. Tables 23 through 25 present tabular summaries of results for full "space-time" or standard simulations of the experiments 201, 202, and 203, experiments whose times of insertions were typical of those undertaken. Tables 26 through 28 represent tabular summaries of the adiabatic simulations of these same experiments, while Tables 29 through 31 represent the "mixed-methods" simulations, where the fast group was treated adiabatically and the thermal group was treated with the space-time method. The detector positions correspond to those listed in Table 13 for the reported experiments, and the relative initial flux values for each detector position can be inferred from the analytical flux shapes and ratios presented in Chapter V.

Table 22. KINET Mathematical Controls Used in Experimental Simulations

Control	Value
Theta Weighting	1.000
Maximum Fractional Change in Flux per Time Step	.050
Maximum Time Step Allowed (sec)	.055
Minimum Time Step Allowed (sec)	.001
Over-Relaxation Time Step (sec)	.050
Print Time Step (sec)	.050
Fractional Error Allowed in Average Flux in Outer Iteration	.001

Table 23. Representative Results of the Space-Time Simulation of Experiment 201

Time (sec)	Depth (cm)	Prediction of Fractional Changes for Detectors 1	2	3	4
.00	.00	1.00000	1.00000	1.00000	1.00000
.05	.43	.99444	.99443	.99446	.99448
.10	.86	.98433	.98420	.98450	.98453
.15	1.29	.97171	.97136	.97198	.97203
.20	1.72	.95660	.95617	.95693	.95700
.25	2.32	.93668	.93499	.93624	.93683
.30	3.73	.90336	.90160	.90304	.90393
.35	5.90	.85643	.85199	.85524	.85693
.40	7.89	.80403	.79904	.80247	.80456
.45	10.14	.74516	.73924	.74355	.74637
.50	12.55	.66985	.66101	.66786	.67143
.55	14.42	.59864	.59027	.59660	.60000
.60	16.33	.54330	.53265	.54151	.54517
.65	18.46	.48807	.47441	.48642	.49046
.70	20.67	.43379	.41847	.43213	.43618
.75	22.90	.39107	.37518	.38947	.39347
.80	25.15	.35257	.32991	.35181	.35593
.85	27.40	.31223	.28617	.31218	.31619
.90	29.63	.28173	.25371	.28186	.28566
.95	31.83	.25739	.21882	.25933	.26300
1.00	33.99	.23181	.18308	.23575	.23926
1.05	36.16	.20995	.15537	.21505	.21833
1.10	38.31	.19337	.13519	.19980	.20291
1.15	40.40	.17487	.11724	.18609	.18894
1.20	42.47	.15813	.10186	.17213	.17471
1.25	44.59	.14533	.09006	.16116	.16350
1.30	46.77	.13043	.08176	.15237	.15444
1.35	49.24	.11085	.07518	.14301	.14475
1.40	51.46	.09607	.06940	.13388	.13534
1.45	53.16	.08736	.06593	.12847	.12976
1.50	54.83	.07934	.06341	.12448	.12557
1.55	56.48	.07249	.06095	.12008	.12096
1.60	58.18	.06652	.05865	.11582	.11652
1.65	59.93	.06153	.05667	.11214	.11268
1.70	61.70	.05794	.05489	.10896	.10936
1.75	63.47	.05555	.05323	.10595	.10621
1.80	65.24	.05344	.05183	.10321	.10333
1.85	66.85	.05173	.05067	.10092	.10093
1.90	68.11	.05045	.04979	.09917	.09910
1.95	69.10	.04946	.04904	.09770	.09756
2.00	69.86	.04870	.04840	.09644	.09625
2.05	70.49	.04804	.04784	.09531	.09507
2.10	71.12	.04743	.04730	.09422	.09398

Table 23. Representative Results of the Space-Time Simulation of Experiment 201 (Concluded)

Time (sec)	Depth (cm)	Prediction of Fractional Changes for Detectors 1	2	3	4
2.15	71.65	.04689	.04683	.09330	.09301
2.20	72.10	.04642	.04639	.09243	.09213
2.25	72.55	.04587	.04587	.09139	.09109
2.30	73.00	.04539	.04542	.09052	.09019
2.35	73.45	.04495	.04502	.08973	.08938
2.40	73.90	.04445	.04456	.08881	.08845
2.45	74.35	.04398	.04412	.08792	.08755
2.50	74.80	.04362	.04379	.08727	.08688
2.55	75.61	.04310	.04338	.08646	.08603
2.60	76.20	.04260	.04290	.08549	.08505
2.65	76.20	.04224	.04255	.08479	.08433
2.70	76.20	.04194	.04227	.08416	.08372
2.75	76.20	.04166	.04200	.08361	.08317
2.80	76.20	.04134	.04167	.08298	.08253
2.85	76.20	.04099	.04131	.08230	.08184
2.90	76.20	.04068	.04099	.08168	.08121
2.95	76.20	.04043	.04073	.08118	.08072
3.00	76.20	.04022	.04052	.08075	.08030
3.50	76.20	.03755	.03784	.07541	.07500
4.00	76.20	.03524	.03552	.07077	.07038
4.50	76.20	.03320	.03346	.06666	.06629
5.00	76.20	.03139	.03163	.06302	.06267

Table 24. Representative Results of the Space-Time Simulation of Experiment 202

Time (sec)	Depth (cm)	Prediction of Fractional Changes for Detectors 1	2	3	4
.00	.00	1.00000	1.00000	1.00000	1.00000
.05	.00	.99958	.99958	.99957	.99958
.10	.00	.99902	.99901	.99902	.99903
.15	.00	.99845	.99845	.99848	.99849
.20	.13	.99715	.99714	.99722	.99723
.25	1.41	.96947	.98389	.98438	.98347
.30	4.19	.81968	.93796	.94012	.93629
.35	8.46	.64972	.85496	.85943	.85206
.40	16.12	.40388	.67746	.69074	.67771
.45	25.58	.24591	.42974	.46325	.45033
.50	35.71	.14695	.20671	.28392	.27544
.55	48.17	.09578	.09697	.18459	.18027
.60	47.30	.07581	.07266	.14372	.14151
.65	62.55	.06962	.06572	.13069	.12933
.70	66.25	.06638	.06221	.12383	.12293
.75	68.14	.06495	.06052	.12050	.11980
.80	69.48	.06390	.05926	.11805	.11747
.85	70.40	.06292	.05818	.11589	.11542
.90	71.21	.06208	.05724	.11402	.11364
.95	71.80	.06132	.05643	.11239	.11205
1.00	72.38	.06065	.05568	.11092	.11062
1.05	72.85	.05993	.05493	.10942	.10915
1.10	73.31	.05927	.05423	.10803	.10780
1.15	73.73	.05868	.05360	.10678	.10659
1.20	74.15	.05806	.05295	.10548	.10533
1.25	74.55	.05746	.05232	.10423	.10410
1.30	74.94	.05691	.05173	.10306	.10297
1.35	76.20	.05645	.05103	.10170	.10173
1.40	76.20	.05581	.05048	.10055	.10061
1.45	76.20	.05532	.05003	.09965	.09971
1.50	76.20	.05481	.04957	.09873	.09879
2.00	76.20	.05027	.04545	.09052	.09057
2.50	76.20	.04652	.04207	.08379	.08383
3.00	76.20	.04334	.03919	.07807	.07812
3.50	76.20	.04061	.03672	.07315	.07319
4.00	76.20	.03815	.03450	.06872	.06775
4.50	76.20	.03603	.03259	.06490	.06494
5.00	76.20	.03414	.03087	.06149	.06152

Table 25. Representative Results of the Space-Time Simulation of Experiment 203

Time (sec)	Depth (cm)	Prediction of Fractional Changes for Detectors 1	2	3	4
.00	.00	1.00000	1.00000	1.00000	1.00000
.05	.77	.97998	.99069	.99073	.99076
.10	1.26	.96386	.97673	.97716	.97678
.15	1.47	.94755	.96480	.96515	.96417
.20	1.67	.92937	.95555	.95565	.95461
.25	1.95	.90799	.94395	.94459	.94350
.30	3.25	.82900	.91378	.91503	.91230
.35	6.15	.70384	.86175	.86476	.85899
.40	9.16	.58173	.79099	.79459	.78698
.45	11.47	.47683	.70552	.71189	.70237
.50	13.93	.38981	.62220	.62937	.61931
.55	16.82	.32197	.54440	.55500	.54413
.60	19.88	.26470	.46089	.47469	.46364
.65	22.98	.22130	.39028	.40640	.39594
.70	26.12	.18620	.32438	.34962	.33973
.75	29.21	.15803	.27070	.29961	.29064
.80	32.27	.13826	.21940	.26479	.25671
.85	35.28	.12108	.17356	.23257	.22552
.90	38.24	.10844	.14223	.20871	.20241
.95	41.16	.09841	.11606	.18985	.18442
1.00	44.11	.08938	.09661	.17192	.16732
1.05	46.97	.08267	.08484	.15887	.15482
1.10	49.72	.07684	.07687	.14710	.14382
1.15	52.34	.07204	.07110	.13754	.13469
1.20	54.85	.06876	.06654	.13074	.12839
1.25	57.35	.06566	.06301	.12432	.12236
1.30	59.83	.06302	.06004	.11883	.11723
1.35	62.30	.06095	.05764	.11448	.11320
1.40	64.52	.05912	.05559	.11072	.10962
1.45	66.48	.05770	.05407	.10771	.10683
1.50	68.09	.05681	.05295	.10549	.10477
1.55	69.05	.05610	.05211	.10382	.10324
1.60	69.74	.05552	.05145	.10250	.10200
1.65	70.42	.05496	.05082	.10124	.10081
1.70	71.10	.05441	.05019	.10000	.09963
1.75	71.79	.05386	.04957	.09876	.09841
1.80	72.36	.05343	.04905	.09772	.09741
1.85	72.81	.05301	.04859	.09683	.09656
1.90	73.23	.05257	.04810	.09586	.09562
1.95	73.66	.05202	.04753	.09471	.09448
2.00	74.09	.05165	.04710	.09385	.09366
2.05	74.52	.05126	.04668	.09301	.09286
2.10	74.91	.05087	.04624	.09217	.09205

Table 25. Representative Results of the Space-Time Simulation of Experiment 203 (Concluded)

Time (sec)	Depth (cm)	Prediction of Fractional Changes for Detectors			
		1	2	3	4
2.15	75.65	.05045	.04569	.09107	.09099
2.20	76.20	.05003	.04519	.09008	.09005
2.25	76.20	.04959	.04484	.08937	.08939
2.30	76.20	.04921	.04452	.08865	.08870
2.35	76.20	.04878	.04414	.08791	.08794
2.40	76.20	.04845	.04382	.08730	.08733
2.45	76.20	.04813	.04352	.08671	.08674
2.50	76.20	.04778	.04321	.08609	.08611
3.00	76.20	.04435	.04011	.07992	.07997
3.50	76.20	.04146	.03749	.07468	.07473
4.00	76.20	.03902	.03528	.07026	.07030
4.50	76.20	.03682	.03330	.06631	.06634
5.00	76.20	.03484	.03151	.06276	.06279

Table 26. Representative Results of the Adiabatic Simulation of Experiment 201

Time (sec)	Depth (cm)	Prediction of Fractional Changes for Detectors 1	2	3	4
.00	.00	1.00000	1.00000	1.00000	1.00000
.05	.43	.99611	.99579	.99595	.99610
.10	.86	.98957	.98894	.98926	.98954
.15	1.29	.98108	.98015	.98062	.98105
.20	1.72	.96963	.96840	.96902	.96959
.25	2.32	.95416	.95253	.95335	.95411
.30	3.73	.92981	.92725	.92854	.92972
.35	5.90	.89761	.89370	.89567	.89747
.40	7.89	.86570	.86067	.86321	.86553
.45	10.14	.81665	.80910	.81355	.81665
.50	12.55	.75505	.74547	.75146	.75519
.55	14.42	.69745	.68673	.69361	.69768
.60	16.33	.64241	.62957	.63857	.64298
.65	18.46	.57887	.56334	.57523	.57992
.70	20.67	.51773	.50018	.51431	.51918
.75	22.90	.46560	.44650	.46237	.46736
.80	25.15	.41241	.38795	.41036	.41528
.85	27.40	.36349	.33533	.36237	.36716
.90	29.63	.32375	.29282	.32337	.32803
.95	31.83	.28972	.25020	.29095	.29538
1.00	33.99	.25758	.20816	.26066	.26477
1.05	36.16	.23127	.17386	.23584	.23970
1.10	38.31	.21098	.14667	.21681	.22048
1.15	40.40	.18895	.12707	.19880	.20207
1.20	42.47	.17033	.11004	.18325	.18621
1.25	44.59	.15497	.09570	.17069	.17337
1.30	46.77	.13862	.08573	.16012	.16251
1.35	49.24	.11850	.07850	.14928	.15129
1.40	51.46	.10211	.07244	.14006	.14176
1.45	53.16	.09088	.06828	.13372	.13520
1.50	54.83	.08326	.06546	.12875	.13001
1.55	56.48	.07585	.06238	.12309	.12412
1.60	58.18	.06945	.05997	.11874	.11957
1.65	59.93	.06356	.05790	.11504	.11567
1.70	61.70	.05815	.05608	.11182	.11228
1.75	63.47	.05676	.05434	.10833	.10861
1.80	65.24	.05446	.05277	.10528	.10541
1.85	66.85	.05257	.05150	.10285	.10284
1.90	68.11	.05114	.05054	.10099	.10088
1.95	69.10	.04998	.04973	.09943	.09924
2.00	69.86	.04919	.04892	.09778	.09756
2.05	70.49	.04841	.04821	.09637	.09611
2.10	71.12	.04771	.04757	.09510	.09481

Table 26. Representative Results of the Adiabatic Simulation of Experiment 201 (Concluded)

Time (sec)	Depth (cm)	Prediction of Fractional Changes for Detectors			
		1	2	3	4
2.15	71.65	.04707	.04699	.09395	.09363
2.20	72.10	.04650	.04647	.09290	.09257
2.25	72.55	.04597	.04598	.09193	.09157
2.30	73.00	.04546	.04552	.09101	.09063
2.35	73.45	.04497	.04508	.09013	.08973
2.40	73.90	.04451	.04466	.08930	.08888
2.45	74.35	.04407	.04426	.08850	.08806
2.50	74.80	.04365	.04388	.08775	.08729
2.55	75.61	.04319	.04350	.08700	.08650
2.60	76.20	.04278	.04315	.08629	.08577
2.65	76.20	.04244	.04280	.08561	.08508
2.70	76.20	.04212	.04247	.08494	.08443
2.75	76.20	.04180	.04215	.08430	.08379
2.80	76.20	.04148	.04183	.08367	.08316
2.85	76.20	.04118	.04153	.08305	.08254
2.90	76.20	.04088	.04122	.08244	.08194
2.95	76.20	.04058	.04092	.08184	.08135
3.00	76.20	.04029	.04063	.08126	.08076
3.50	76.20	.03761	.03792	.07585	.07538
4.00	76.20	.03528	.03557	.07115	.07072
4.50	76.20	.03323	.03351	.06702	.06661
5.00	76.20	.03141	.03167	.06335	.06296

Table 27. Representative Results of the Adiabatic Simulation of Experiment 202

Time (sec)	Depth (cm)	Prediction of Fractional Changes for Detectors 1	2	3	4
.00	.00	1.00000	1.00000	1.00000	1.00000
.05	.00	.99966	.99966	.99966	.99966
.10	.00	.99938	.99938	.99938	.99938
.15	.00	.99915	.99915	.99915	.99915
.20	.13	.99426	.99786	.99790	.99776
.25	1.41	.94618	.98631	.98683	.98521
.30	4.19	.83586	.95079	.95228	.94763
.35	8.46	.68252	.90310	.90597	.89705
.40	16.12	.46150	.79525	.80465	.78856
.45	25.58	.34184	.60101	.63830	.61927
.50	35.71	.22901	.33060	.44077	.42614
.55	48.17	.14292	.14564	.27478	.26759
.60	57.30	.09559	.09186	.18156	.17848
.65	62.55	.07709	.07281	.14508	.14341
.70	66.25	.06981	.06530	.13036	.12934
.75	68.14	.06674	.06212	.12414	.12338
.80	69.48	.06522	.06050	.12097	.12040
.85	70.40	.06395	.05904	.11802	.11754
.90	71.21	.06286	.05785	.11565	.11526
.95	71.80	.06193	.05686	.11367	.11334
1.00	72.38	.06111	.05598	.11192	.11165
1.05	72.85	.06035	.05518	.11034	.11021
1.10	73.31	.05966	.05445	.10888	.10871
1.15	73.73	.05901	.05377	.10752	.10739
1.20	74.15	.05840	.05313	.10625	.10616
1.25	74.55	.05783	.05253	.10504	.10499
1.30	74.94	.05728	.05195	.10389	.10387
1.35	76.20	.05693	.05139	.10278	.10287
1.40	76.20	.05633	.05085	.10170	.10179
1.45	76.20	.05577	.05034	.10068	.10077
1.50	76.20	.05523	.04985	.09970	.09979
2.00	76.20	.05052	.04560	.09119	.09127
2.50	76.20	.04670	.04216	.08431	.08439
3.00	76.20	.04349	.03926	.07852	.07859
3.50	76.20	.04072	.03676	.07351	.07358
4.00	76.20	.03829	.03456	.06913	.06919
4.50	76.20	.03614	.03262	.06525	.06530
5.00	76.20	.03423	.03089	.06179	.06184

Table 25. Representative Results of the Space-Time Simulation of Experiment 203 (Concluded)

Time (sec)	Depth (cm)	Prediction of Fractional Changes for Detectors			
		1	2	3	4
2.15	75.65	.05045	.04569	.09107	.09099
2.20	76.20	.05003	.04519	.09008	.09005
2.25	76.20	.04959	.04484	.08937	.08939
2.30	76.20	.04921	.04452	.08865	.08870
2.35	76.20	.04878	.04414	.08791	.08794
2.40	76.20	.04845	.04382	.08730	.08733
2.45	76.20	.04813	.04352	.08671	.08674
2.50	76.20	.04778	.04321	.08609	.08611
3.00	76.20	.04435	.04011	.07992	.07997
3.50	76.20	.04146	.03749	.07468	.07473
4.00	76.20	.03902	.03528	.07026	.07030
4.50	76.20	.03682	.03330	.06631	.06634
5.00	76.20	.03484	.03151	.06276	.06279

Table 28. Representative Results of the Adiabatic Simulation of Experiment 203

Time (sec)	Depth (cm)	Prediction of Fractional Changes for Detectors 1	2	3	4
.00	.00	1.00000	1.00000	1.00000	1.00000
.05	.77	.97110	.99325	.99354	.99264
.10	1.26	.94832	.98411	.98458	.98313
.15	1.47	.93357	.97474	.97528	.97361
.20	1.67	.91838	.96479	.96540	.96352
.25	1.95	.90001	.95363	.95433	.95216
.30	3.25	.84500	.93225	.93338	.92986
.35	6.15	.73734	.89660	.89867	.89223
.40	9.16	.62939	.85572	.85866	.84951
.45	11.47	.54479	.78959	.79504	.78398
.50	13.93	.45684	.72276	.72962	.71712
.55	16.82	.38573	.65041	.66073	.64703
.60	19.88	.32581	.56450	.57899	.56487
.65	22.98	.27308	.48697	.50440	.49024
.70	26.12	.22970	.40279	.42994	.41698
.75	29.21	.19226	.33192	.36505	.35326
.80	32.27	.16368	.26561	.31345	.30305
.85	35.28	.13958	.20460	.26847	.25956
.90	38.24	.12188	.15975	.23546	.22764
.95	41.16	.10769	.12990	.20784	.20132
1.00	44.11	.09644	.10598	.18600	.18051
1.05	46.97	.08834	.09093	.17006	.16541
1.10	49.72	.08113	.08159	.15571	.15186
1.15	52.34	.07569	.07442	.14485	.14163
1.20	54.85	.07152	.06934	.13639	.13371
1.25	57.35	.06776	.06511	.12870	.12653
1.30	59.83	.06491	.06181	.12278	.12103
1.35	62.30	.06279	.05935	.11823	.11684
1.40	64.52	.06062	.05696	.11361	.11252
1.45	66.48	.05908	.05523	.11028	.10943
1.50	68.09	.05797	.05397	.10783	.10718
1.55	69.05	.05705	.05298	.10592	.10538
1.60	69.74	.05625	.05206	.10406	.10358
1.65	70.42	.05551	.05124	.10243	.10202
1.70	71.10	.05486	.05050	.10096	.10061
1.75	71.79	.05426	.04982	.09960	.09932
1.80	72.36	.05371	.04920	.09837	.09814
1.85	72.81	.05319	.04864	.09726	.09706
1.90	73.23	.05271	.04812	.09622	.09606
1.95	73.66	.05226	.04763	.09524	.09512
2.00	74.09	.05183	.04717	.09431	.09423
2.05	74.52	.05143	.04672	.09343	.09338
2.10	74.91	.05104	.04630	.09259	.09257

Table 28. Representative Results of the Adiabatic Simulation of Experiment 203 (Concluded)

Time (sec)	Depth (cm)	Prediction of Fractional Changes for Detectors			
		1	2	3	4
2.15	75.65	.05072	.04588	.09176	.09180
2.20	76.20	.05039	.04548	.09096	.09105
2.25	76.20	.04996	.04510	.09019	.09028
2.30	76.20	.04955	.04473	.08945	.08953
2.35	76.20	.04915	.04437	.08873	.08881
2.40	76.20	.04876	.04401	.08803	.08811
2.45	76.20	.04838	.04367	.08734	.08742
2.50	76.20	.04801	.04333	.08666	.08674
3.00	76.20	.04459	.04025	.08050	.08058
3.50	76.20	.04168	.03762	.07524	.07530
4.00	76.20	.03913	.03532	.07065	.07071
4.50	76.20	.03689	.03330	.06660	.06666
5.00	76.20	.03490	.03150	.06300	.06305

Table 29. Representative Results of the Mixed-Methods Simulation of Experiment 201

Time (sec)	Depth (cm)	Prediction of Fractional Changes for Detectors 1	2	3	4
.00	.00	1.00000	1.00000	1.00000	1.00000
.05	.43	.99485	.99456	.99461	.99475
.10	.86	.98548	.98488	.98514	.98544
.15	1.29	.97422	.97321	.97370	.97414
.20	1.72	.96082	.95956	.96015	.96069
.25	2.32	.94128	.93922	.94072	.94153
.30	3.73	.90823	.90678	.90779	.90899
.35	5.90	.85990	.85518	.85856	.86037
.40	7.89	.80383	.79841	.80199	.80420
.45	10.14	.74368	.73785	.74156	.74462
.50	12.55	.66815	.65938	.66595	.66947
.55	14.42	.59864	.59008	.59624	.59984
.60	16.33	.54424	.53360	.54226	.54610
.65	18.46	.48936	.47576	.48743	.49155
.70	20.67	.43551	.41997	.43348	.43768
.75	22.90	.39276	.37604	.39051	.39480
.80	25.15	.35373	.33093	.35253	.35688
.85	27.40	.31437	.28797	.31392	.31816
.90	29.63	.28385	.25506	.28338	.28752
.95	31.83	.25899	.21978	.26029	.26431
1.00	33.99	.23380	.18439	.23724	.24107
1.05	36.16	.21193	.15653	.21665	.22026
1.10	38.31	.19484	.13584	.20094	.20439
1.15	40.40	.17603	.11703	.18678	.18992
1.20	42.47	.15944	.10171	.17310	.17595
1.25	44.59	.14635	.08988	.16206	.16466
1.30	46.77	.13045	.08158	.15283	.15515
1.35	49.24	.11067	.07493	.14320	.14516
1.40	51.46	.09636	.06947	.13442	.13602
1.45	53.16	.08746	.06587	.12883	.13025
1.50	54.83	.07925	.06314	.12442	.12566
1.55	56.48	.07241	.06073	.12000	.12099
1.60	58.18	.06651	.05853	.11595	.11674
1.65	59.93	.06150	.05657	.11235	.11296
1.70	61.70	.05781	.05473	.10908	.10951
1.75	63.47	.05537	.05303	.10593	.10620
1.80	65.24	.05323	.05160	.10314	.10326
1.85	66.85	.05149	.05044	.10085	.10084
1.90	68.11	.05017	.04954	.09908	.09897
1.95	69.10	.04914	.04875	.09754	.09736
2.00	69.86	.04838	.04810	.09622	.09600
2.05	70.49	.04771	.04751	.09505	.09479
2.10	71.12	.04708	.04696	.09394	.09366

Table 29. Representative Results of the Mixed-Methods Simulation of Experiment 201 (Concluded)

Time (sec)	Depth (cm)	Prediction of Fractional Changes for Detectors 1	2	3	4
2.15	71.65	.04651	.04645	.09292	.09261
2.20	72.10	.04601	.04598	.09200	.09166
2.25	72.55	.04552	.04554	.09112	.09076
2.30	73.00	.04504	.04510	.09024	.08986
2.35	73.45	.04456	.04466	.08938	.08898
2.40	73.90	.04410	.04424	.08853	.08812
2.45	74.35	.04365	.04383	.08772	.08728
2.50	74.80	.04322	.04344	.08693	.08648
2.55	75.61	.04268	.04299	.08605	.08555
2.60	76.20	.04224	.04259	.08523	.08471
2.65	76.20	.04193	.04228	.08460	.08408
2.70	76.20	.04166	.04198	.08399	.08348
2.75	76.20	.04135	.04168	.08336	.08286
2.80	76.20	.04103	.04137	.08274	.08223
2.85	76.20	.04071	.04106	.08211	.08161
2.90	76.20	.04039	.04075	.08150	.08100
2.95	76.20	.04010	.04046	.08091	.08042
3.00	76.20	.03982	.04017	.08035	.07986
3.50	76.20	.03722	.03753	.07507	.07461
4.00	76.20	.03494	.03523	.07048	.07005
4.50	76.20	.03293	.03321	.06642	.06602
5.00	76.20	.03114	.03140	.06281	.06243

Table 30. Representative Results of the Mixed-Methods Simulation of Experiment 202

Time (sec)	Depth (cm)	Prediction of Fractional Changes for Detectors 1	2	3	4
.00	.00	1.00000	1.00000	1.00000	1.00000
.05	.00	.99966	.99966	.99965	.99965
.10	.00	.99927	.99927	.99926	.99926
.15	.00	.99888	.99888	.99888	.99888
.20	.13	.99706	.99707	.99715	.99701
.25	1.41	.96522	.98087	.98158	.98009
.30	4.19	.81675	.92934	.93315	.92882
.35	8.46	.64206	.85037	.85330	.84553
.40	16.12	.41264	.69202	.70441	.69125
.45	25.58	.25715	.44884	.48361	.47018
.50	35.71	.15062	.21312	.29176	.28266
.55	48.17	.09633	.09785	.18632	.18163
.60	57.30	.07530	.07230	.14334	.14094
.65	62.55	.06891	.06505	.12992	.12844
.70	66.25	.06585	.06168	.12329	.12230
.75	68.14	.06453	.06002	.12007	.11931
.80	69.48	.06356	.05882	.11773	.11716
.85	70.40	.06269	.05786	.11578	.11530
.90	71.21	.06187	.05695	.11395	.11356
.95	71.80	.06112	.05612	.11228	.11194
1.00	72.38	.06044	.05534	.11075	.11046
1.05	72.85	.05976	.05463	.10934	.10910
1.10	73.31	.05912	.05394	.10796	.10777
1.15	73.73	.05849	.05328	.10664	.10649
1.20	74.15	.05788	.05265	.10536	.10525
1.25	74.55	.05731	.05204	.10414	.10407
13.0	74.94	.05676	.05145	.10296	.10293
1.35	76.20	.05626	.05073	.10156	.10165
1.40	76.20	.05567	.05024	.10054	.10063
1.45	76.20	.05516	.04977	.09960	.09969
1.50	76.20	.05466	.04933	.09868	.09878
2.00	76.20	.05005	.04518	.09037	.09046
2.50	76.20	.04631	.04181	.08362	.08370
3.00	76.20	.04316	.03896	.07793	.07800
3.50	76.20	.04043	.03649	.07300	.07306
4.00	76.20	.03804	.03433	.06867	.06874
4.50	76.20	.03591	.03242	.06484	.06490
5.00	76.20	.03402	.03071	.06142	.06048

Table 31. Representative Results of the Mixed-Methods Simulation of Experiment 203

Time (sec)	Depth (cm)	Prediction of Fractional Changes for Detectors 1	2	3	4
.00	.00	1.00000	1.00000	1.00000	1.00000
.05	.77	.97833	.99094	.99100	.99044
.10	1.26	.96310	.97784	.97827	.97710
.15	1.47	.94739	.96644	.96686	.96530
.20	1.67	.92850	.95663	.95703	.95523
.25	1.95	.90842	.94545	.94625	.94418
.30	3.25	.83360	.91879	.91994	.91646
.35	6.15	.70695	.86609	.86885	.86286
.40	9.16	.58283	.79360	.79674	.78844
.45	11.47	.47761	.70643	.71259	.70297
.50	13.93	.38914	.62282	.62905	.61869
.55	16.82	.32180	.54475	.55474	.54356
.60	19.88	.26572	.46271	.47618	.46487
.65	22.98	.22164	.39253	.40843	.39727
.70	26.12	.18714	.32683	.35174	.34136
.75	29.21	.15886	.27230	.30188	.29234
.80	32.27	.13856	.22083	.26629	.25758
.85	35.28	.12151	.17417	.23436	.22670
.90	38.24	.10862	.14285	.21007	.20319
.95	41.16	.09842	.11645	.19053	.18462
1.00	44.11	.08920	.09712	.17246	.16741
1.05	46.97	.08247	.08487	.15931	.15491
1.10	49.72	.07672	.07701	.14761	.14399
1.15	52.34	.07204	.07090	.13814	.13509
1.20	54.85	.06852	.06641	.13084	.12828
1.25	57.35	.06539	.06280	.12434	.12225
1.30	59.83	.06284	.05989	.11899	.11728
1.35	62.30	.06079	.05744	.11461	.11326
1.40	64.52	.05898	.05546	.11079	.10972
1.45	66.48	.05756	.05386	.10769	.10684
1.50	68.09	.05664	.05270	.10542	.10475
1.55	69.05	.05589	.05183	.10370	.10315
1.60	69.74	.05525	.05113	.10228	.10181
1.65	70.42	.05467	.05047	.10096	.10055
1.70	71.10	.05410	.04983	.09968	.09933
1.75	71.79	.05357	.04921	.09846	.09817
1.80	72.36	.05309	.04864	.09732	.09707
1.85	72.81	.05264	.04813	.09631	.09610
1.90	73.23	.05220	.04765	.09536	.09519
1.95	73.66	.05177	.04718	.09441	.09428
2.00	74.09	.05135	.04671	.09348	.09338
2.05	74.52	.05094	.04626	.09258	.09251
2.10	74.91	.05054	.04582	.09170	.09167

Table 31. Representative Results of the Mixed-Methods Simulation of Experiment 203 (Concluded)

Time (sec)	Depth (cm)	Prediction of Fractional Changes for Detectors			
		1	2	3	4
2.15	75.65	.05014	.04534	.09074	.09078
2.20	76.20	.04982	.04489	.08984	.08991
2.25	76.20	.04938	.04454	.08914	.08922
2.30	76.20	.04900	.04421	.08845	.08853
2.35	76.20	.04862	.04387	.08775	.08783
2.40	76.20	.04823	.04353	.08705	.08713
2.45	76.20	.04784	.04318	.08635	.08643
2.50	76.20	.04745	.04284	.08568	.08575
3.00	76.20	.04415	.03985	.07970	.07977
3.50	76.20	.04129	.03726	.07454	.07460
4.00	76.20	.03879	.03501	.07003	.07009
4.50	76.20	.03658	.03302	.06605	.06611
5.00	76.20	.03462	.03125	.06251	.06256

BIBLIOGRAPHY

1. A. F. Henry, "Analytical Methods in Reactor Kinetics," Bettis Atomic Power Laboratory, WAPD-OP-10 (1960).

2. J. R. Lamarsh, Nuclear Reactor Theory, Addison-Wesley Publishing Company, Inc., Reading, Massachusetts, 1966.

3. A. F. Henry, "The Application of Reactor Kinetics to the Analysis of Experiments," Nuclear Science & Engineering, 3, 52 (1958).

4. M. Becker, "A Generalized Formulation of the Point Nuclear Reactor Kinetics Equations," Nucl. Sci. Eng., 31, 458 (1968).

5. J. B. Yasinsky, "On the Use of Point Kinetics for the Analysis of Rod-Ejection Accidents," Nucl. Sci. Eng., 39, 241 (1970).

6. T. J. Thompson and J. G. Beckerley, eds., The Technology of Nuclear Reactor Safety, The MIT Press, Cambridge, Massachusetts, 1964.

7. K. A. Ott and D. A. Meneley, "Accuracy of the Quasistatic Treatment of Spatial Reactor Kinetics," Nucl. Sci. Eng., 36, 402 (1969).

8. K. F. Hansen, et al., "Stable Numerical Solutions of the Reactor Kinetics Equations," Nucl. Sci. Eng., 22, 51 (1968).

9. Z. Akasu, "General Solution of the Reactor Kinetic Equations Without Feedback," Nucl. Sci. Eng., 3, 456 (1958).

10. T. A. Porsching, "Numerical Solution of the Reactor Kinetics Equations by Approximate Exponentials," Nucl. Sci. Eng., 25, 183 (1966).

11. K. F. Hansen, et al., "A New Method of Integrating the Point Kinetics Equations," Transactions of the American Nuclear Society, 12, 617 (1969).

12. J. C. Vigil, "Solution of the Reactor Kinetics Equations by Analytic Continuation," Nucl. Sci. Eng., 29, 392 (1967).

13. P. A. Secker, "Solution of the Reactor Kinetics Equations by Optimum Integrating Factors," Trans. Am. Nucl. Soc., 12, 618 (1969).

14. J. P. W. da Nóbrega and A. F. Henry, "A New Solution of the Point Kinetics Equations," Nucl. Sci. Eng., 46, 366 (1971).

BIBLIOGRAPHY (Continued)

15. S. Kaplan, et al., "Space-Time Reactor Dynamics," Third United Nations International Conference on the Peaceful Uses of Atomic Energy, 1964, Geneva, Vol. 4.

16. T. W. Kerlin, "Status of Space-Time Analysis," Nuclear Safety, 6 (4), 395 (1966).

17. P. R. Kasten, "Accident Analysis," Nuclear Safety, 7 (2), 162 (1966).

18. D. K. Butler and D. A. Meneley, "Recent Developments in Fast Reactor Kinetics," Nuclear Safety, 11 (4), 289 (1970).

19. W. M. Stacey, "Space- and Energy-Dependent Neutronics in Reactor Transient Analysis," Reactor Technology, 14 (2), 169 (1971).

20. W. R. Cadwell, "WIGLE - A Program for the Two Group, Space-Time Diffusion Equations in Slab Geometry," Bettis Atomic Power Laboratory, WAPD-TM-416 (1964).

21. A. F. Henry and A. V. Vota, "WIGL2 - A Program for the Solution of the One-Dimensional, Two-Group, Space-Time Diffusion Equations Accounting for Temperature, Xenon, and Control Feedback," Bettis Atomic Power Laboratory, WAPD-TM-532 (1965).

22. J. B. Yasinsky, et al., "TWIGL - A Program to Solve the Two-Dimensional, Two-Group, Space-Time Neutron Diffusion Equations with Temperature Feedback," Bettis Atomic Power Laboratory, WAPD-TM-743 (1968).

23. S. D. Conte, Elementary Numerical Analysis, McGraw-Hill Book Company, New York, 1965.

24. A. L. Wight and K. F. Hansen, "Solving Reactor Kinetics Equations by Alternating Direction Implicit Method," Trans. Am. Nucl. Soc., 12, 120 (1969).

25. H. L. Garabedian and C. B. Leffert, "A Time Dependent Analysis of Spatial Flux Distributions," Nucl. Sci. Eng., 6, 26 (1959).

26. E. L. Wachpress, "Multichannel Flux Synthesis," Nucl. Sci. Eng., 12, 381 (1962).

27. J. B. Yasinsky, "Notes on Nuclear Reactor Kinetics," Bettis Atomic Power Laboratory, WAPD-TM-960 (1970).

BIBLIOGRAPHY (Continued)

28. S. Kaplan, et al., "Application of Synthesis Techniques to Problems Involving Time Dependence," Nucl. Sci. Eng., 18, 163 (1964).

29. Seminar, Georgia Institute of Technology (January, 1972).

30. A. F. Henry and N. J. Curlee, "Verification of a Method for Treating Neutron Space-Time Problems," Nucl. Sci. Eng., 4, 727 (1958).

31. D. L. West, et al., "Use of the Adiabatic Approximation in Prompt-Critical, Large Core Reactor Excursion Analyses," Trans. Am. Nucl. Soc., 8, 497 (1965).

32. K. O. Ott and J. T. Madell, "Quasistatic Treatment of Spatial Phenomena in Reactor Dynamics," Nucl. Sci. Eng., 26, 562 (1966).

33. W. M. Stacey and C. H. Adams, "The Time-Integrated Method: A Quasistatic Neutron Space-Time Approximation," Trans. Am. Nucl. Soc., 10, 251 (1967).

34. K. O. Ott and D. A. Meneley, "Accuracy of the Quasistatic Treatment of Spatial Reactor Kinetics," Nucl. Sci. Eng., 36, 402 (1969).

35. E. L. Wachpress, "Numerical Studies of Multichannel Variational Synthesis," Nucl. Sci. Eng., 34, 158 (1968).

36. J. B. Yasinsky, "Numerical Studies of Combined Space-Time Synthesis," Nucl. Sci. Eng., 34, 158 (1968).

37. R. S. Denning, "Space-Time Kinetics Studies for Commercial Power Reactors," Trans. Am. Nucl. Soc., 13 (2), 676 (1970).

38. J. B. Yasinsky and A. F. Henry, "Some Numerical Experiments Concerning Space-Time Reactor Kinetics Behavior," Nucl. Sci. Eng., 22, 171 (1965).

39. H. H. Hassan and G. H. Miley, "Verification of Space-Time Reactor Kinetics Analysis by Experiments," Nucl. Sci. Eng., 40, 449 (1970).

40. R. A. Rydin, et al., "Noise and Transient Kinetics Experiments and Calculations for Loosely Coupled Cores," Nucl. Sci. Eng., 46, 179 (1971).

41. S. G. V. S. Raju and R. S. Stone, "Dynamics of Coupled Core Reactors," Nuclear Safety, 9, 125 (1968).

BIBLIOGRAPHY (Continued)

42. J. E. Houghtaling, et al., "Temperature-Dependent Kinetic Behavior of the SPERT-III E-Core," Trans. Am. Nucl. Soc., 10, 2 (1967).

43. G. R. Freund, et al., "Design Summary Report in the Transient Reactor Test Facility TREAT," ANL-6034.

44. J. C. Robinson, Approximate Solution to the Time-Dependent, Multi-Group Neutron Diffusion Equations Using a Restricted Variational Principle, Ph.D. Dissertation, University of Tennessee (1966).

45. H. Christensen, "A Review of NORA Project Noise Experiments," CONF-660206 (1966).

46. R. J. Johnson, Investigation of the Space-Dependent Zero Power Reactor Source Transfer Function, Ph.D. Dissertation, Georgia Institute of Technology (1966).

47. D. N. Bridges, An Investigation of the Spatially-Dependent Reactor Source Transfer Function with Temperature Feedback, Ph.D. Dissertation, Georgia Institute of Technology (1970).

48. N. J. Diaz and M. J. Ohanian, "Space-Time Kinetics Studies in a Large, Close-to-Critical H_2O-UO_2 Assembly," Trans. Am. Nucl. Soc., 13, 236 (1970).

49. G. H. Weaver, Reactor Space-Time Analysis and Experiments, Ph.D. Dissertation, Georgia Institute of Technology (1971).

50. Safeguards Report for the Georgia Tech Research Reactor, Georgia Institute of Technology, Atlanta, Georgia (1960).

51. Fluid Power Data Book, Womack Machine Supply Company, Dallas, Texas (1967).

52. Introduction to Programming, Digital Equipment Corporation, Maynard, Massachusetts (1970).

53. Small Computer Handbook, Digital Equipment Corporation, Maynard, Massachusetts (1970).

54. L. R. Foulke, "Examination of Errors Introduced by the Few-Group Diffusion Theory Approximation in Space-Dependent Kinetics Calculations," Trans. Am. Nucl. Soc., 13, 702 (1970).

55. J. J. Seidler, et al., "Reactor Physics Calculations for the 5 MW Georgia Tech Research Reactor," Technical Report GT-NE-9, Nuclear Engineering Series, Georgia Institute of Technology, Atlanta, Georgia (1968).

BIBLIOGRAPHY (Concluded)

56. D. J. McGoff, "FORM - A Fourier Transfer Fast Spectrum Code for the IBM 709," NAA-SR-MEMO-5766 (1960).

57. R. H. Shudde and J. Dyer, "TEMPEST-II, A Neutron Thermalization Code," Atomics International, AMTD-111 (1962).

58. G. R. Keepin, "Neutron Data for Reactor Kinetics. 1. Delayed Neutrons from Fission. 2. Photoneutrons from D_2O and Beryllium," Nucleonics, 20 (8), 150 (1962).

59. W. W. Graham and D. S. Harmer, "The Determination of Effective Delayed Neutron and Photoneutron Kinetics Parameters in a Highly Enriched Heavy Water Reactor," Technical Report GT-NE-3, Nuclear Engineering Series, Georgia Institute of Technology, Atlanta, Georgia (1965).

60. M. Ash, Nuclear Reactor Kinetics, McGraw-Hill Book Company, New York, 1965.

61. P. R. Bevington, Data Reduction and Error Analysis for Physicists, McGraw-Hill Book Company, New York, 1969.

VITA

Anthony Joseph Foltman, II was born in Dallas, Texas on October 16, 1944. He attended public schools in Tampa, Florida and graduated from C. Leon King High School in 1963. He then attended the Georgia Institute of Technology in Atlanta, Georgia where he received a Bachelor of Science degree in Physics in 1967.

Mr. Foltman subsequently enrolled in the graduate program at Georgia Tech and was awarded a Master of Science degree in Nuclear Engineering in 1968. While engaged in this graduate work he was employed by the Engineering Experiment Station where he was involved in neutron diffraction research.

Mr. Foltman continued his graduate studies toward a doctorate in Nuclear Engineering at Georgia Tech. The work was supported by a National Science Foundation Traineeship and a Graduate Research Assistantship.

Mr. Foltman is married to the former Karen Angela Kovac of Tampa, Florida. He is a member of the American Nuclear Society and the Society of the Sigma Xi.